STABILITY OF TWIN SQUARE AND CIRCULAR TUNNELS PLACED AT RELATIVE DEPTHS IN CLAYEY DEPOSIT USING ADAPTIVE LOWER BOUND – FINITE ELEMENT LIMIT ANALYSIS

A Dissertation

Submitted for the partial fulfilment of the requirement

for the award of the degree of

MASTER OF ENGINEERING

In

CIVIL ENGINEERING

By

INDRANIL CHOWDHURY

(M.E in Civil Engineering)

(Examination Roll No. – M4CIV23026)

Registration No. – 160037 of 2021-2022

Under the supervision of

Dr. Obaidur Rahaman

FACULTY OF ENGINEERING AND TECHNOLOGY

DEPARTMENT OF CIVIL ENGINEERING

(SOIL MECHNICS AND FOUNDATION ENGINEERING DIVISION)

JADAVPUR UNIVERSITY

KOLKATA – 700032, WEST BENGAL

2023

DECLARATION

This is to certify that the thesis entitled "Stability of Twin Square and Circular Tunnels placed at Relative Depths in Clayey Deposit using Adaptive Lower Bound – Finite Element Limit Analysis" which is prepared and submitted by Indranil Chowdhury, be accepted for the partial fulfillment of the requirements for the award of Master of Engineering in Civil Engineering from Jadavpur University. This thesis is prepared under my supervision and neither this thesis nor any part of this thesis has been submitted for any degree or any other academic award anywhere before.

Indranil Chowdhury
Class Roll No.: 002110402022
Examination Roll No.: M44CIV23026
Class: M.C.E. 2nd Year

Date:

Place: Civil Engineering Department

Jadavpur University, Kolkata

JADAVPUR UNIVERSITY

Faculty of Engineering & Technology

Department of Civil Engineering

CERTIFICATE OF RECOMMENDATION

This is to certify that the thesis entitled "Stability of Twin Square and Circular Tunnels Placed at Relative Depths in Clayey Deposit Using Adaptive Lower Bound – Finite Element Limit Analysis" which is prepared and submitted by Indranil Chowdhury, be accepted for the partial fulfillment of the requirements for the award of Master of Engineering in Civil Engineering from Jadavpur University. This thesis is prepared under my supervision and neither this thesis nor any part of this thesis has been submitted for any degree or any other academic award anywhere before.

Signature of Supervisor

Dr. Obaidur Rahaman
Assistant Professor,
Department of Civil Engineering
Jadavpur University

Countersigned by:

Dean
Faculty of engineering and Technology
Jadavpur University

Head of The Department
Jadavpur University

JADAVPUR UNIVERSITY

Faculty of Engineering & Technology

Department of Civil Engineering

CERTIFICATE OF APPROVAL

This is to certify that this thesis is hereby approved as an original work conducted and presented satisfactory to warrant its acceptance as a prerequisite to the degree for which it has been submitted. It is implied that by this approval the undersigned does not necessarily endorse or approve any statement made, opinion expressed, or conclusion drawn therein, but approves the thesis only for the purpose for which it is submitted.

The final examination for evaluation of the thesis Committee of Thesis Paper Examiners.

_____

Signature of Examiner

_____

Signature of Examiner

ACKNOWLEDGEMENT

I gratefully acknowledge the innovative guidance, active supervision and consistent motivation of our reverent Professor **Dr. Obaidur Rahaman** of the Department of Civil Engineering, Jadavpur University, Kolkata, who regardless of his other commitments, always guided and in spite of his other commitments counseled and resolved in every part of this thesis in a way that it would not be in this shape without him. I do convey my sincere thanks and gratitude to him.

I also acknowledge the cooperation, guidance and assistance provided by Prof. Ramendu Bikas Sahu, Prof. Gupinath Bhandari, Prof. Pritam Aitch, Prof. Arghadeep Biswas and Prof. Narayan Roy during this work.

I am also indebted and grateful to all Professors and staffs of Civil Engineering Department, Jadavpur University, Kolkata, for extending all facilities to carry out the present study.

I would also like this opportunity to express my gratitude to my classmates who helped me through the entire semester for this work.

I am also grateful to my colleagues in my organization along with our Senior General Manager Mr. Sudip Nath of C. E. Testing Company Pvt. Ltd. for valuable suggestions and constant motivation.

Indranil Chowdhury
Class Roll No.: 002110402022
Examination Roll No.: M44CIV23026
Class: M.C.E. 2nd Year

CONTENTS

List of figures

List of tables

Abstract

Owing to the space restraints, the changes in soil formations, the presence of important structures on the ground surface, the presence of a largely confined aquifer; the tunnels in the 'twin-tunnel' may be required to be placed at two different depths relative to each other. In view of this possible scenario, this study utilizes the lower bound finite element limit analysis technique to determine the stability factors of twin tunnels placed at different relative depths in a clayey deposit. The tunnels are assumed to be unsupported, straight and infinitely long; thus, modeled as a plain strain problem. The soil surrounding the tunnels in assumed to be clayey soil in undrained condition. Two categories of shapes are taken into account, namely square, and circular tunnel. The stability number is obtained by following two different approaches: (i) load multiplier method where the objective function, i.e., the collapse multiplier in the limit analysis, is the net surface surcharge, and (ii) gravity multiplier method where the acceleration due to gravity becomes the objective function of the optimization problem.

The analysis conducted in this thesis utilizes the OptumG2, a finite element limit analysis software and it leverages the feature ‘adaptive meshing’ to obtain precise results within lesser computation time. The impacts of different depth ratios, spacing between the tunnels, and soil properties on the stability factors as well as the failure mechanism have been studied thoroughly. For the ease of interpretation, all the parameters have been expressed as dimensionless parameter and stability charts are obtained in terms of stability number for various combinations of these dimensionless parameters. Variation of the collapse mechanism based on state of yield for different parameters is also presented in this study. Accuracy of the adopted methodology is verified by comparing the results with that of a standard stability problem of square tunnel and circular tunnel.

CHAPTER – 1: INTRODUCTION

1.1. GENERAL

The demand for community services (sewers, water pipelines), as well as transportation infrastructure (roads, trains, and metros), has increased as urban population growth has continued to rise. Tunnels and underground buildings are employed to accommodate the necessary infrastructures due to the lack of available spaces and surface congestion. In the modern world, tunneling has been widely exploited to create effective transit systems within big cities. With rising urbanization and population, tunnels are being used more frequently to bypass populated regions, ease traffic, and create public transportation networks. Such tunnels are reaching saturation in some cities, so additional tunnels are being built next to the existing infrastructure. Due to the fact that building multiple tunnels is typically a more cost-effective choice than building a single larger tunnel, dual tunnels are frequently used in engineering. Additionally, in order to support one-way traffic, highways and railways often construct separate tunnels. The stability of dual tunnels must therefore be evaluated. In fact, using multiple tunnels is a method that is becoming more and more common when designing new infrastructure. Utilizing two or more tunnels improves safety by separating traffic, facilitating better access and providing escape in case of emergencies.

Due to the growth of mining, subterranean openings, large aquifer, pipelines, and transportation networks new tunnels may be built close to the existing tunnels. Moreover, due to presence of important or heavy structures at the ground level and changes in the subsoil formation, the tunnels may be required to be placed at different depths. Therefore, it is necessary to perform the stability analysis of two tunnels placed at various relative depths.

In Geotechnical engineering, stability issues are concerned with understanding the magnitude of the loads that may be safely maintained by the soil, and dealing with the eventual collapse circumstances of a mass of soil mass. In this category, issues with ground pressure, bearing capacity, and slope stability are frequently taken into account. In the case of tunnels, stability problems are often posed to calculate the maximum loads that can be applied to the ground surface above the tunnel or to determine the pressure needed inside the tunnel to prevent soil collapse. Another common method to evaluate stability is to assume condition with no surcharge loads but determining the maximum density of soil that which can be permitted by

the tunnels without any collapse.

Tunnel stability refers to the ability of a tunnel to maintain its shape and support the surrounding ground. According to Peck's theory (1969), a tunnel gets stability in the ground through deformation of its shape and/or support from the surrounding ground. There are various methods available for assessing tunnel stability, including the use of safety factors and numerical techniques. The applied loads, the tunnel geometry (i.e. the form, size and depth of a tunnel), and the strength of the surrounding material are only a few of the many parameters that have effect on tunnel stability. The unit weight (γ) of the soil is also important in determining the stability of many geotechnical structures. For tunnels, the weight of the soil typically acts to drive collapse. However, for deep tunnels in which collapse involves heaving of the floor, part of the soil mass moves upwards against gravity and the unit weight acts to resist collapse of the soil into the tunnel.

The stability of a tunnel depends on how well it can resist the stresses and strains imposed by the surrounding ground, which vary according to subsoil formation of the tunnel. The geometry of tunnel is another important aspect. For example, a circular tunnel may have more stability than a square one, as it can distribute the load more evenly. However, square tunnels offer more utilization of the excavated space. Moreover, a tunnel in a soft soil may have more stability than a tunnel in a hard rock, as it can deform more easily without cracking. Analyzing the stability of tunnels is not a straightforward task, as there are many complex and uncertain factors involved, such as the soil properties, the groundwater conditions, the construction methods, and the long-term effects of aging and weathering. Therefore, engineers need to use advanced methods and tools to assess the stability of tunnels and design appropriate measures to enhance it.

The issue of stability is prevailing before the construction of the secondary support. The stability of tunnel has been analyzed for several scenarios by various researchers. From cohesive to cohesionless soil, from weathered to heavily jointed rock, from circular to horse-shoe shaped tunnels, the researchers analyzed stability of tunnels for single and multiple tunnels. The researchers adopt analytical or semi-analytical approach, empirical and experimental approaches to analyze the tunnels.

However, with increasing demand, the subsoil condition and the tunnel system is being complicated which cannot be analyzed through conventional approaches, especially in soils.

Sloan (2013) pointed out that limit equilibrium analysis although simple and widely used, fails to address the equilibrium of all the points within the domain. This method also requires an assumption of a general failure surface which makes the analysis very difficult specially the case of heterogeneity and anisotropy. With the growing advancement in speed and capacity of computers, the usage of numerical methods is becoming more popular. The specific numerical methods include finite element method (FEM), finite difference method (FDM), boundary element method (BEM), discontinuous deformation analysis (DDA), smoothed particle hydrodynamics (SPH), material point method (MPM), etc.

The tunnel stability problems can also be handled well by using the principles of the limit analysis which is based on the plasticity theory and it provides two limit theorems – lower bound and upper bound (Chen, 1975). The lower bound solution is computed from a statically admissible stress field with a check that the yield condition gets nowhere violated in the domain. On the other hand, a kinematically admissible velocity field is generated with a condition that the total power dissipation becomes minimum. An approximate magnitude of the limit load for a simple stability problem can be computed from an assumed failure/collapse mechanism. However, for the problems involving irregular geometry or complex loading or complicated boundary conditions, and, moreover, to improve the accuracy of the solution, the concept of the finite element discretization along with some mathematical optimization procedure is usually integrated in the limit analysis technique (Bottero et al. 1980, Sloan 1988). This combined procedure is usually termed as the finite element limit analysis (FELA), and it inherits several advantages over the other stability methods, such as:

I. The limit analysis considers the problem only at the verge of failure. Therefore, instead of computing the complete stress-strain relationship (model) of the material, it requires only the values of different material shear strength parameters, associated with a chosen yield criterion, for performing the stability analysis.

II. It does not require any predefined failure surface or the collapse mechanism.

III. Similar to the elasto-plastic finite element analysis, it can handle irregular geometry, difficult boundary condition, complex loading condition, material anisotropy as well as inhomogeneity. However, unlike the elasto-plastic finite element analysis, there is no need to generate the complete load-deformation response before predicting the collapse magnitude which results in a significant reduction in the overall computational time in solving a given problem.

IV. The obtained solutions are quite accurate since the solution is obtained numerically based on the principle of optimization satisfying both statically admissible stress field as well as kinematically admissible velocity field.

V. This method is capable of generating the actual collapse mechanism which helps to generate the failure surface in soil/rock media in event of collapse.

Among the two limit theorems, the predicted magnitude of the collapse load on the basis of the lower bound theorem remains always equal to or less than the true value. Therefore, the lower bound finite elements limit analysis (LB-FELA) provides a conservative (safe) estimate of the true collapse load. The work presented in this thesis is focused on the application of the LB-FELA in the stability analysis of two tunnels.

1.2. MOTIVATION AND OBJECTIVES

In practical applications, the construction of dual tunnels is often regarded as a superior choice compared to a single large tunnel. This preference is based on considerations of soil characteristics, geological conditions, and various practical and economic concerns. Several factors, such as scarcity of available land, the presence of large aquifers, increasing traffic demands, and the existence of substantial surface structures, may necessitate the placement of tunnels at two distinct levels. However, it has been observed that existing research predominantly focuses on tunnels situated at the same level. Therefore, a limited information is available regarding tunnels positioned at different depths. Consequently, this study aims to assess the stability of twin tunnels located at varying relative depths. The comprehensive objectives of this thesis are summarized as follows:

1. To analyze the stability of dual square tunnels in clayey soil using adaptive lower bound finite element limit analysis considering both the load multiplier and gravity multiplier methods.
2. To assess the stability of twin circular tunnels in clayey soil through adaptive lower bound finite element limit analysis, encompassing both load multiplier and gravity multiplier methods.
3. To perform an extensive parametric investigation aimed at assessing how the unit weight and the cohesion of soil, tunnel geometry, tunnel shapes, and the relative horizontal and vertical spacing between twin tunnels influence the stability number.

4. To explore the characteristics of the failure surface in diverse scenarios.

1.3. ORGANIZATION OF THE THESIS

This thesis is organized into following five main chapters.

Chapter one gives an overview and brief introduction on stability of tunnels using different methods and objectives of thesis.

Chapter two discusses review of previous literatures covering analytical, semi-analytical, experimental, and numerical methods of stability analysis of tunnels.

Chapter three describes the methodology and stability analysis techniques in OptumG2.

Chapter four describes the problem statement and range of various parameters which have been considered in this study.

The results are discussed in detail in chapter five.

Chapter six deals with the conclusions and future scopes.

CHAPTER – 2: LITERATURE REVIEW

The literature concerning tunnel stability analysis has been classified into three distinct categories: (i) analytical and semi-analytical approaches, (ii) case studies and experimental methodologies, and (iii) numerical methods. Within each of these categories, detailed discussions have been conducted on the influence of factors such as (i) the number of tunnels, (ii) tunnel shapes and geometries, and (iii) soil characteristics.

2.1. ANALYTICAL AND SEMI-ANALYTICAL METHODS

Analytical approach comprises different proposed mathematical and empirical perspectives of design of single and dual tunnels. The following literatures covers different aspects of the findings by the researchers over the years.

1. **Terzaghi (1946)** recommended methods to ascertain loadings on tunnel linings. The stability of the tunnel then can be calculated using the loads on the tunnel and resistance offered by the tunnel lining. A zone of arching is assumed above the tunnel. This zone was divided into zone carried by roof and zones carried by the wedges. In this study, rock mass is considered to be loading on the tunnel for a height less than the depth of the tunnel. The passive vertical pressure on the tunnel and active horizontal pressures are then calculated to determine the loading.

2. Purely analytical studies of the two-tunnel problem are scarce. However one is described by **Fotieva and Sheinin (1966)** this study was based on the assumption of an elastic soil and use a Laplace transformation technique the analysis was applied to an example problem of a lined tunnel of six meter diameter at a depth of 36 meter the soil and the liner oil assigned material properties of lock and concrete separately a second tunnel of the same size was considered to be excavated to the existing one at a central distance of 8 meter the driving of the second tunnel cost additional stress in the liner.

3. The stresses, strains, and displacements surrounding a circular tunnel in rock are determined using an elasto-plastic solution by **Hendron and Aiyer (1972)**. The Coulomb-Navier failure criteria are utilized to determine the correlation among the principal stresses in the plastic zone, and the notion of normality is employed to relate the plastic strains to the yield surface. When the material's angle of shearing resistance is larger than zero, the normality concept leads the material to dilate during yielding. As a result, the displacements computed using this method

takes into account the impact of dilatancy in the yielding zone surrounding the tunnel.

4. **Atkinson and Potts (1977)** discussed the stability of a tunnel in cohesionless soil. They primarily kept focus on radial pressure to be supported by compressed air, bentonite slurry, a shield or by other means in order to achieve stability.

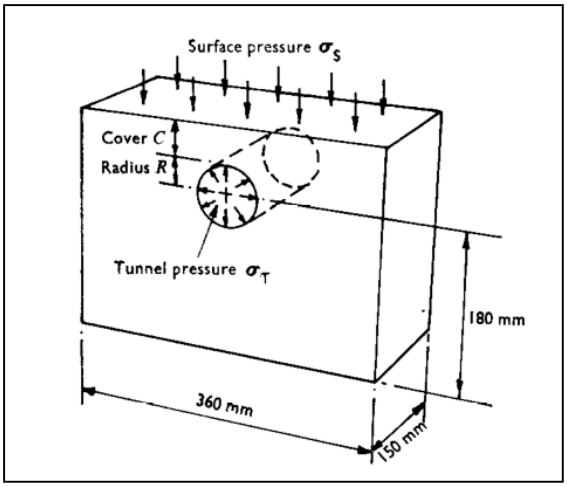

Fig. 2.1: Boundary conditions and dimensions of model tunnel tests, (Atkinson and Potts, 1977)

Both the theoretical as well as numerical analysis were performed. The theoretical analysis was done using lower bound solution of the Coulmb failure criteria, considering it is valid even for non-associated flow rule in upper bound solution. The theoretical solutions were compared with the experimental results which were obtained from the model test at the Cambridge University. While this study is entirely concerned with stress at failure, the theory assumes that the tunnel support can readily adapt itself to the radial deformations of the ground for compliance with the mechanisms of the upper bound solution and the states of stress of the lower bound solution.

5. **Davis et al. (1980)** investigated about the pressure which is necessary to maintain stability of the tunnel heading in cohesive soil. The soil was assumed to be homogeneous with a constant c_u throughout the depth. According to the theory of plasticity, the collapse load for a particular configuration of loading on a perfectly plastic body is unique, i.e. the load carrying capacity of the body cannot be changed by applying the various loads in a different order. The authors derived the expressions for limit theorems of plasticity for different scenarios and applied them. They considered the case of unlined circular tunnel, plain strain in the heading and the case of circular heading. In each of the cases the authors analyzed for upper and lower bound solutions with or without the self-weight of the soil. It is seen that local collapse, blow-out are possible failure scenarios in the theoretical calculations also.

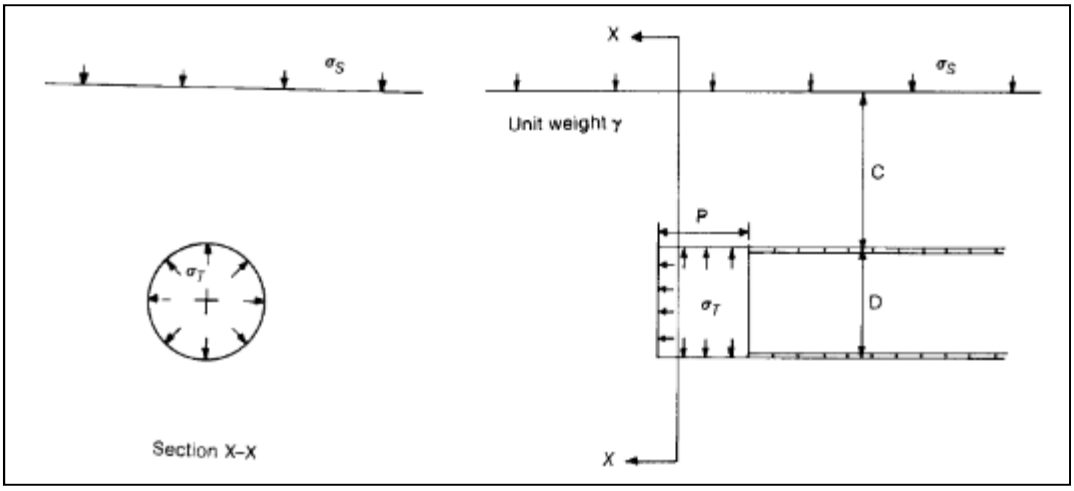

Fig. 2.2: An Idealization of Shield tunnel, (Davis et al., 1980)

It is seen that higher tunnel pressure is required in unlined circular tunnels than in circular tunnels. The authors suggested not use the average pressure as safe one as it violates the theory of plasticity. The experimental evidence currently available indicates that the results presented in this study can be used with confidence for the calculation of the undrained stability of tunnels when C/D < 3 (C being the depth of the crown of the tunnel and D is the diameter of the circular tunnel).

6. **Fritz (1984)** offered a circular hole loaded by an axisymmetric internal and far-field pressure, an analytical solution for the time-dependent stresses and displacements in plane strain. The material is taken to be elasto-viscoplastic with dilatant plastic deformations governing by non-associated flow rule. A modified St. Venant slider that takes into account strain softening is defined by Mohr-Coulomb yield conditions for both the peak and residual strengths. In this way, the pressure necessary to maintain stability of the tunnel heading in cohesive soil is determined.

7. In this study, **Sulem et al. (1987)** considered the face advance effect a time-dependent model for ground-support interaction. A closed form solution is developed for a circular tunnel in a homogeneous and isotropic medium with time-dependent behavior. The "convergence confinement method" is offered as a generalization that takes time effects into account. The illustration of this model for the prediction of the time-dependent behavior of the lining is also presented in the case of an actual tunnel.

8. **Liu et al. (2018)** proposes a new 2D analytical model based on the kinematic approach of

the limit analysis and slip-line theories. This model can be used to assess collapse support pressure corresponding to face stability of circular tunnels in purely cohesive soil. The analytical model takes into account the normalcy conditions, the yield criterion, and the vertical soil arching impact. When analyzing the mechanisms based on the motion of rigid multi-blocks, two upper bound solutions for the ratio of the cover to the diameter (C/D) are obtained. The outcomes from this study are found to be very similar to real-world engineering solutions. This produces smaller failure plane than Davis (1980) because of inclusion of the normality condition. The comparison is reproduced below.

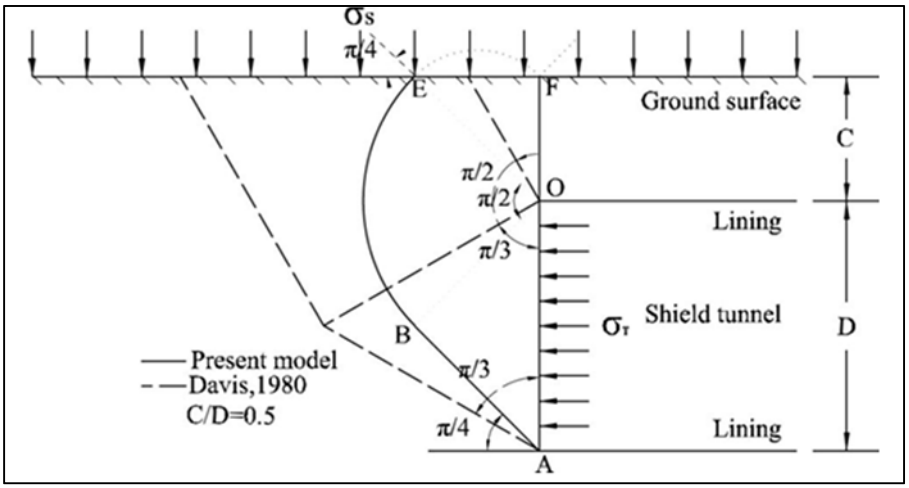

Fig. 2.3: Comparison between the failure zones (Liu et al., 2018)

9. **Wang et al. (2018)** solved A sequence of two types of problems on a simply connected domain, such as a non-circular hole in an infinite plane and a half-plane without holes. Schwartz alternating technique and complex variable theory is used. The solutions from all alternating iterations are finally superimposed to produce convergent and correct analytical solutions. The solutions are found when the stresses / displacements calculated from all iterations are superimposed. With the exception of the horizontal displacement along the line close to the ground surface, the analytical solutions show good agreement with the numerical results. A parametric analysis of the elliptical/square tunnel loaded with infinite surcharges is also carried out. It is found that the concentration factors of shallow tunnels are larger than those of the corresponding deeply buried tunnels with the same shape.

10. **Ma et al. (2022)** proposed an analytical solution is proposed for the plastic zones developed around two circular tunnels of different sizes. The tunnels are considered to be deep and under uniform in-situ stress with unequal size excavated in intact rock. The stress continuity condition

in the along the interfaces in the rock considered to be Mohr-Coulomb medium yields the solution. In accordance, the complex variable approach is then used to calculate the stress field in the elastic zone, whereas the stress field in the plastic zone is statically determined. Following that, a set of nonlinear equations involving the mapping function coefficients is built, which reduces the challenge of identifying elastic-plastic interfaces to the challenge of resolving the mapping function coefficients. The coefficients as design variables in the differential-evolution algorithm is used to solve the nonlinear equations. This solution is also validated using a numerical solution.

2.2. CASE STUDIES & EXPERIMENTAL METHODS

Several literatures study different techniques used by the researchers to observe the practical behavior of tunnels. The results were then compared with numerical and field data in several cases. Some of the prominent and successful experimental literatures are outlined below.

1. **Kimura and Mair (1981)** used centrifuge to determine the relationship of 2-D tunneling idealization and 3-D tunneling. The analysis of a tunnel is more complex when it is near the ground-surface which can be idealized through 3-D analysis. The experiments in soft clay were done on a 4m working radius Cambridge Geotechnical Centrifuge facility. The models were constructed using kaolinite slurry and consolidating to achieve an undrained strength of 26 kPa. The tunnels used were of 60mm diameter and used in 75g and 125g, resulting in stability problem of 4.5m and 7.5m diameter prototype tunnels, respectively. After observing the failure mechanisms, the slope between the points of maximum slope on the surface settlement trough is found (Mair, 1979) to be in line with the field data observed by Peck (1969) and Clough and Schmidt (1977).

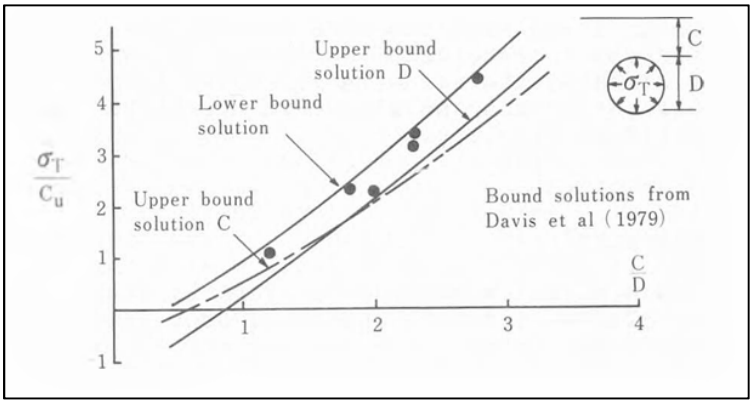

Fig. 2.4: Predicted and observed tunnel support pressures at collapse (Kimura and Mair, 1980)

2. According to the timing of their occurrence in relation to the tunnel construction, the two mechanisms of tunneling-induced ground movements were distinguished by **Rankin (1988)** as follows: (a) short-term settlements brought on by stress relief from the tunnel excavation; and (b) long-term settlements brought on by consolidation effects. The mechanical characteristics of the ground surrounding the tunnel, the building method used, and the level of craftsmanship are just a few of the variables that have an impact on the size and shape of these soil displacements.

3. **Kim et. al. (1996, 1998)** performed physical tests to investigate the effect of lining of the first tunnel on the second tunnel. Seven sets of carefully controlled tests were performed in two main series: (a) parallel tunnels; and (b) perpendicular tunnels. Two different test tanks were developed and used to produce clay samples of Speswhite kaolin.: a plane strain tank for the parallel tunnels; and a cylindrical tank for the perpendicular tunnels. The outcomes of the tests show that the interaction effect is more prominent at the spring and crown of the tunnel.

4. **Caporaletti et. al. (2005)** conducted a number of plane strain centrifuge tests at City university, Londan to model the tunnel excavation at layered ground. The subsoil was considered to be moderately stiff clay overlain by a thick medium dense sand. The tunnel is considered to be excavated below high and thin structures and then analyzed the effect. The ground strains including vertical horizontal shear principle and their directions volumetric and maximum shear strength are also evaluated. It is observed that the soil above the tunnel crown experiences a decrease in the volume whereas soil in other locations within the clay layer shows negative volumetric strains. A dilative behavior was assessed at the bottom of the sand layer, which was attributed by values of lesser volume loss in clay.

5. The sprayed-concrete lined tunnels at Heathrow Express Terminal 4 station were fitted with a wide range of sensors. The study by **Clayton et. al. (2006)** provides data on instrument performance and survivability, as well as an overall assessment of the displacements resulting from tunnel excavation. Data are presented from the in-tunnel displacement monitoring system and for towns above the tunnels. demonstrated that the empirical Gaussian settlement curves for each tunnel (shown in dashed lines) gives a good estimate of the profile resulting from the excavation of both tunnels when they are accumulated together (solid line). This implies that the presence of an existing tunnel does not alter the expected pattern of ground movements into a new tunnel.

6. **Chapman et. al. (2006)** modeled a set of multiple tunnels by building a test tank in 1/50 scale. The experiment was conducted on soft clay and the soil is consolidated from slurry to a soil of specified strength. After consolidation, a surcharge is kept at the soil's surface using a water bag setup in order to create a realistic over-consolidation ratio. Consolidation pressure was applied using loading stages of 4, 12, 25, 50 and 98 kPa respectively. The total time for the consolidation was approximately five weeks. By using an auguring technology and a shield and liner configuration, the tunnels (0.08m in diameter) are built with a predictable "volume loss" throughout construction. The side faces of the tank are made of transparent Perspex, making it possible to see how the soil moves close to these faces. Digital cameras are used to record and analyze the soil displacements.

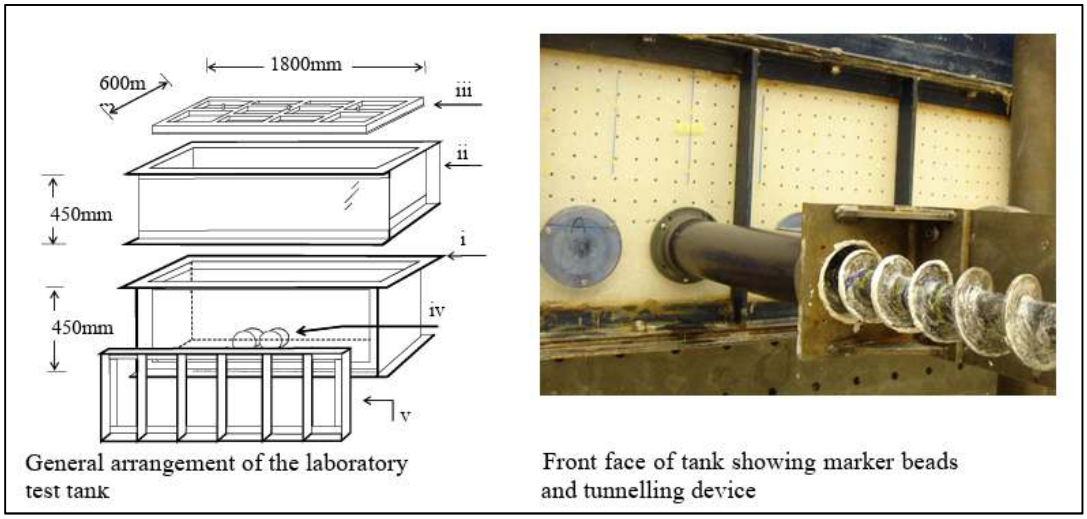

Fig. 2.5: Arrangement and experimental setup (Chapman et. al. 2006)

7. Using case study data and centrifuge modeling, **Farrel (2011)** examined the dynamics involved in soil structure interaction during tunneling beneath buildings. The response of two buildings to the construction of a 12m diameter tunnel with extensive jet grouting in river deposits has allowed to gather field observations of the interaction between soil and structure. In the University of Cambridge, an 8m diameter beam centrifuge has been the subject of centrifuge modeling. Buildings are modeled as microbeams of concrete, masonry, and aluminum on fine, dry sand. The reaction of buildings with a range of stiffnesses is examined by altering the construction materials and shape. The advantages of centrifuge modeling were clear from the observed mechanisms' strong agreement with those found in the case study. These findings show that, in both the vertical and horizontal axes, structures can dramatically alter and lessen the Greenfield ground distortions. An alternative empirical method for

assessing the soil structure interaction is suggested in light of these data. However, settlements beneath stiffness responsive buildings can be bigger than Greenfield values, as evidenced by centrifuge modeling and field data. This results from redistributing the weight of the building and could have an impact on nearby infrastructure.

8. **Marshall et al. (2012)** investigated for the effect of tunnel size, depth and volume loss on greenfield soil displacements above tunnels in sandy ground. The outcomes of many plane-strain centrifuge experiments conducted on tunnels in dry silica sand are examined. The tunnels' cover-to-diameter ratio, or C/D, varied from 1.3 to 4.4. By looking at soil displacement data generated using an image-based deformation measurement technique, characteristics of the surface and subsurface greenfield settlement trough shape are demonstrated. Demonstrations of the impacts of tunnel size, depth, and volume loss are explored, along with the applicability of standard fitting curves. It is found that for practical reasons, volume of soil moving into the tunnel is generally estimated through measurements at soil surface level, neglecting that the soil volume moving into the tunnel may be different from the volume of the settlement trough measured at soil surface. A number of geotechnical centrifuge experiments were carried out to investigate the issue of tunnels in sands. To isolate the influence of geometric and tunneling-related elements on the observed settling trough forms, a single sand was employed and prepared uniformly throughout the testing. Comparing tunnel volume loss to the volume loss that the soil experiences serves as an illustration of the complex volumetric behavior of drained soil. A system of equations is created that offers a way to assess how tunnel size, depth, and volume loss affect the geometry of the settlement trough.

9. **Giardina et al. (2015)** evaluated the interaction between surface surcharge and sand during tunneling by both centrifuge and computational models. In order to demonstrate and validate a two-dimensional finite element model, test results from centrifuge experiments with and without structures are compared. The effect of the weight of the building assuming that for realistic values of weight and ground loss, no gap can develop between the soil and the building was analysed. A sensitivity analysis of the impact of building weight on soil movements and structural deformations is then conducted using the model. The spin-off of the centrifuge ranged from 0 to 75g. The validation results show that in order to accurately represent the soil-structure interaction that was experimentally observed, it is crucial to assume a no-tension contact between the soil and the structure. The parametric analyses demonstrate that the weight of the building affects the relationship between the stiffness of the building and the

deformations brought on by tunneling. The horizontal displacement in the buildings in experiment as well as in the numerical analysis is found to be negligible.

2.3. NUMERICAL METHODS

Numerical analysis may need higher resources and rigorous calculations; however, it provides some useable approach to analyze complex problems. Tunneling involves different stresses behind and ahead of the tunnel faces. Even in plane strain problem, as already discussed above gaussian distribution may not provide correct answers. In problems like this, numerical analysis in form of Finite element (Strength reduction and deformation based) analysis and finite element limit analysis may yield excellent solutions. Some of the landmark research works are discussed in this section below.

1. The use of finite elements and linear programming to compute rigorous lower bounds for soil mechanics problems appears to have been first proposed by **Lysmer (1970)**. He considered only plane strain problem in Mohr-Coulomb soil medium. This formulation employed 3-noded triangular elements to model the stress field with stresses varying linearly within each element and illustrated the advantages of computing lower bounds numerically. The Method of Linear Programming is used to isolate an optimal statically admissible stress field corresponding to a lower bound solution.

2. A tunnel's failure or collapse can be classified as either active or passive. These two types were analyzed by **Assadi and Sloan (1991)** in their study of stability of a square tunnel. They defined active collapse as "collapse of the tunnel is triggered by application of the surcharge and self-weight, with the internal tunnel pressure providing resistance against failure". Additionally, according to these writers, passive collapse (also known as "blow out") occurs when the roles of internal pressure and external pressure are reversed. As a result, passive collapse is produced by internal pressure while external pressure and self-weight offer resistance. The most common use of active collapse, which involves subsidence of the ground surface after collapse, is tunneling. In this study, the loading was applied to the tunnel by an internal pressure, a surcharge and self-weight. The bound solutions from this finite element limit analysis generally bracket the exact stability number for the variety of shallow-tunnel geometries addressed in this study to within 15% or better. In situations where the stability number approaches 0, the gap between the boundaries may rise above 15%.

3. **Sloan and Assadi (1991)** studied the same scenario again but when the soil has strength increasing linearly depth. Tight bounds on exact collapse pressures have been determined by the use of two numerical approaches that combine the classical limit theorems with finite elements. The offered solutions are completely rigorous since they adhere to all of the requirements of the static and kinematic theorems.

4. A new method for computing rigorous upper bounds on the limit loads for one to three dimensional continua are described by **Lyamin and Sloan (2002)** described. The formulation used linear finite elements as its foundation, permitted kinematically admissible velocity discontinuities at all interelement boundaries. A kinematically admissible velocity field is considered solving a non-linear programming problem. The study demonstrated the method's applicability to a variety of plasticity issues, including those involving inhomogeneous materials, difficult loading, and intricate geometry. In the final optimization, the power dissipated by plastic deformation in the continuum and lost through plastic slide across velocity discontinuities are both represented by the objective function. The accuracy and effectiveness of the strategy were also shown by comparison with other approaches that were already in use.

5. **Osman et al. (2006)** developed upper bound calculations of collapse loads in tunnels using distributed shear deformation mechanism. Within the boundaries of this deformation mechanism, the soil was found to be deforming compatibly following a Gaussian distribution. Outside this mechanism the soil was assumed to be rigid. This mechanism does not incorporate slip surfaces and displacement discontinuities. This mechanism is observed to be consistent with the centrifuge data reported by Mair (1979).

6. **Lee et. al. (2006)** investigated the surface settlement troughs, excess pore water pressure generation, tunnel stability and arching effects that develop during tunneling in soft clayey soil. Both centrifuge and numerical modeling are used to simulate the tunneling process and to compare the results. The centrifuge modeling can measure the tunnel deformation, surface settlement, and pore water pressure, while the numerical modeling can estimate the stress distribution and the arching ratio in the soil mass around the tunnel. It is observed that the centrifuge and numerical modeling provide consistent results of the tunnel stability, surface settlement, and pore water pressure. The concept of arching ratio is introduced to quantify the arching effects on the soil mass surrounding tunnels and the boundaries of the arching zones

are determined for both single and parallel tunneling. The tunnel stability is found to be improving with increasing cover-to-diameter ratio and decreasing with increasing center-to-center distance for parallel tunnels. The arching effect is discovered to be more significant for shallower tunneling and that the arching zones can be divided into positive and negative zones depending on the stress transfer mechanism.

7. **Meguid and Rowe (2006)** considered the near-face stability of D-shaped tunnels excavated in a Mohr–Coulomb material subjected to anisotropic in situ stress conditions in their study. The analysis of the construction of the intake tunnel of the Darlington Nuclear Generating Station using three-dimensional elasto-plastic finite element analysis are done in this study. The quantification of the effect of rock mass strength reduction on the tunnel deformation, face stability, and distribution of stresses at the tunnel circumference is investigated for different in situ stress conditions are done. The induced displacement and stresses around the tunnel opening as the face advances are also compared to the field measurements.

The strength reduction is established by reducing the cohesion and tangent of the friction angle in the same proportion. A design line was suggested to limit the induced strains to within tolerable limits. The suggested design line in this study is based on an additional 50% of the elastic strain.

8. The solutions to the issue of twin tunnel excavation stability in soft ground are presented by **Osman (2010)** offers. Because of undrained condition direct used superimpose approach is considered. This way, the behavior of each tunnel is determined separately and then the total displacement and other parameters are accumulated. It is common practice when dealing with multiple tunnels to superimpose the independent settlement profiles predicted for each tunnel independently to obtain the final accumulated settlement. To idealize the ground deformations surrounding shallow, unlined twin tunnels buried inside an undrained clay layer, a suitable displacement field has been developed. Upper limits on the loads needed to prevent the collapse are calculated and presented as dimensionless stability graphs that take into account the shear strength's fluctuation with depth, the embedded depth of tunnels, and the distance between tunnels. The spacing between tunnels is found to be have a significant influence on their stability. The interaction between tunnels reduces the stability number N_c by up to 35% in shallower tunnels (Crown distance to Dia. = 1) and by up to 22% in deeper tunnels (Crown to Dia. ≥ 3).

9. **Wilson et al. (2011)** investigated the undrained stability of a plane strain circular tunnel in clay, where the shear strength profile is assumed to increase linearly with depth. Stability solutions for a variety of geometries and soil conditions are found using rigid-block upper bound methods as well as finite element limit analysis (which gives both upper and lower bounds). The tunnel considered is shown below, the stability analysis proceeds by fixing values of H/D, $\gamma D/c_{u0}$, and $\rho D/c_{u0}$, with $D = c_{u0} = 1$ and $\sigma_s = 0$. This reduces the number of variables in the parametric study to the tunnel depth (H), the soil unit weight (g), and the rate of strength increase with depth (r).

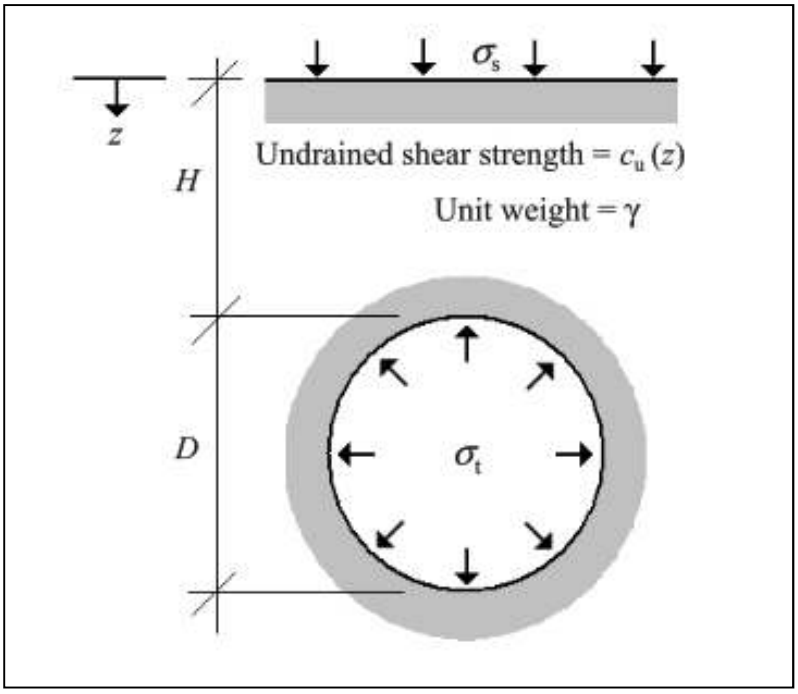

Fig. 2.6: Plane strain circular tunnel in a heterogeneous Tresca material (Wilson et al., 2011)

A parametric equation has been developed to describe the undrained stability of a circular tunnel in terms of the three dimensionless variables.

$$N = N_0 + \left(\frac{\gamma D}{c_{u0}}\right) N_\gamma \text{.....(1.1)}$$

where N_0 is the stability number for the weightless case (i.e., $\gamma D/c_{u0} = 0$), N_γ is a factor accounting for the weight of the soil, and both these factors are nonlinear functions of the parameters H/D and $\rho D/c_{u0}$. Fitting a curve to all finite element results for the weightless cases give another equation which is then presented in a convenient series of graphs.

10. The stability of circular tunnels in cohesive-frictional soils subjected to surcharge loading

has been investigated theoretically and numerically assuming plane strain conditions by **Yamamoto et al. (2011a)**. The ground is modeled as a uniform Mohr–Coulomb material with a cohesion c', friction angle, Φ' and unit weight c, assuming drained loading conditions. Semi-analytical rigid-block methods were used to find upper-bound solutions for the cases considered. With an associated flow rule, it is assumed that the dilatancy angle is equal to the friction angle. The soil mass is assumed to be governed by the Mohr–Coulomb failure criterion and an associated flow rule, with the geometry of the blocks being allowed to vary while being constrained such that their areas and boundary segment lengths remain non-negative. An empirical equation for estimating the ultimate surcharge load that can be applied to the surface of a cohesive-frictional soil above a shallow circular tunnel has been proposed. This equation is based on average values of the lower- and upper-bound solutions from finite element limit analysis and predicts these values to within 5%.

11. The stability of a plane strain square tunnel, in a cohesive–frictional soil subjected to surcharge loading was also investigated analytically and numerically by **Yamamoto et al. (2011b).** The results of these analyses were presented in the form of dimensionless stability charts. The lower and upper bounds obtained using numerical limit analysis bracket the actual ultimate surcharge load to within ±10% or better for the range of moderate tunnel depths and soil friction angles.

12. **Yamamoto et. al. (2013)** studied the stability of dual circular tunnels in cohesive-frictional soils under surcharge loading using both theoretical and numerical methods. The finite element limit analysis techniques is employed to obtain rigorous lower and upper-bound solutions for the ultimate surcharge loading. This study also compared the solutions with upper-bound rigid-block mechanisms to check the accuracy of the results. The ground is modeled as a uniform Mohr–Coulomb material with cohesion, friction angle and unit weight. A range of values of different dimensionless parameters were considered for the study. The effects of interaction between dual tunnels and the location of the critical tunnel spacing where interaction no longer occurs were also discussed. The three rigid-block mechanisms to obtain upper-bound solutions for the ultimate surcharge loading is also used to compare the results with that from finite element limit analysis to check the accuracy and efficiency of the mechanisms.

13. The stability of two long, horizontally aligned, circular, unsupported tunnels in cohesive and cohesive-frictional soils was assessed by **Sahoo and Kumar (2013)**. The finite element

limit analysis was performed using linear programming in an upper bound limit. The tunnel stability was described in the study using a non-dimensional stability number that depended on the tunnel cover, soil cohesion, unit weight of soil mass, diameter of each tunnel, internal friction angle of soil, and the rate at which the cohesion improved linearly with depth. On account of the symmetry about the vertical plane, passing through the centre line between the two tunnels, only one half of the total domain was considered for the analysis. The chosen problem domain was discretized into a variety of triangular elements with three nodes. The size of the elements gradually decreases near tunnel's edge. Each node continues to be exclusive to one element, and the line of velocity discontinuity is always the interface between any two adjacent elements. It is found that as tunnel cover rose, soil friction angle and cohesion gradient decreased, and the optimal tunnel distance required to entirely eliminate the interference effect increased. The study confirmed the results of previously employed remedies.

14. The stability of dual square tunnels in cohesive-frictional soils under surcharge loading is investigated by **Yamamoto (2014)** using theoretical and numerical methods. The potential impacts of interaction between dual tunnels are also explored using finite element limit analysis techniques to obtain rigorous lower and upper-bound solutions for the ultimate surcharge loading. The solutions found with upper-bound rigid-block mechanisms are compared to check the accuracy of the results.

15. **Wilson et. al. (2014)** discussed the stability of twin circular tunnels placed parallelly side by side. The finite-element limit analysis and semi-analytical rigid block techniques are used to obtain bounds on the stability of the tunnels for a range of geometries in a Tresca soil. These techniques use linear finite elements to model the stress or velocity fields and collapsed solid elements at all interelement boundaries to simulate stress or velocity discontinuities. The upper bound estimates of the stability of the dual tunnels are also presented using two rigid block mechanisms that can reduce to a simpler trap door mechanism if required. These mechanisms are optimized using a constructed hodograph and the Hook-Jeeves optimization algorithm. The rigid block upper bounds give a close approximation to the finite-element solutions, especially for small tunnel spacings. It is seen that, as the tunnel depth increases, the stability number decreases rapidly for small tunnel spacings, but remains almost constant for large tunnel spacings. This is because, for deep tunnels, the soil weight dominates the collapse mechanism, whereas, for shallow tunnels, the surcharge pressure and the tunnel support have more

influence on the stability. For very deep tunnels, the stability number is found to be approaching zero, which means that no tunnel support is required to prevent collapse.

16. **Wilson et. al. (2015)** further expanded their work on two square tunnels built side by side in an undrained clay soil. Two methods to analyze the stability are assessed: finite element limit analysis and rigid block upper bound methods. Different factors that affect the stability, such as the depth of the tunnels, the weight of the soil, and the distance between the tunnels are also taken into account. It is observed that the stability of the tunnels does not always increase as they move further apart. For some cases, the stability actually decreases as the distance between the tunnels increases. The failure modes of the tunnels depend on the depth, weight, and distance factors. For shallow tunnels, the failure is mainly in the roof and pillar. For deeper tunnels, the failure also involves the outer walls and floor of the tunnels. The finite element limit analysis and rigid block methods give close estimates of the stability. The finite element method gives both upper and lower bounds on the stability, which bracket the true solution to be found within 5% range, whereas the rigid block method gives only upper bounds, which are close to the finite element upper bounds.

17. **Zhang et al (2016)** studied the stability of dual unlined elliptical tunnels in cohesive-frictional soils using upper-bound finite element methods with rigid translatory moving elements (UBFEM-RTME). The authors obtained the results in terms of dimensionless stability numbers, which increase with / and decrease with increasing B/D (dimensionless width), C/D (dimensionless depth) & dimensionless center-to-center distance S/D and collapse mechanisms, which mainly include two wedge-shaped zones and a complete non-plastic wedge. No pressure is applied at the tunnel boundary or along the ground surface. The collapse mechanisms are mostly constituted by two wedge-shaped zones around the tunnel and a complete non-plastic wedge located close to the ground surface. For cases with $S/D < S_c/D$, the tunnel span has no significant influence on the maximum horizontal portion (R) of the collapse mechanism. When $S/D < S_c/D$, the interaction between the two elliptical tunnels tends to disappear, and the value of R/B clearly decreases, especially for $\Phi = 10°$.

18. **Zhang et al. (2018)** considered dual unlined horseshoe-shaped tunnels using the upper-bound finite element method (UBFEM) to investigate the stability of dual horseshoe-shaped tunnels. A system of higher-order triangle elements (six-nodal triangle elements) in

combination with a plastic-dissipation-based mesh adaptive strategy are used to improve the accuracy of computations with plain strain problem description. The quantitative results of this study confirm that horseshoe-shaped tunnels utilize underground space more efficiently than circular tunnels and minimize the volume of soil excavated and they provide better stability than rectangular tunnels due to their soil-arching effects.

19. **Shiau and Al-Asadi (2020)** studied on the 3D heading stability of parallel twin circular tunnels in cohesive undrained soil. The analysis was done using finite element limit analysis in OptumCE on elastic-perfectly plastic Tresca material. Solutions for rigorous upper bound and lower bound critical stability numbers for collapse and blow-out were obtained. The stability was described by Broms and Bennermarks' dimensionless undrained stability number. In the UB and LB simulations, an adaptive mesh refinement was used. The interaction effects of the distance between the tunnels on the stability for a series of tunnel cover-to diameter ratios are assessed in this study. In absence of other 3-D analysis of twin tunnels, the results of this study are validated with that of available 2-D analysis. It is observed that the 3D stability results are approximately 2.5 times higher than those in the 2D analysis, in general. This 3-D analysis is found to be providing more realistic data over the conservative two-dimensional analysis.

20. **Li et al. (2021)** solved the issue of calculation accuracy by using equivalent area method, a non-circular tunnel is studied by the author to assess its face stability by kinematical approach where the discretization-based failure mechanism is used to describe the face failure. In the laboratory tests, it is also found that the soil strength in tensile regime is significantly reduced which is much smaller than the one described by the classical Mohr-Coulomb yield criterion. For this purpose, the tensile strength cut-off is introduced to define a linearly varying soil dilatancy angle with the rotation angle when the tensile stress can be expected in soils. The proposed approach is compared with the existing methods in literature and the finite difference method of FLAC3D which proves that the proposed approach has sufficient accuracy and great efficiency. Finally, an engineering example of a tunnel in Hunan Province, China is studied using the proposed approach and some suggestions are given for practical tunnel excavations.

21. **Keawsawasvong and Ukritchon (2022)** in their study assessed the safety of tunnel stability in unlined circular tunnels in anisotropic and non-homogeneous clays. The lower-bound approach along with finite element analysis and second-order cone programming are

utilized to examine the effects of undrained strength anisotropy and strength non-homogeneity on tunnel stability. The anisotropic shear strength of the clay was modeled using an elliptical yield function. The proposed new stability equation for unlined circular tunnels in anisotropic and non-homogeneous clays, includes four new stability factors: constant undrained strength (s_{UPSC0}), linearly increasing strength gradient (ρ), undrained strength anisotropy (r_e) and soil unit weight (γ). There are power functions used in N_c, N_ρ, N_{a1} and N_{a2}, whereas a linear function for N_c. the factor of safety can be given as

$$FS = \frac{s_{uPSC0} N_c N_{a1} + \rho D N_\rho N_{a2}}{\sigma_s + \gamma D N_\gamma - \sigma_t} \quad \text{.....(1.2)}$$

This equation provides a fast and accurate tool for predicting the undrained stability of circular tunnels in practice.

22. In this study, **Nguyen and Nguyen-Son (2022)** presented a cell-based smoothed finite element method (CS-FEM) to assess the static and seismic stability of a single square tunnel. The subsoil is considered to be governed by Mohr-Coulomb Model whose shear strength varies linearly with depth. By using uniform quadrilateral elements and the CS-FEM technique to approximate the kinematically admissible displacement fields, volumetric locking problems and the singularity associated with the Mohr-Coulomb model are eliminated. Different stability charts and tables are developed for practical use in the tunnel design, along with a newly proposed formulation for predicting the undrained stability. Moreover, a seismic stability number using the same numerical approach is presented. Considering only half of the tunnel new upper bound solutions are obtained on the undrained stability.

CHAPTER – 3: NUMERICAL MODELING

3.1. INTRODUCTION:

The genuine collapse load is bracketed by the lower and upper bound limit theorems, which form the foundation of the limit analysis. The upper bound theorem and lower bound theorem determine the top and lower limits of the collapse load, respectively. Since the limit loads are conservatively estimated by the lower bound theorem, the appropriate solution is always safe from a design perspective. The obtained answer becomes closer to the actual solution for a particular problem when the difference between the two bounds of the solution becomes small.

To arrive at a solution using the limit analysis, the following presumptions should be required:

1. It must be a pure plastic material. Soil tends to either soften or harden under force. The stress-strain curve's softening or hardening portions should be ignored to use limit theorems, and they should be roughly represented by the average strength to enable continuous plastic flow at a constant stress level.
2. To satisfy Drucker's stability postulate, the yield surface must be convex.
3. For the theory of virtual work to continue to hold, the material shouldn't experience significant deformation.

3.2. LOWER BOUND THEOREM:

The lower bound theorem **(Drucker et al. 1951)** is stated as: "If there is any stress field (σ_{ij}^{s}) which satisfies equilibrium equations, balances the tractions T_i along the traction boundary ∂R and nowhere violates the yield condition f(σ_{ij}^{s}) $\leq$ 0, then the traction T_i together with the body forces F_i will not be greater than the true collapse loads caused by the actual traction and body forces."

3.3. UPPER BOUND THEOREM:

The upper bound theorem (Drucker et al. 1951) is stated as: "If there is any compatible plastic deformation field comprised of the velocity field (v_i^k) and strain-rate field (ε_i^k) which satisfies the velocity boundary condition $v_i^p = 0$ = along the boundary ∂R and the normality condition $\varepsilon_{ij}^k = \lambda \frac{\partial f}{\partial \sigma_{ij}}$, then the tractions T_i and the body force F_i determined by equating the rate of

external work done to the rate of dissipation of internal energy will not be lesser than the true collapse loads comprised of tractions T_i^c and body forces F_i^c.

When the lower bound theorem is used with a flow rule material's failure load is always safely estimated from a design and stability perspective; the computed collapse load always decreases by an amount that is less than or equal to the exact collapse load.

3.4. LOWER BOUND FINITE ELEMENT LIMIT ANALYSIS FORMULATION WITH LINEAR PROGRAMMING FOR A PLANAR PROBLEM:

In this study, we used the lower bound only to simulate the statically acceptable stress field for a variety of planar stability problems with complex geometry, challenging loading, and nonhomogeneous soil mass. One of the best techniques for performing the numerical analysis using the lower bound limit analysis and optimization is the finite element method. The following is a broad description of the optimization problem that can be solved by combining linear programming and the lower bound finite element method:

$$\text{Minimize } P_u(\sigma) = 0 \quad \ldots\ldots\ldots\ldots\ldots\ldots (3.1a)$$

Subjected to: $A_i(\sigma) = 0$; $i = 1, \ldots, m$ ……..(3.1b)

$B_j(\sigma) = 0$; $j = 1, \ldots, k$ ……(3.1c)

where the basic unknown variable is a non-dimensional stress vector (σ) and P_u is the collapse load (objective function). For a linear programming problem P_u, A_i, and B_j become linear functions of the basic unknown variables (σ).

3.4.1. LINEAR FINITE ELEMENT:

The entire stress field is split using linear elements as illustrated in Fig. 3.1(a) as the initial step in carrying out the lower bound finite element limit analysis. A three-noded triangular element is the simplest version of a two-dimensional linear element. The shape functions that are utilized (i) to map the domain geometry and (ii) to define the variation of stresses are maintained the same in the isoparametric three-noded triangular elements. Within a three-noded triangular linear element, stresses for two-dimensional planar issues fluctuate linearly.

The following are some benefits of using a linear element to simulate the stress field:

- Constraints on linear equality are defined by linear finite elements.
- Using linear elements makes it simpler to create the statically permissible stress discontinuities along the interfaces of adjacent elements.
- Any internal point of a linear element will automatically satisfy the corresponding yield condition if the yield condition is met at all of the nodes of the element. Since the yield criteria are used, the use of linear elements lowers the overall amount of inequality constraints.

Statically permissible stress discontinuities are allowed along the interfaces of several nearby elements, unlike the standard displacement-based finite element method, in the lower bound finite element limit analysis. In the lower bound finite element limit analysis, several nodes might have the same coordinates while maintaining their individuality for each element. Three fundamental unknown stresses- σ_x, σ_y and τ_{xy} are linked to each node.

Following are some examples of the linear changes in stresses across the element:

$$\sigma_x = \sum_{i=1}^{3} N_i \sigma_{x,i} \quad \text{..... (3.2a)}$$

$$\sigma_y = \sum_{i=1}^{3} N_i \sigma_{y,i} \quad \text{..... (3.2b)}$$

$$\tau_{xy} = \sum_{i=1}^{3} N_i \tau_{xy,i} \quad \text{..... (3.2c)}$$

where, N_i is the shape function and, $\sigma_{x,i}$, $\sigma_{y,i}$ and $\tau_{xy,i}$ are the stresses at the i^{th} node. The shape function for the i^{th} node is defined by the following expression:

$$N_i = \frac{1}{2|A|}(\xi_i + \eta_i X + \xi_i X) \quad \text{.....(3.3)}$$

Where , $A = \det \begin{bmatrix} 1 & X_1 & Y_1 \\ 1 & X_2 & Y_2 \\ 1 & X_3 & Y_3 \end{bmatrix}$; $\xi_i = A_{jk}$; $\eta_i = y_j - y_k$; $\xi_i = X_k - X_j$;

$A_{jk}$is the area covered by the corners j and k of a triangular element and the origin of the Cartesian coordinate system (x-y); where, i, j, and k are the three nodes of a triangular element numbered in a counter-clockwise direction.

3.4.2. ELEMENT EQUILIBRIUM:

The equilibrium conditions are given below-

$$\frac{\partial \sigma_x}{\partial x} + \frac{\partial \tau_{xy}}{\partial y} = b_x \quad \text{.....(3.4a)}$$

$$\frac{\partial \tau_{xy}}{\partial x} + \frac{\partial \sigma_y}{\partial y} = b_y \quad \text{.....(3.4b)}$$

where b_x and b_y are the required body forces for the material's specific volume. Keep in mind that tensile stresses are regarded as positive, and the Fig. 3.1(b). illustrates the positive σ_x, σ_y, and τ_{xy} directions. When Equation (3.2) is substituted into Eq. (3.4), it is evident that-

$$\sum_{i=1}^{3} \frac{\partial N_i}{\partial x} \sigma_{X,i} + \sum_{i=1}^{3} \frac{\partial N_i}{\partial y} \tau_{XY,i} = b_X \quad \text{.....(3.5a)}$$

$$\sum_{i=1}^{3} \frac{\partial N_i}{\partial x} \tau_{XY,i} + \sum_{i=1}^{3} \frac{\partial N_i}{\partial y} \sigma_{y,i} = b_Y \quad \text{.....(3.5b)}$$

We can rewrite these two equations in the below matrix form:

$$[\mathbf{A^e_{eq}}]_{2x9} \{\boldsymbol{\sigma^e}\}_{9x1} = \{\mathbf{b^e_{eq}}\}_{2x1} \quad \text{.....(3.6)}$$

The basic unknowns for each element are thus determined by the fulfillment of equilibrium requirements, which yields two linear equality constraints involving nine nodal stresses. The i subscript denotes the i^{th} node.

3.4.3. DISCONTINUITY EQUILIBRIUM:

As previously established, a jump in the state of stress is permitted along any interface shared by two neighboring elements in the lower bound finite element limit analysis. However, this increase in stress must be statistically acceptable. This is done by keeping the normal and shear loads constant throughout adjacent interface elements. The equality of the normal and shear stresses at each pair of adjacent nodes will therefore naturally ensure the necessary condition of a statically permissible stress discontinuity because stresses change linearly throughout each element. The concept of statically permissible stress discontinuity is shown in Fig. 3.1(c) and (d).

A common edge EE′ connects two nearby elements e_1 and e_2 in the Fig. 3.1.(c). Nodes 2 and 4 of the element e_2 and nodes 1 and 3 of the element e_1 comprise the edge EE'. Note that nodes 1 and 2 and nodes 3 and 4 are two pairs of nearby nodes that share the same coordinates. The edge EE′ makes an angle of β_d with the positive x-axis. At the above mentioned two pairs of adjacent nodes, the following needs to be fulfilled to meet the statically permissible stress field:

$$\sigma_{n,1} = \sigma_{n,2} \quad \text{.....(3.7a)}$$

$$\tau_{nt,1} = \tau_{nt,2} \quad \text{.....(3.7b)}$$

$$\sigma_{n,3} = \sigma_{n,4} \quad \text{.....(3.7c)}$$

$$\tau_{nt,3} = \tau_{nt,4} \quad \text{.....(3.7d)}$$

As shown in the above figure, the normal (σ_n) and shear (τ_{nt}) forces operating along a plane inclined by an angle β can be expressed as follows:

$$\begin{Bmatrix} \sigma_n \\ \tau_{nt} \end{Bmatrix} = \begin{bmatrix} sin^2\beta & cos^2\beta & -sin2\beta \\ -\frac{1}{2}sin2\beta & \frac{1}{2}sin2\beta & cos2\beta \end{bmatrix} \begin{Bmatrix} \sigma_x \\ \sigma_y \\ \tau_{xy} \end{Bmatrix} \quad \text{.....(3.8)}$$

The following relations are provided by Equations (3.7) and (3.8) and are expressed as matrices:

$$\left[A_{eq}^{dc}\right]_{4x12} \{\sigma^{dc}\}_{12x1} = \{b_{eq}^{dc}\}_{4x1} \quad \text{.....(3.9)}$$

The discontinuity equilibrium condition, therefore, imposes four linear equality requirements on the nodal stresses of the two pairs of adjacent nodes in terms of 12 unknown fundamental factors along the interface shared by two adjacent elements.

3.4.4. STRESS BOUNDARY CONDITION:

By connecting nodes 1 and 2 as illustrated in Fig. 3.1.(e), the stress boundary conditions along any boundary edge can be represented as follows:

$$\sigma_{n,1} = q_1; \qquad \tau_{nt,1} = t_1 \text{.....(3.10a)}$$

$$\sigma_{n,2} = q_2; \qquad \tau_{nt,2} = t_2 \text{.....(3.10b)}$$

In this instance, the boundary edge is at an angle α with the positive x-axis of the x-y Cartesian coordinate system. The stresses –

i $\sigma_{n,i}$ and $\tau_{nt,i}$ refer to normal and shear stresses at the ith node;

ii The known normal stresses q_1 and q_2, which are connected to nodes 1 and 2, along the boundary edge 1-2, respectively;

iii The boundary edge 1-2's known shear stresses, t1, and t2, are connected to nodes 1 and 2, respectively.

Concerning the Cartesian coordinate system x-y, the stress boundary conditions along any edge can be rewritten using the matrix notation shown below:

$$\left[A_{eq}^{bound}\right]_{4x6} \{\sigma^{bound}\}_{6x1} = \{b_{eq}^{bound}\}_{4x1} \quad \text{.....(3.11)}$$

Four linear equality constraints are constructed at each boundary edge in terms of six unknown nodal stresses, each of which is subject to a different set of boundary conditions.

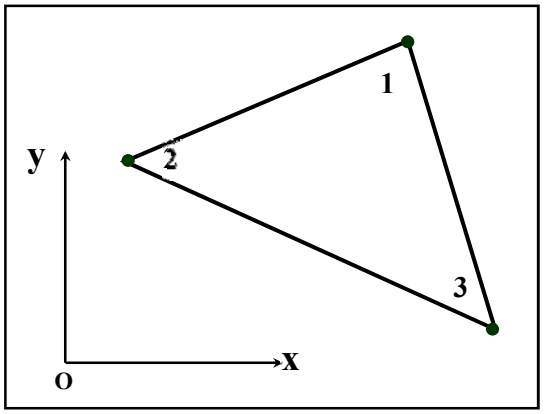

(a)

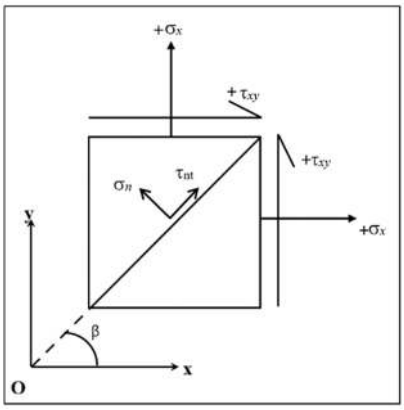

(b)

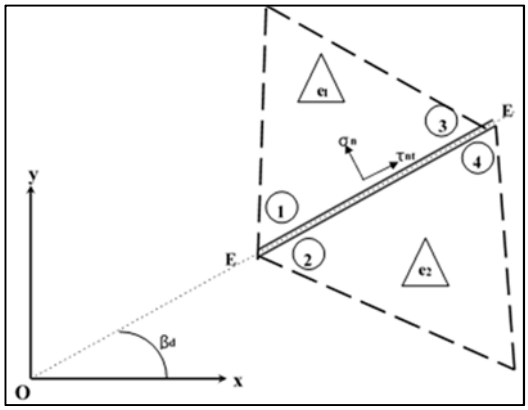

(c)

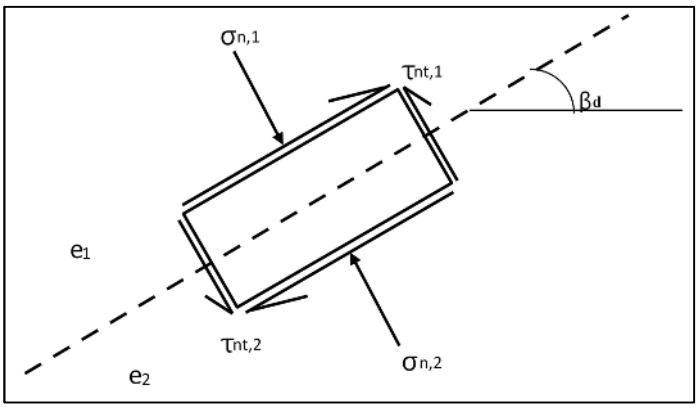

(d)

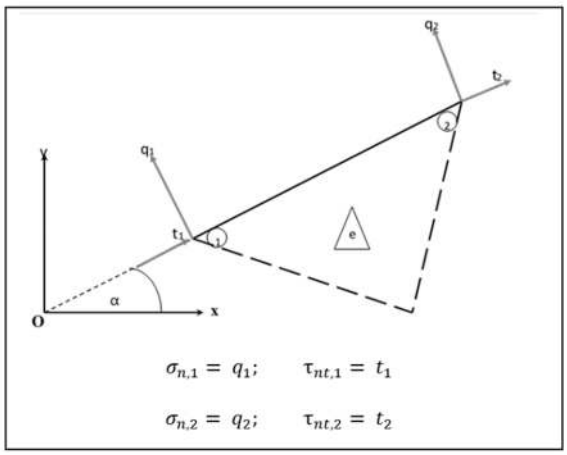

(e)

Figure 3.1.: (a) A typical triangular linear finite element in a two dimension, (b) Positive sign conventions for stresses, (c) Statically admissible stress discontinuity along any edge shared by two adjacent elements, (d) Close view of stresses around corner E, (e) Stress boundary condition along any edge

3.4.5. ASSEMBLING OF CONSTRAINTS AND OPTIMIZATION:

Putting together all local equality and inequality constraint matrices and determining the local objective function formulations are the next stage in the lower bound finite element limit analysis. The objective of the assembly process is to create the global vector related to the objective function and the global constraint matrices.

The following expressions can be used to provide the global equality constraints:

$$[A_1]\{\sigma\} = [b_1] \quad \text{.....(3.12)}$$

Where,

$$[A_1]=\sum_{e=1}^{E}\left[\mathrm{A}_{\mathrm{eq}}^{\mathrm{e}}\right]+\sum_{dc=1}^{D_c}\left[\mathrm{A}_{\mathrm{eq}}^{\mathrm{dc}}\right]+\sum_{bound=1}^{N_b}\left[\mathrm{A}_{\mathrm{eq}}^{\mathrm{bound}}\right];$$

$$[b_1]=\sum_{e=1}^{E}\left[\mathrm{b}_{\mathrm{eq}}^{\mathrm{e}}\right]+\sum_{dc=1}^{D_c}\left[\mathrm{b}_{\mathrm{eq}}^{\mathrm{dc}}\right]+\sum_{bound=1}^{N_f}\left[\mathrm{b}_{\mathrm{eq}}^{\mathrm{bound}}\right]$$

And $\{\sigma\}=\{\sigma_{x,1}\ \sigma_{y,1}\ \tau_{xy,1}\ \sigma_{x,2}\ \sigma_{y,2}\ \tau_{xy,2} \dots\dots\dots \sigma_{x,N}\ \sigma_{y,1}\ \sigma_{xy,N}\}^T$;

Similarly, the matrix notation used to represent the global inequality restrictions is as follows:

$$[A_2]\{\sigma\} \leq \{b_2\} \quad \text{.....(3.13)}$$

Where:

$$[A_2]=\sum_{i=1}^{N}\left[\mathrm{A}_{\mathrm{yield}}^{\mathrm{i}}\right]+\sum_{in=1}^{N_i}\left[\mathrm{A}_{\mathrm{int}}^{\mathrm{in}}\right]$$

$$[b_2]=\sum_{i=1}^{N}\left[\mathrm{b}_{\mathrm{yield}}^{\mathrm{i}}\right]+\sum_{in=1}^{N_i}\left[\mathrm{b}_{\mathrm{int}}^{\mathrm{in}}\right]$$

$\{\sigma\}=\{\sigma_{x,1}\ \sigma_{y,1}\ \tau_{xy,1}\ \sigma_{x,2}\ \sigma_{y,2}\ \tau_{xy,2} \dots\dots\dots \sigma_{x,N}\ \sigma_{y,1}\ \sigma_{xy,N}\}^T$

where (i) N, E, and D_c represent the total number of nodes, elements, and discontinuities, respectively; (ii) N_b indicates how many nodes are located along the boundary where the stresses are determined; and (iii) N_f indicates how many nodes are located at the soil-structure interface.

3.4.6. MODELLING IN OPTUMG2 SOFTWARE:

Optum G2 is a finite element limit analysis software program designed to solve geotechnical problems. The program contains a myriad of features for solving simple problems right through to complex multi-staged projects. Upon opening the program, the user will be greeted with a screen. The pop-up in the foreground contains the option to start a new project, load an existing one, access the user manual, watch a number of instructional videos or run a variety of pre-

programmed examples. The design grid is in the background with the stage, properties, project, and customization manager to the right, with the taskbar containing the four functional tabs; geometry, materials, features, and results, above.

The first step is to model the geometry of the problem. The geometry tab contains a number of options such as; point, line, arc, circle, and rectangle to create the 2D model. All points are assigned their own number and coordinates and can be manually inputted or snapped to pre-existing nodes. Familiar tools; copy, paste, move, scale, rotate, delete, undo and redo are used to finish the model geometry and make any necessary changes. Buttons on the design grid give the user the ability to select, zoom in and out, zoom to selection, pan and turn the gridlines on and off.

Once the model geometry has been established, the materials can be chosen. The program comes with a broad range of pre-programmed materials but it is also possible to input a new material. There are eight different categories of materials available; solids, fluids, plates, connectors, geogrids, hinges, pile rows, and nail rows. The solid category is used to represent materials such as soil, concrete, and rock. A number of soil modelling options are available including Mohr-Coulomb (MC) and Tresca. MC materials assume linear elasticity and exhibit a yield function dependent on the cohesive strength (c) and angle of friction of the soil (φ). There is a wide variety of predefined Mohr-Coulomb materials including; soft clay, firm clay, stiff clay, loose sand, medium sand, and dense sand. Tresca materials are dependent only on undrained shear strength (S_u). Once the desired material type has been chosen, a number of properties related to that material can be manually varied in the "Properties" bar that appears on the right-hand side of the screen. For a Mohr-Coulomb material, these variable properties include; drainage, stiffness, strength, flow rule, tension cut-off, compression cap, fissures, unit weight, initial conditions, and hydraulic model. For a Tresca material these variable properties are limited to; stiffness, strength, tension cut-off, unit weight, initial conditions and hydraulic conductivity.

The features tab allows the user to set: flow BC, consolidation BC, boundaries, fixed loads, multiplier loads, anchors and connectors, soil support, mesh size, and the focus section. It is necessary to set boundary conditions to prevent the model from moving in the 'x' or 'y' directions. A 'full' support prevents the model from moving in all directions, while 'normal' support only prevents movement in the parallel direction and 'tangential' support only prevents movement in the perpendicular direction. A fixed load is applied to represent constant loads

such as a surcharge on the soil or permanent internal tunnel support. A multiplier load is applied with a unit load to allow the solver to amplify the load until a state of failure is reached, this feature can be used to find the limiting load on a soil structure. A water table or fixed pressure can be easily added at this stage along with any soil supports such as anchors, geogrids, piles, and soil nails.

The stage manager can be selected from the tabs towards the bottom right of the screen. It is here that the analysis is set up and a multi-staged project can be created. The drop-down box titled 'analysis' is used to select the type of analysis to be performed, options include; limit analysis, strength reduction, mesh, seepage, initial stress, elastic, elastoplastic, and multiplier elastoplastic and consolidation. This research focuses on using only the limit analysis and strength reduction options. Selecting limit analysis allows the user to choose either gravity or load multiplier while selecting strength reduction allows the user to choose whether the strength of the solids or structures will be reduced. Both methods require that a time scope be chosen, either short or long term, to indicate whether the changes to the model will happen immediately or over a longer period of time. When analysing a problem in undrained clay it is necessary to use a long-term analysis, but for sand, gravel, or other coarse materials, a short and long-term analysis should be assigned to fully evaluate the problem. The element type can be set to upper, lower, six, or fifteen elements Gauss or a custom user-specified element type. This study will focus on using only the lower element type to ascertain the lower bound factor of safety values.

The number of elements in the initial mesh can be defined to influence the accuracy of the solution. Mesh adaptivity is a feature unique to Optum G2 and is used to perform adaptive mesh iterations to refine the failure mechanism and further increase the accuracy of results. For the gravity reduction and strength reduction methods it is recommended that at least three iterations be adopted along with shear dissipation as the adaptivity control (Optum CE 2013). The design approach can be set to provide a key factor of safety based on design codes but will be ignored and left as the default unity setting for this research.

Once the analysis has been performed through the stage manager window the outcome will be displayed on a pop-up screen and can be examined further through the results tab. A number of options are available to plot different features such as; displacement, strain, stress, material parameters, plastic multiplier, yield function, and shear dissipation. An animation can be run to demonstrate the failure mechanism of the model. Results can be graphed, exported, generated in a report, or viewed through a log.

CHAPTER – 4: PROBLEM DEFINITION

4.1. SHAPE OF THE TUNNELS:

The shape of the cross section of a tunnel is often governed by its intended use and the method by which the tunnel can be most economically constructed. Circular tunnels are common as they are readily constructed using tunnel boring machines and are relatively stable since the stresses are smoothly distributed around the tunnel opening. Rectangular, square and arch shaped tunnels are also adopted as these shapes are well suited for carrying trains and traffic. Also, the tunnel of these shapes and can be constructed with minimal excavation beyond the required envelope. In this study, both the square and the circular tunnels have been considered for the stability analysis.

4.2. GEOMETRY OF THE TUNNELS:

In addition to its shape, the size and the depth of the tunnel have a significant influence on its stability. The tunnel depth (H), or cover, is typically defined as the depth of soil above its crown below the ground level. The size of a circular tunnel is defined by its diameter (D), while the square tunnels are described by its width (B). These dimensions are shown in Figure 4.1.

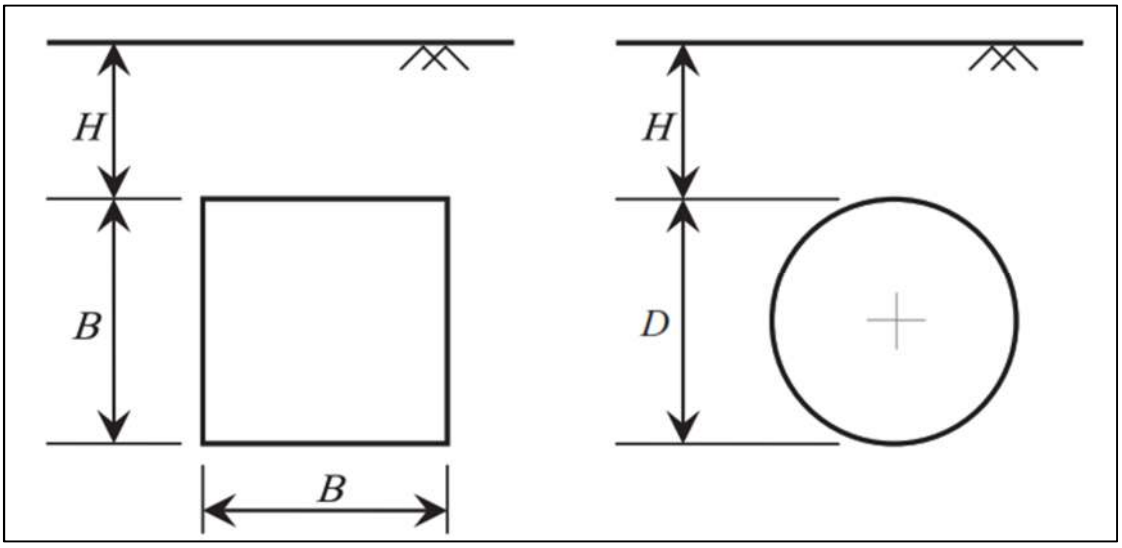

Fig. 4.1: Geometry of (a) Square Tunnel and (b) Circular Tunnel

4.3. STRENGTH OF THE SURROUNDING SOIL:

The strength of the surrounding soil is one of the most important factors to influence stability of a tunnel system.

The stability analysis for both the square and the circular tunnels are performed considering only undrained cohesion (c_u). The medium, in this case, is considered to be governed by the following Mohr-Coulomb's yield function.

$$F = |\sigma_1 - \sigma_3| + (\sigma_1 - \sigma_3)\sin\phi - 2c_u\cos\phi \quad \text{.....(4.1)}$$

4.4. UNIT WEIGHT OF THE SOIL:

The unit weight (γ) of the soil is also important in determining the stability of geotechnical structures. For tunnels, the weight of the soil typically acts to drive collapse. However, for deep tunnels in which collapse involves heaving of the floor, part of the soil mass moves upwards against gravity and the unit weight acts to resist collapse of the soil.

4.5. PROBLEM STATEMENT:

The geometries of the problems are shown under Fig. 4.2 and 4.3. The size of both the square tunnels are *B* whereas the diameter of both the circular tunnels are *D*. The first tunnel is placed with a clear-cover of *H* below the ground level. The second tunnel is placed at a horizontal center to center distance of S_H and vertical center to center distance of S_V from the first tunnel. The ground surface is assumed to be horizontal. The length of the tunnel is assumed to be considerably large compared to the cross-section of the tunnels so that the problem can be solved with plain strain analysis. The surrounding soil is assumed to be linearly elastic perfectly plastic and it obeys an associated flow rule. The subsoil is modeled as a Mohr-Coulomnb media as explained under Section 4.3.

In this study, the number of the elements are increased from 5000 to the target element number in five adaptive iterations. At first, the analysis is done considering target elements of 5000 and then, it is increased by 1000 in each stage until the difference between the two subsequent collapsible multipliers becomes less than 0.001. The domain of the model is taken sufficiently large so that the boundary elements remains far away from the yield. In this way, the result is not affected by the boundary. The support condition is taken as "Standard Fixities" in the OptumG2 analysis which applies normal support on vertical and full support on horizontal boundary lines.

The various factors that influence the stability of a tunnel can be summarized through the use of dimensionless parameters. In this study, the set of dimensionless parameters as defined by Assadi and Sloan (1991) are adopted. The geometry of the circular and the square tunnel can conveniently be expressed in terms of the dimensionless parameter *H/D* and *H/B* respectively. The unit weight and cohesion of the soil can also be expressed in terms of $\gamma D/c_u$ for circular tunnel, and $\gamma B/c_u$ for square tunnel. The stability of the twin tunnels is then evaluated varying these dimensionless parameters while considering two different approaches, namely, load multiplier method and gravity multiplier method.

In load multiplier method, the surface is loaded with a uniform distributed surcharge of σ_s while both the tunnels are subjected to a constant internal pressure of σ_t. The stability number (N) for the above systems can be defined as,

$$N = \frac{\sigma_s - \sigma_t}{c_u} \text{.....(4.2)}$$

By assuming σ_t to be zero, it is possible to simplify the calculation procedure. The analysis, hence, can be done optimizing σ_s as the objective function in the two problems shown under Fig. 4.2. As a result, the boundary conditions along the periphery of the tunnels are considered such that both normal and shear stresses become zero (σ_n = 0 and τ_n = 0). Along the ground surface, shear stress is equal to zero and normal stress is equal to the surface surcharge, i.e. σ_n = σ_s.

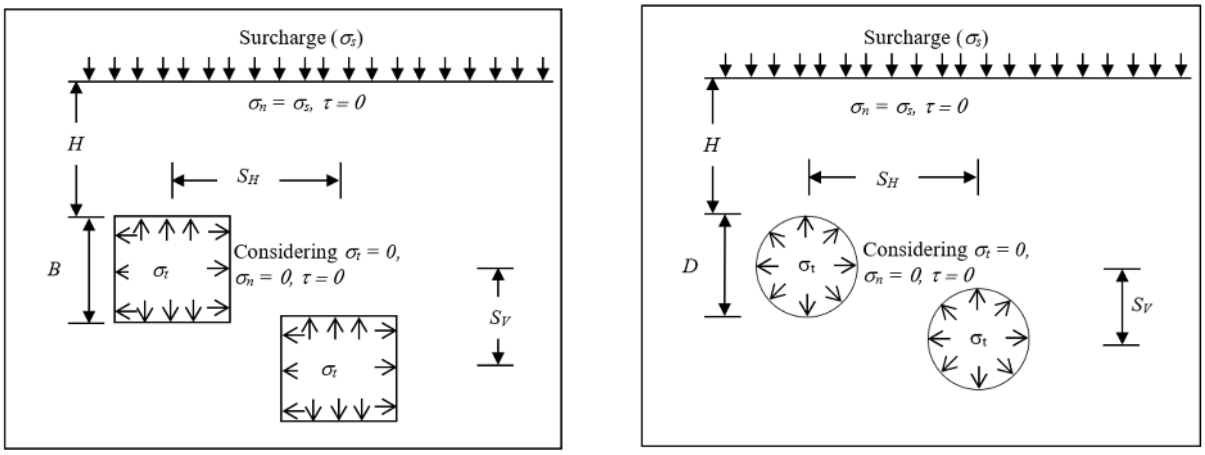

Fig. 4.2: Geometrical Model in Load multiplier method for (a) Dual square tunnels and (b) Dual Circular Tunnels

In gravity multiplier method, the problems are same as in the above. However, there is no surface surcharge as well as no internal tunnel pressure considered as shown Fig. 4.3. Hence, the boundary conditions along the ground surface as well along the tunnel periphery both are such that both the normal stress and shear stress are equal to zero (σ_n = 0 and τ_n = 0). The stability of the tunnel is then assessed with the dimensionless stability number, S_n as defined in equation 4.3. after Sahoo and Kumar (2013).

$$S_n = \frac{\gamma_{max} H}{c_u} \text{.....(4.3)}$$

Here, γ_{max} is the maximum unit weight of soil mass which can be allowed by the unlined pair of tunnels before failure.

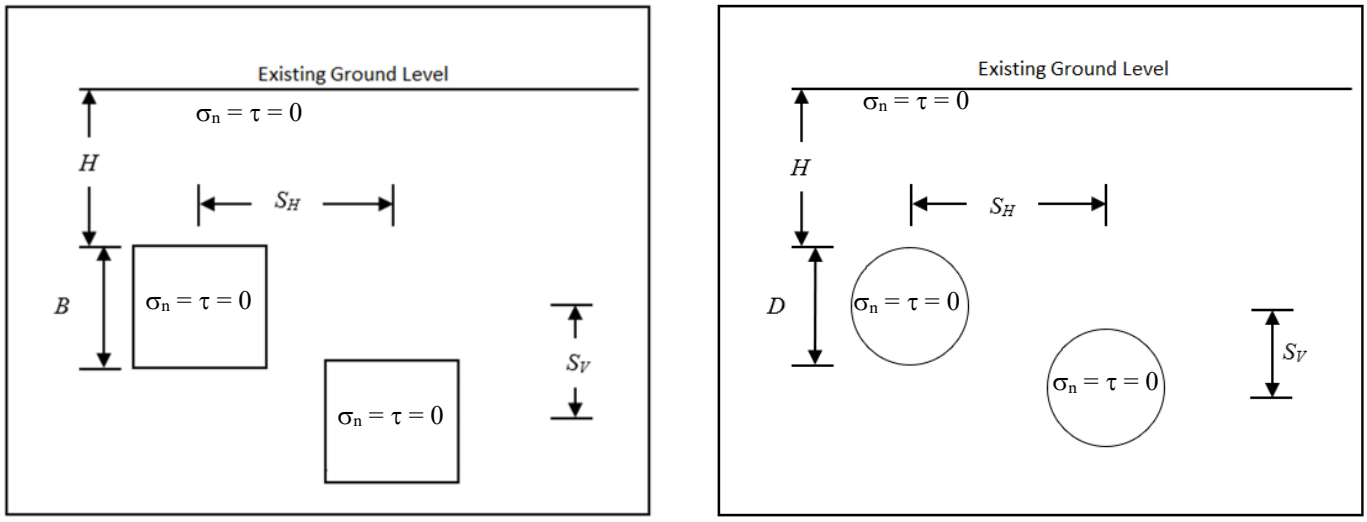

Figure 4.3: Geometrical Model in Gravity multiplier method for (a) Dual square tunnels and (b) Dual Circular Tunnels

CHAPTER – 5: RESULT AND DISCUSSION

5.1. GENERAL:

The results are presented in terms of stability number N and S_n as explained in equation (4.2) and equation (4.3). The findings obtained in this study are initially verified against previously available results. The diverse parameters considered in this investigation are summarized in Table 1.

Table 1: Summary of the design properties

Parameter	Range of Variation
$\gamma B/c_u$ or $\gamma D/c_u$	1 – 3
Angle of Internal Friction, ϕ	0°
H/B or H/D	1 to 3
S_V/B or S_V/D	0 – 3
S_H/B or S_H/D	1.5 – 11

5.2. VALIDATION OF THE PRESENT ANALYSIS:

The results obtained in this study are compared with the available results considering various scenarios.

5.2.1. TUNNELS UNDER LOAD MULTIPLIER METHOD:

For the validation, the stability number of a twin square tunnel with $S_V/B = 0$ and for different H/B, S_H/B, and $\gamma B/c_u$ have been compared with the results of Wilson et al. (2015) as presented in Table 2. The same is also done for twin circular tunnels with $S_V/D = 0$ and for different H/D, S_H/D and $\gamma D/c_u$ with the results of Wilson et al. (2014).

Table 2: Comparison of stability number considering Load Multiplier Method (*N*)

H/B or H/D	$\gamma B/c_u$ or $\gamma D/c_u$	S_H/B or S_H/D	Square Tunnels		Circular Tunnels	
			Wilson et. al. (2015)	Present analysis	Wilson et. al. (2014)	Present analysis
1	1	2	0.13	0.121	0.53	0.531
1	1	3	0.44	0.428	0.94	0.940
1	2	3	-0.87	-0.868	-0.42	-0.439
1	3	3	-2.26	-2.244	-1.84	-1.852
2	3	4	-4.72	-4.687	-4.26	-4.267
2	3	5	-4.59	-4.548	-4.08	-4.086

It is seen that the results of the present analysis are in good agreement with that of Wilson et al. (2014 & 2015). The minor difference of the results may be attributed to the fact that the

present study considers adapting meshing technique while it is not considered by Wilson et al. (2014 & 2015).

5.2.2. TUNNELS UNDER GRAVITY MULTIPLIER METHOD:

The stability numbers N and S_n may be approximately compared as below when the tunnels are at the same level considering the total force acting on the tunnel crown.

$$N + \frac{\gamma B}{c_u} . \frac{H}{B} = S_n \text{.....(5.1)}$$

$$N + \frac{\gamma D}{c_u} . \frac{H}{D} = S_n \text{.....(5.2)}$$

For the validation, the stability number obtained from this analysis are compared with that of the load multiplier method using equation (5.1) and (5.2) and presented in Table 3.

Table 3: Comparison of stability number considering Gravity Multiplier Method (S_n)

H/B or H/D	$\gamma B/c_u$ or $\gamma D/c_u$	S_H/B or S_H/D	Square Tunnels		Circular Tunnels	
			S_n from N	S_n in Present Analysis	S_n from N	S_n in Present Analysis
1	1	4	1.717	1.614	1.891	1.806
2	1	1.25	1.789	1.826	2.047	2.046
2	1	2	1.750	1.776	2.125	2.110
3	1	1.25	2.388	2.451	2.701	2.721
3	1	4.5	2.573	2.622	3.040	3.042

It can be observed that, r the results from both of these methods seamlessly coincide with each other, showcasing their congruence.

5.3. RESULTS OF DUAL SQUARE TUNNEL:

5.3.1. LOAD MULTIPLIER METHOD:

The lower bound of the stability numbers for dual square tunnels are presented in Annexure 1. Here, $S_V/B = 0$ means both the tunnels are at the same level. For ease of the analysis, σ_t is kept 0, so a negative value of the stability number indicates that to maintain stability, additional internal tunnel pressure (σ_t) is required.

5.3.1.1. Variation of stability number with relative depth (S_V/B)

The variation of stability numbers with S_V/B are presented graphically from Fig. 5.1 to Fig. 5.3. It can be seen that the stability number in general decreases exponentially with increase in the relative depth. Hence, when the overburden increases substantially, it is evident that internal tunnel pressure needs to be applied. For all the cases analyzed, N first decreases with S_H/B and then increases to attain a constant value eventually after $S_H/B = 6$ to 8. However, if $H/B = 1$ and $S_V/B = 0$ or 1, the decrease of N values in the beginning, i.e. the concave upward portion of the graph is not clear. It can also be observed from the graphs that when the density of the soil and tunnel cover increases, a too high relative depth may not be stable.

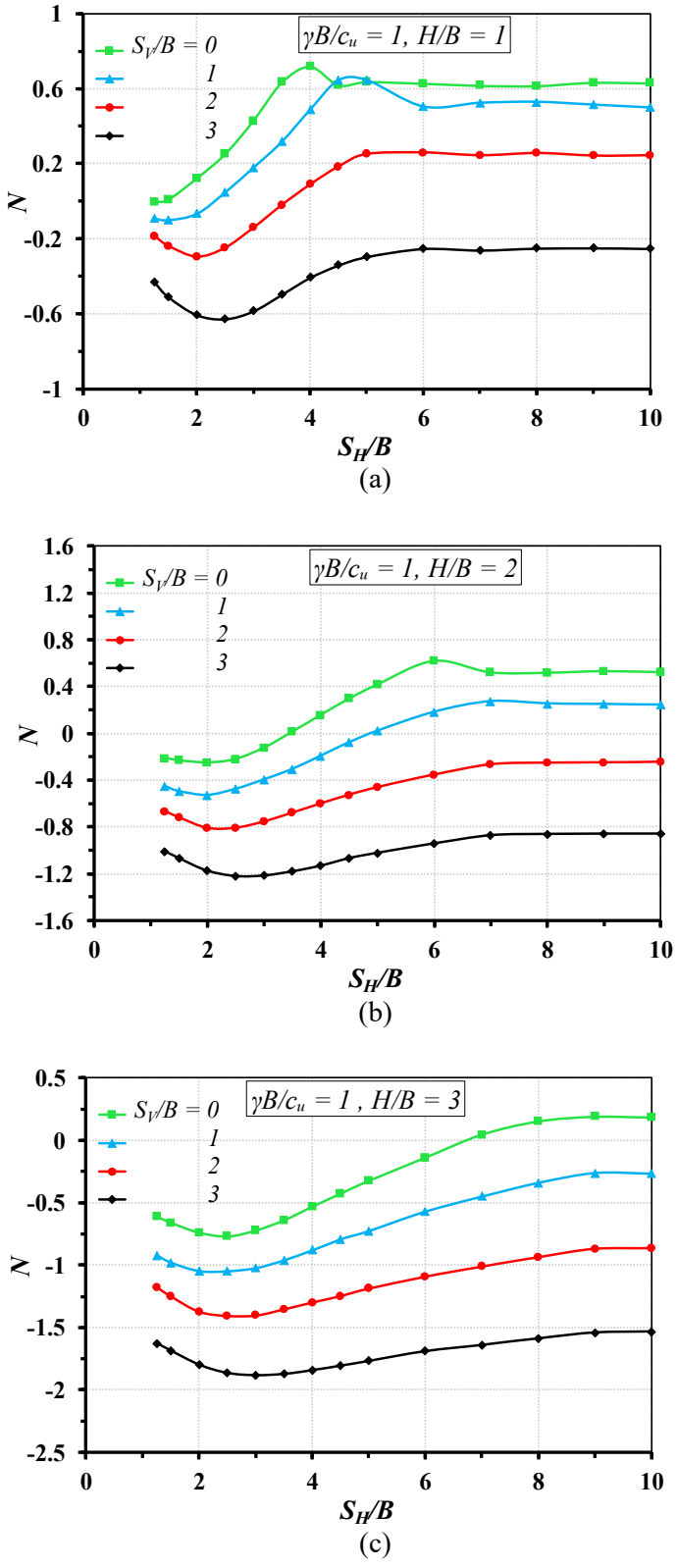

Fig. 5.1: Variation of Stability Numbers (*N*) in Load Multiplier with S_H/B for $\gamma B/c_u = 1$ and for different S_V/B and for (a) $H/B = 1$, (b) $H/B = 2$, and (c) $H/B = 3$

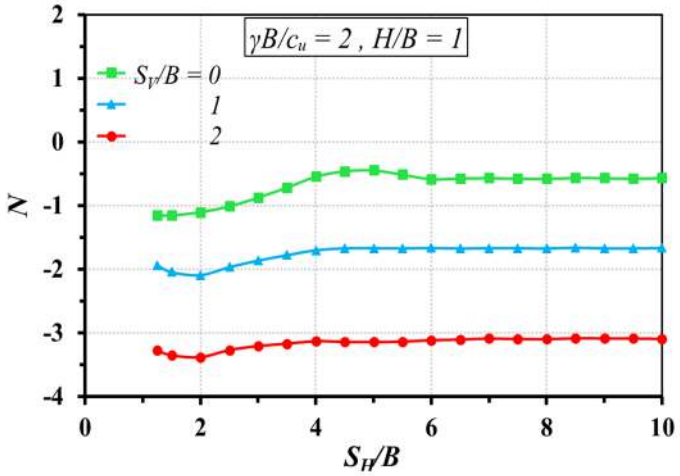

(a)

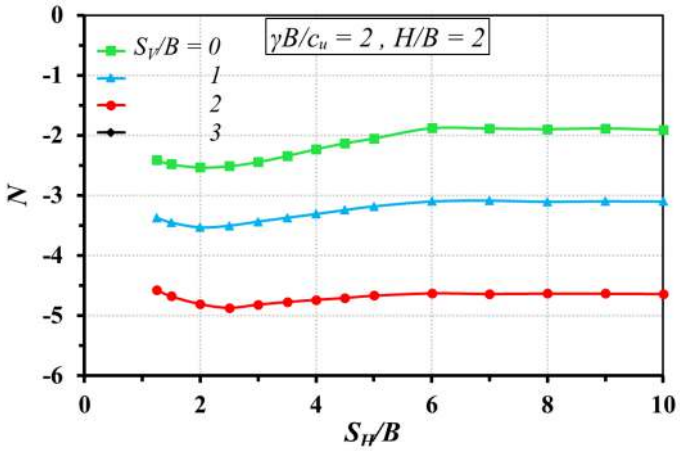

(b)

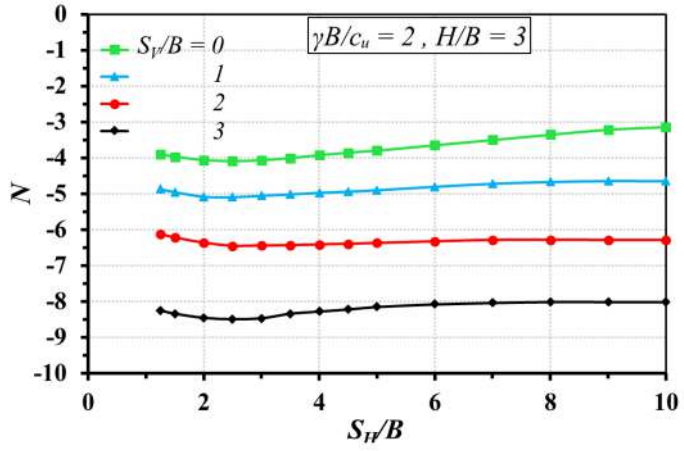

(c)

Fig. 5.2: Variation of Stability Numbers (N) in Load Multiplier with S_H/B for $\gamma B/c_u = 2$ and for different S_V/B and for (a) $H/B = 1$, (b) $H/B = 2$, and (c) $H/B = 3$

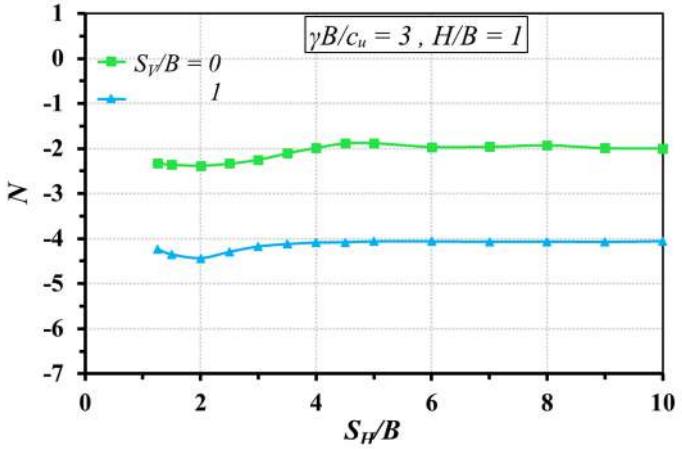

(a)

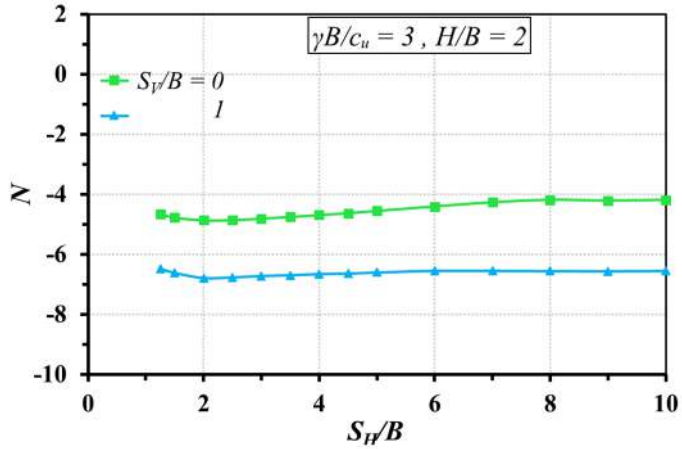

(b)

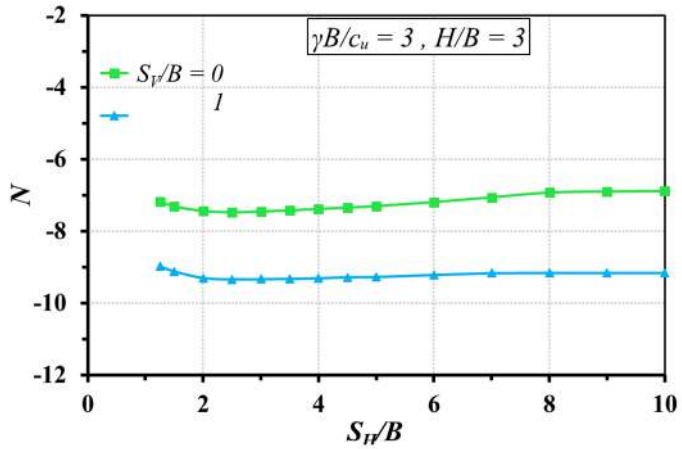

(c)

Fig. 5.3: Variation of Stability Numbers (N) in Load Multiplier with S_H/B for $\gamma B/c_u = 3$ and for different S_V/B and for (a) $H/B = 1$, (b) $H/B = 2$, and (c) $H/B = 3$

5.3.1.2. Variation of stability number clear cover (*H/B*)

The variation of stability numbers with *H/B* are presented graphically from Figure 5.4 to Figure 5.6. It is seen that even with all parameters remaining constant, with the cover of the tunnel (*H*) increasing, the stability factor decreases. However, from the graphs it can be seen that this decrease is not exponential. Moreover, if $\gamma B/c_u$ is as high as 3, S_V/B of 2 and 3 do not render any solutions.

The stability numbers are not similar where it increases with S_H/B, i.e., if the stability plots are not parallel for different *H/B* values. This indicates that, the behavior of the soils surrounding the tunnels somewhat changes with increase in depth if not substantially. Although *N* decreases with increase in *H/B*, it is evident that greater the depth, greater the chance of obtaining a stable ground.

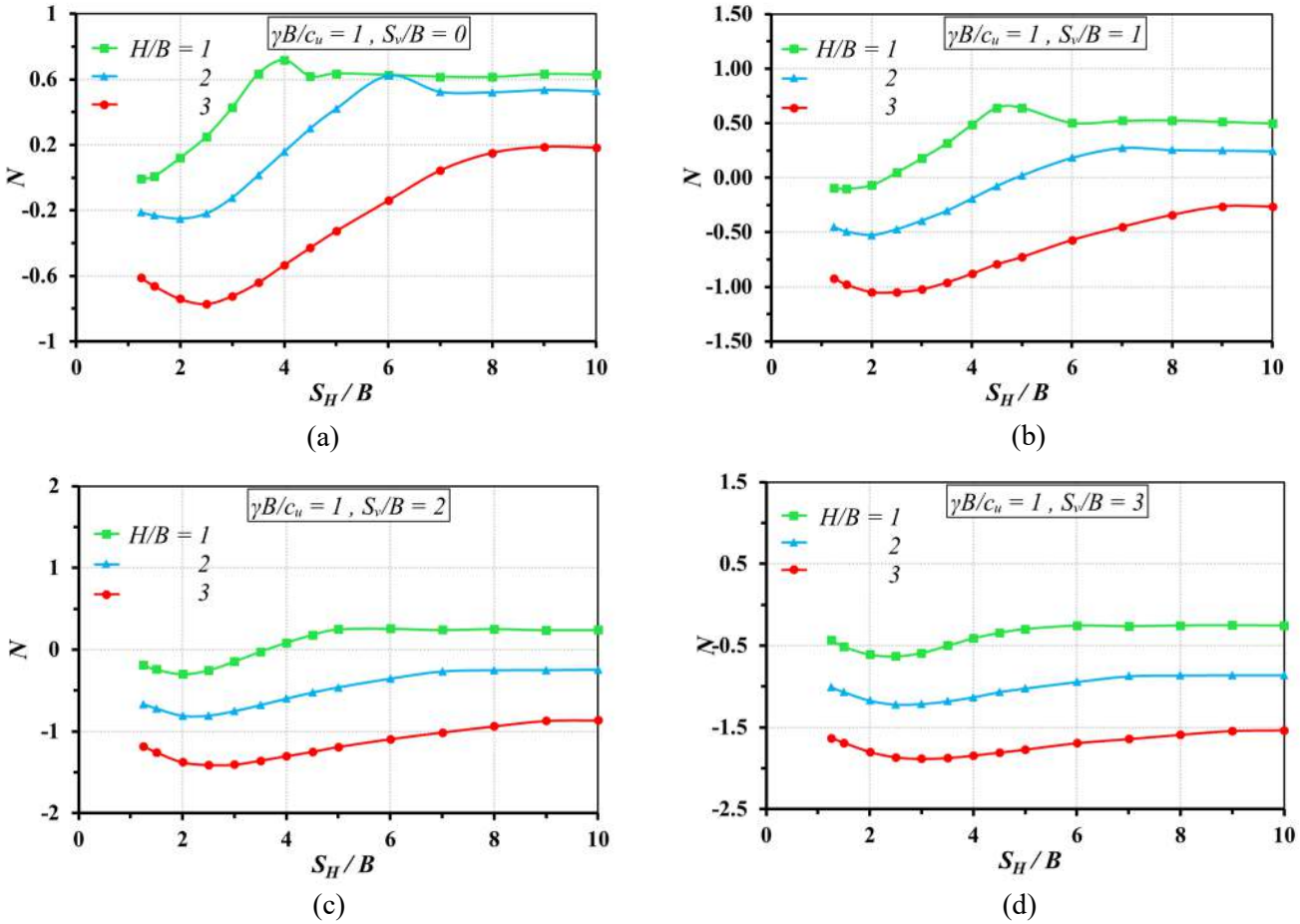

Fig. 5.4: Variation of Stability Numbers (*N*) in Load Multiplier with S_H/B for $\gamma B/c_u = 1$ and different *H/B* and for (a) $S_V/B = 0$, (b) $S_V/B = 1$, (c) $S_V/B = 2$ and (d) $S_V/B = 3$

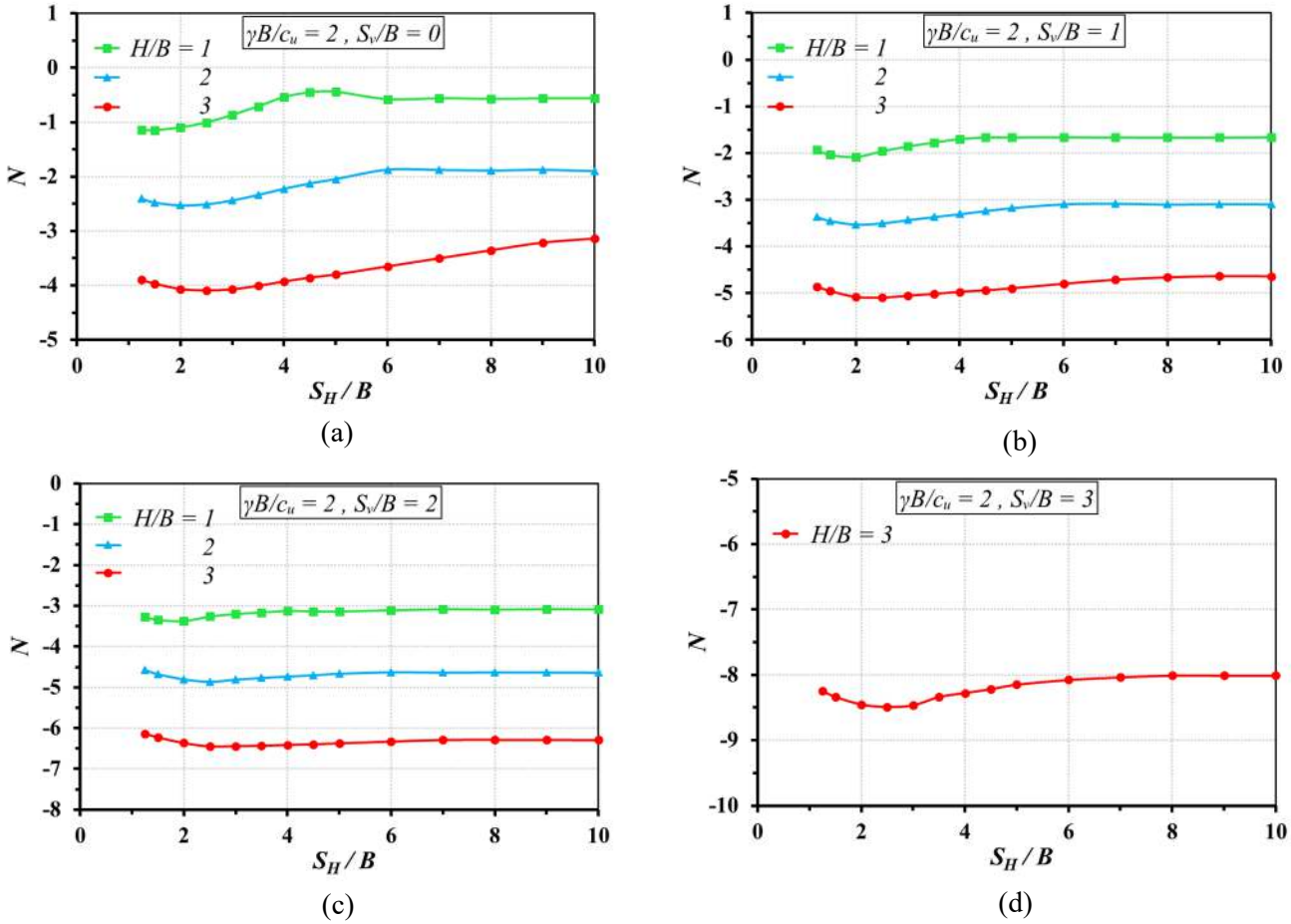

Fig. 5.5: Variation of Stability Numbers (*N*) in Load Multiplier with S_H/B for $\gamma B/c_u = 2$ and different H/B and for (a) $S_V/B = 0$, (b) $S_V/B = 1$, (c) $S_V/B = 2$ and (d) $S_V/B = 3$

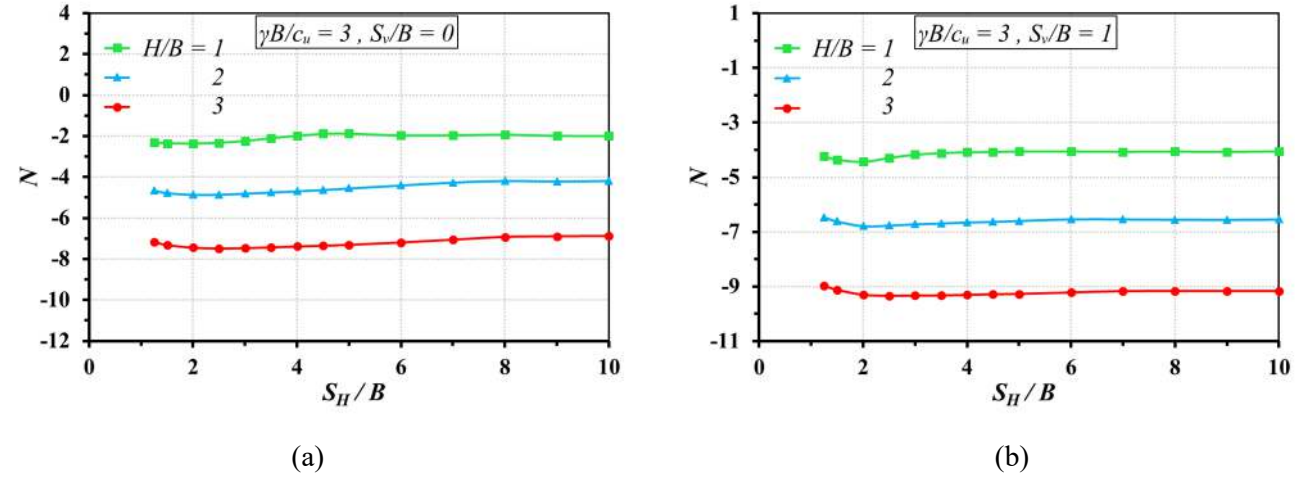

Fig. 5.6: Variation of Stability Numbers (*N*) in Load Multiplier with S_H/B for $H/B = 1$ and for different $\gamma B/c_u = 1$ and for (a) $S_V/B = 0$, (b) $S_V/B = 1$, (c) $S_V/B = 2$ and (d) $S_V/B = 3$

5.3.1.3. Variation of stability number with unit weight of soil and undrained cohesion ($\gamma B/c_u$)

The variation of stability numbers with unit weight and cohesion are assessed in terms of dimensionless parameter of $\gamma B/c_u$. The outcomes are presented graphically from Figure 5.7 to Figure 5.9. It is obvious that with increase in unit weight of soil or decrease in cohesion the stability will also decrease. But it is found that with increase in $\gamma B/c_u$, if the relative depth is high (S_v/B = 2 and 3), the tunnels are stable only under greater cover above the tunnel , i.e. H/B of 2 to 3. Even though in some cases when $\gamma B/c_u$ is 1 and H/B is in between 1 to 2, with small relative depths the initial decrease of the stability factor is not observed, an average decrease of as much as 50% of the stability factor is found in other cases. The increase of the stability factor from bottom, however, varies fin the range of 10% to more than 100%.

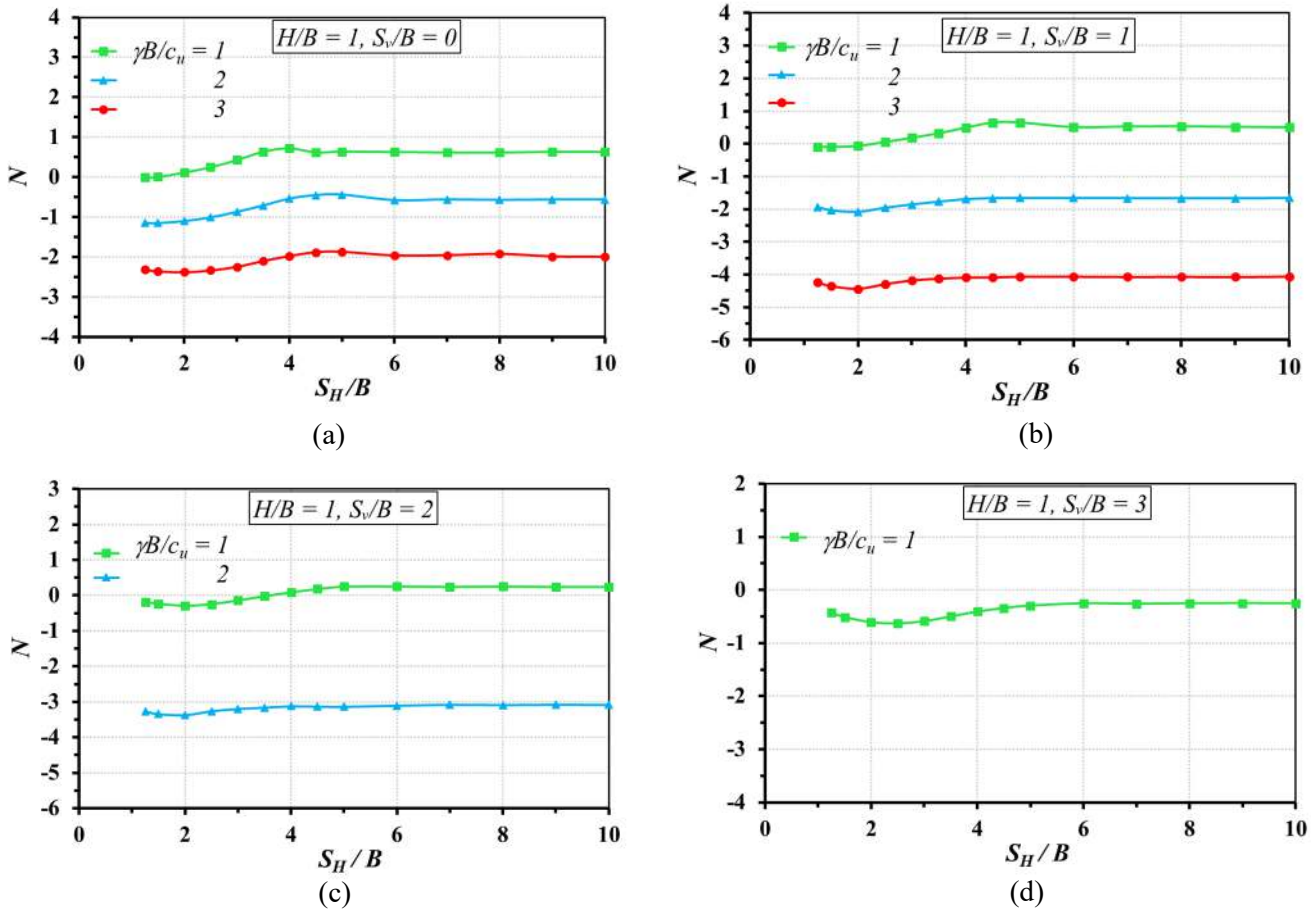

Fig. 5.7: Variation of Stability Numbers (N) in Load Multiplier with S_H/B for H/B = 1 and for different $\gamma B/c_u$ and for (a) S_V/B = 0, (b) S_V/B = 1, (c) S_V/B = 2 and (d) S_V/B = 3

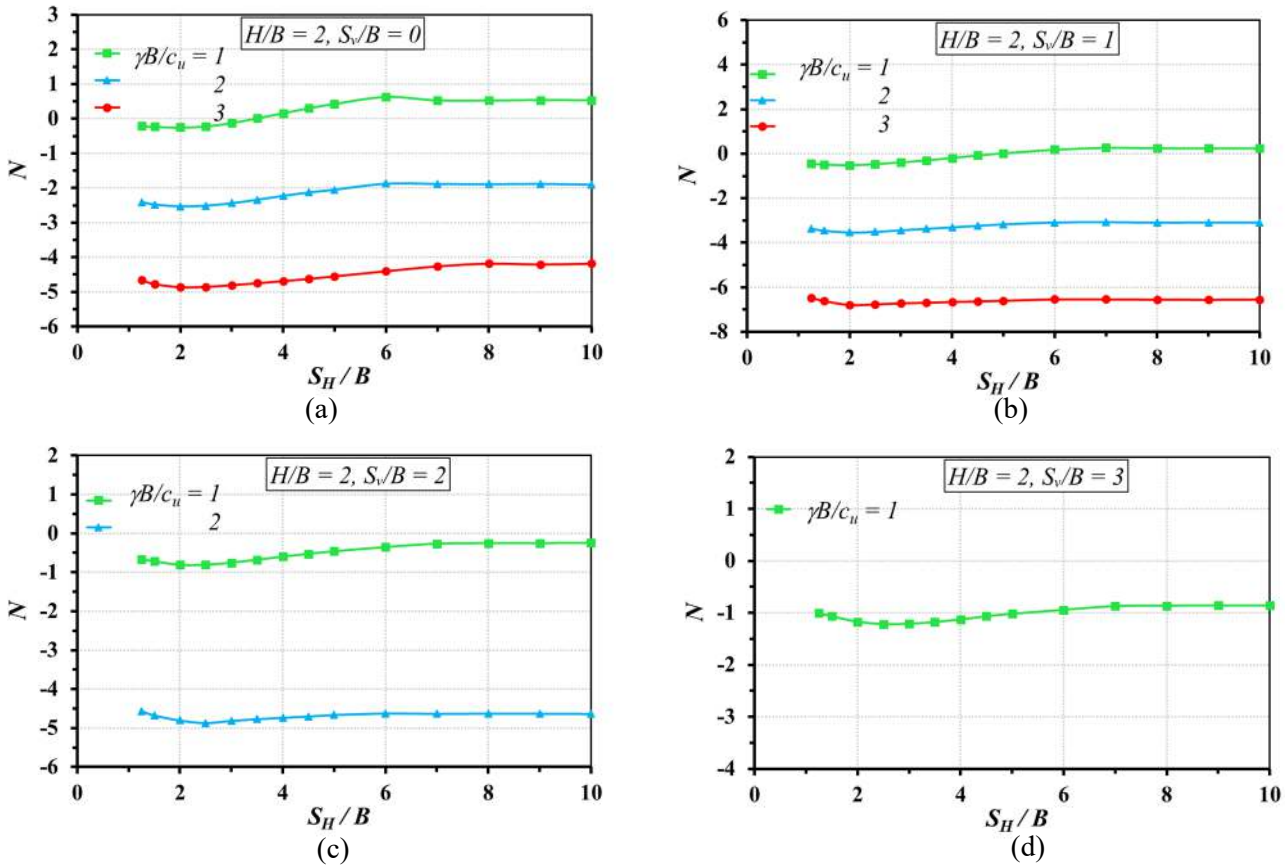

Fig. 5.8: Variation of Stability Numbers (*N*) in Load Multiplier with S_H/B for $H/B = 2$ and for different $\gamma B/c_u$ and for (a) $S_V/B = 0$, (b) $S_V/B = 1$, (c) $S_V/B = 2$ and (d) $S_V/B = 3$

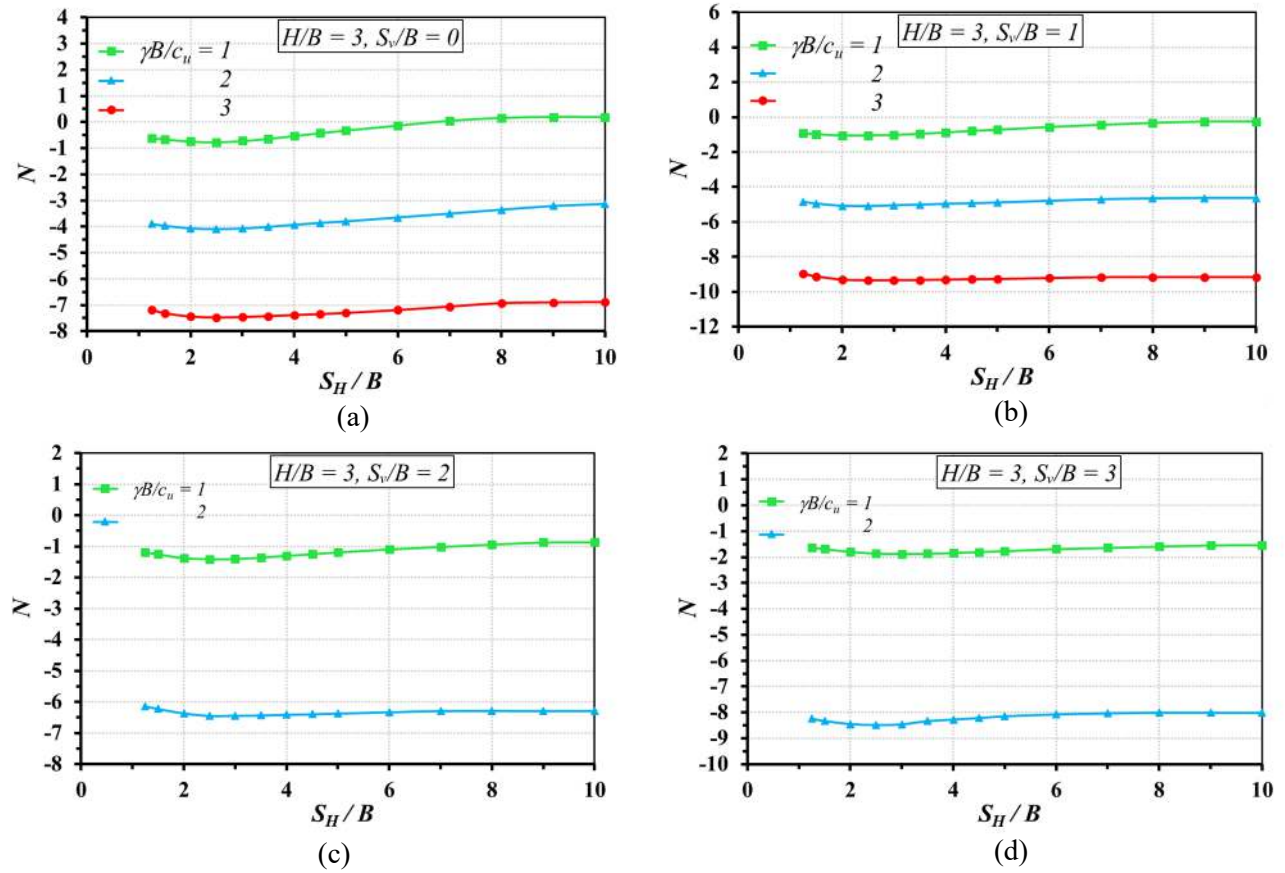

Fig. 5.9: Variation of Stability Numbers (*N*) in Load Multiplier with S_H/B for $H/B = 2$ and for different $\gamma B/c_u$ and for (a) $S_V/B = 0$, (b) $S_V/B = 1$, (c) $S_V/B = 2$ and (d) $S_V/B = 3$

5.3.2. GRAVITY MULTIPLIER METHOD:

The lower bound of the stability numbers for dual square tunnels are presented in Table A2 under Annexure 1 for this method. In OptumG2, the gravity multiplier method optimizes the gravity and consequently γ become the objective function, i.e. collapse multiplier. As already discussed, S_V/B of 0 means both the tunnels are at the same level. Here, it is assumed that there is no internal tunnel pressure, hence a collapse multiplier less than 1 means it is required to apply σ_t to maintain stability.

The optimization by gravity multiplier method expresses the maximum unit weight of soil (hence the downward force) that the unlined tunnels can withstand without failure. No surcharge load is considered above the ground surface. Even though the idea of optimizing the force function in this method is equivalent to that of the load multiplier method, where the surcharge is optimized, the results can only be compared with each other. This due to the fact that N does not count the existing overburden above the tunnel surface, whereas, the distribution of stress is different for gravity multiplier method which optimizes the body force of the subsoil.

5.3.2.1. Variation of stability number with relative depth (S_V/B)

The variation of stability numbers (S_n) with S_V/B are presented graphically from Fig. 5.10. As observed in load multiplier method, it is seen that the stability number decreases with increase in the relative depth. It is observed with increase in S_H/B, S_n first decrease and then increases. This decrease, however, is absent for H/B of 1 and S_V/B of 0 or 1. This may be attributed to the fact that for shallow tunnels, the stability is not achieved well when the tunnels are closely spaced. However, with increase in S_V/B, the stability factor decreases because of increase in the overburden. The exponential reduction of S_n with increment in S_V/B may be seen in order of 10% to 15%.

It is seen that for the range of S_H/B = 6-8, the stability factor becomes constant. This is because the two tunnels tend to behave as single individual tunnels with great distance.

For tunnels placed at the same level, the increasing stability number first achieves a peak and again plummets. This can be because of apparent rigidity of the wall between the tunnels.

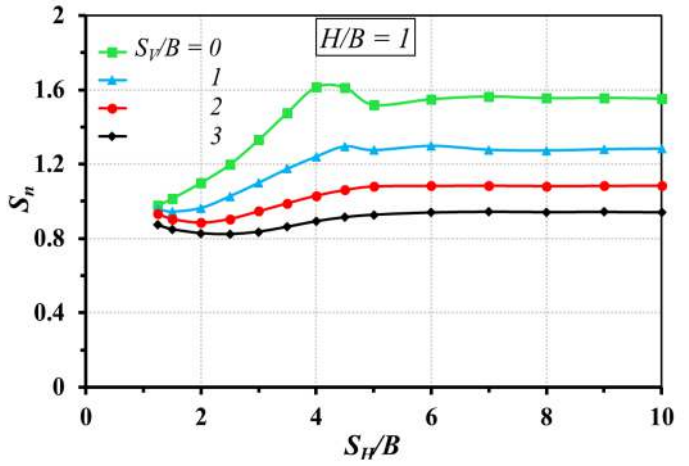

(a)

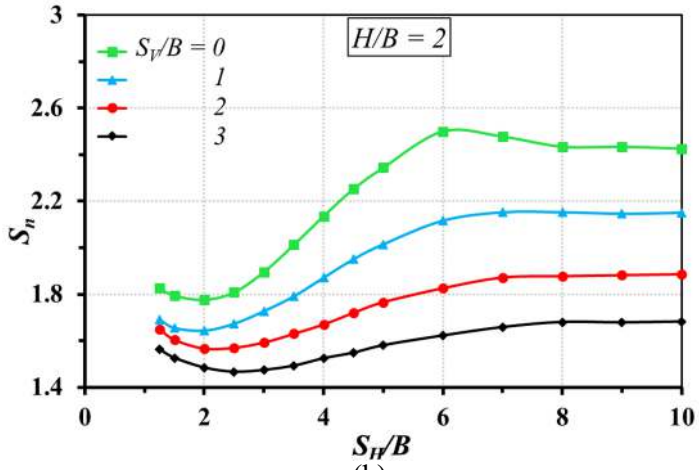

(b)

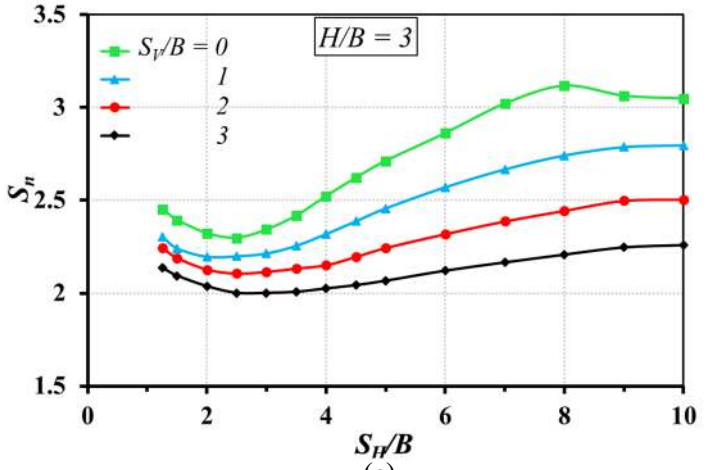

(c)

Fig. 5.10: Variation of Stability Numbers (*N*) in Gravity Multiplier with S_H/B for different S_V/B and for (a) *H/B* = 1, (b) *H/B* = 2 and (c) *H/B* = 3

5.3.2.2. Variation of stability number with clear cover (*H/B*)

The variation of stability numbers (S_n) with depth or cover thickness (presented as a dimensionless parameter of *H/B*) are presented graphically in Fig. 5.11.

It can be noted that as with increase in *H*, S_n increases, the same is reflected in the graphs. This may seem contradictory with *N* as shown in the previous section; however, this is because the manner S_n is calculated as is evident from equation 5.2.

Whatsoever, as S_V/B increases, the increase in S_n with H/B seems to be in lesser margin, by about 50% - 60% only. This means, the greater the relative depth, there will be lesser benefit of the increasing tunnel cover.

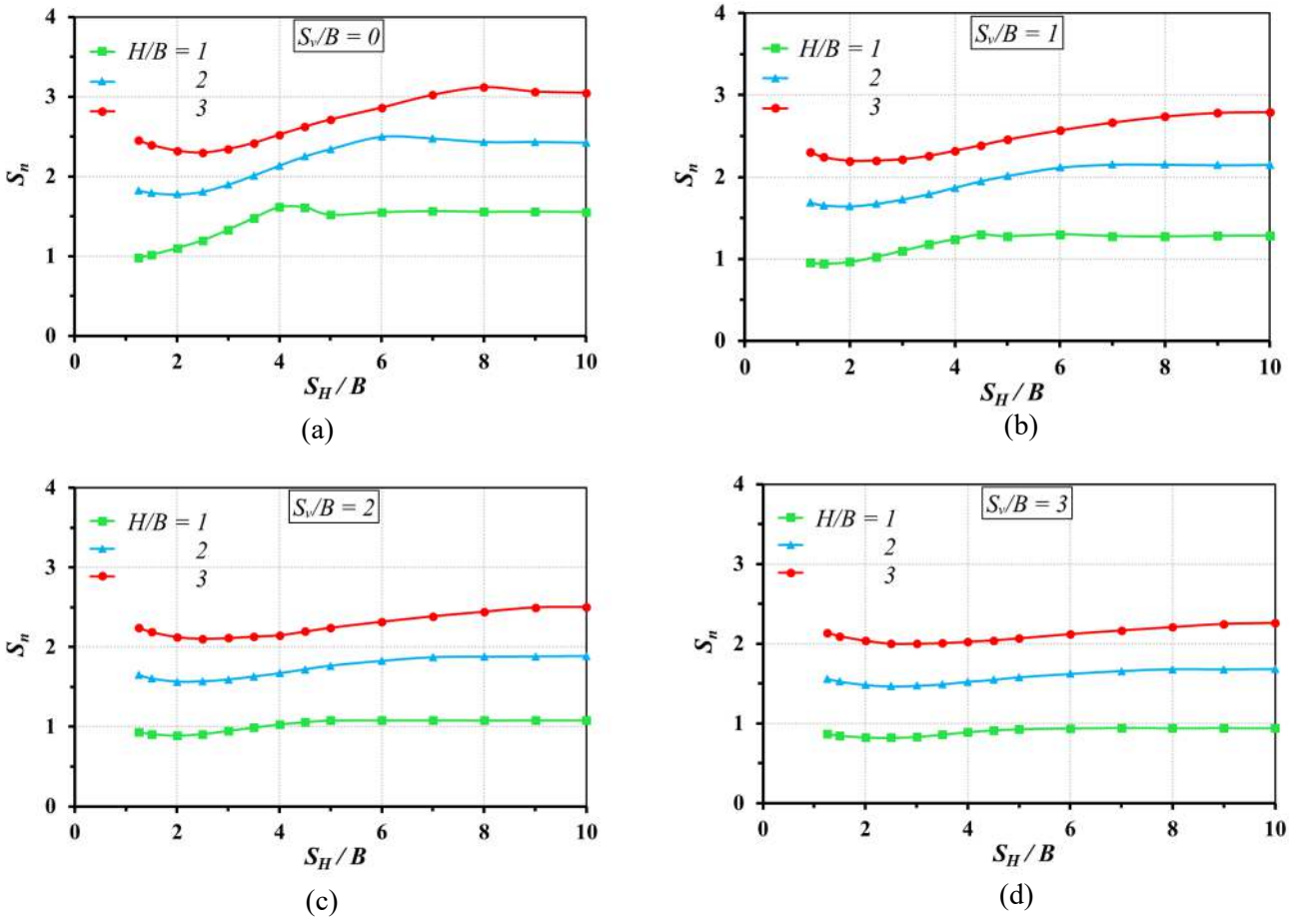

Fig. 5.11: Variation of Stability Numbers (*N*) in Gravity Multiplier with S_H/B for different S_V/B and for (a) *H/B* = 1, (b) *H/B* = 2 and (c) *H/B* = 3

5.4. RESULTS OF DUAL CIRCULAR TUNNEL:

5.4.1. LOAD MULTIPLIER METHOD:

For dual circular tunnels the lower bound of the stability numbers from load multiplier method are summarized in Table A3 under Annexure 1. As σ_t is kept 0 as discussed, so a negative value of the stability number means that to maintain stability, additional internal tunnel pressure (σ_t) is required.

5.4.1.1. Variation of stability number with relative depth (S_V/D)

The variation of stability numbers with S_V/D are shown graphically from Fig. 5.12 to 5.14. From the graphs, it is seen that with increase in the relative depth, the stability factor reduces exponentially. In all the cases where S_V/D is 3, N is almost negative. This means internal pressure of σ_t is needed in excess of σ_s. In all of the analysis it is found that the stability is most likely to be achieved when overburden pressure is low as well as relative depth is low. However, as S_V/D increases, the stability factor decreases drastically by more than 100% and eventually stability becomes impossible to achieve with greater density.

It is also observed that with incremental S_H/D, the stability factor first decreases by about 20% - 30% and then increases to attain a constant value. This constant N indicates the tunnels tend to behave as single individual tunnels. Although the critical distance varies from case to case, in general this is about S_H/D of 5 to 7.

When relative depth increases, it is evident that internal tunnel pressure needs to be applied. It can be observed from the graphs that when the density of the soil and tunnel cover increases, a too large relative depth may not be stable.

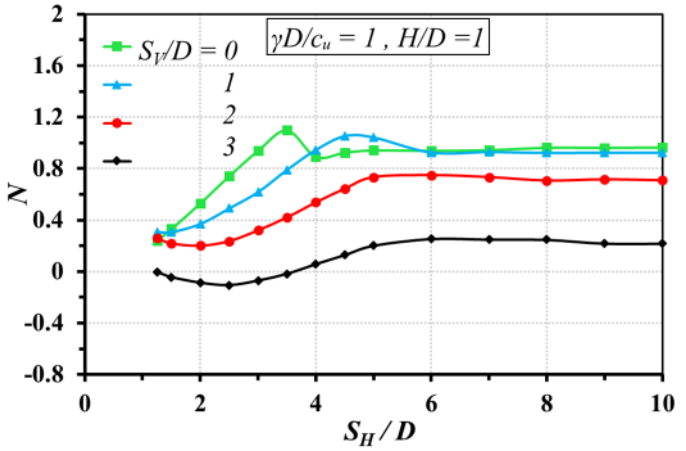

(a)

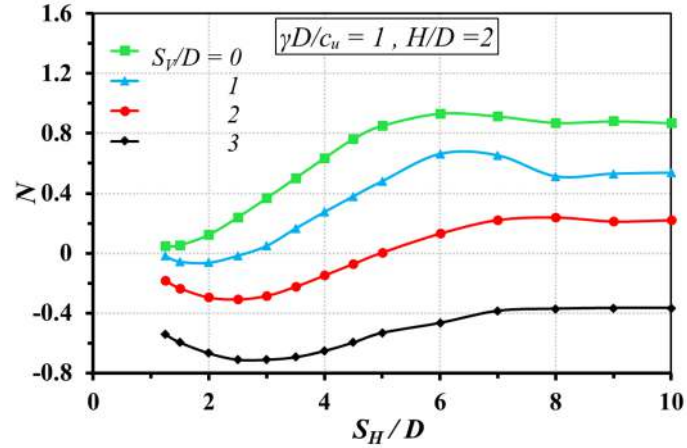

(b)

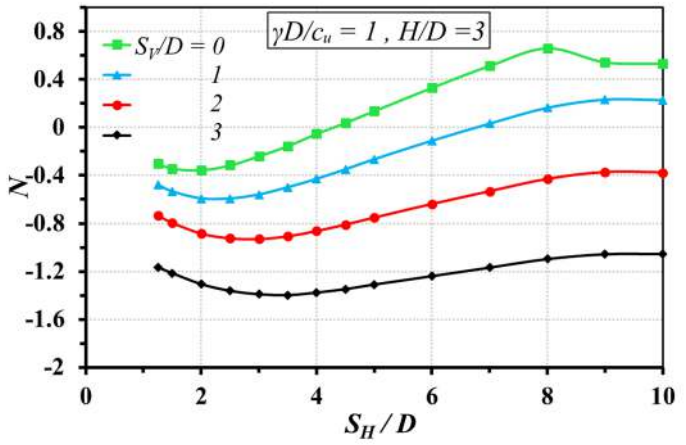

(c)

Fig. 5.12: Variation of Stability Numbers (*N*) in Load Multiplier with S_H/D for $\gamma B/c_u$ =1 and for different S_V/D and for (a) H/D = 1, (b) H/D = 2, and (c) H/D = 3

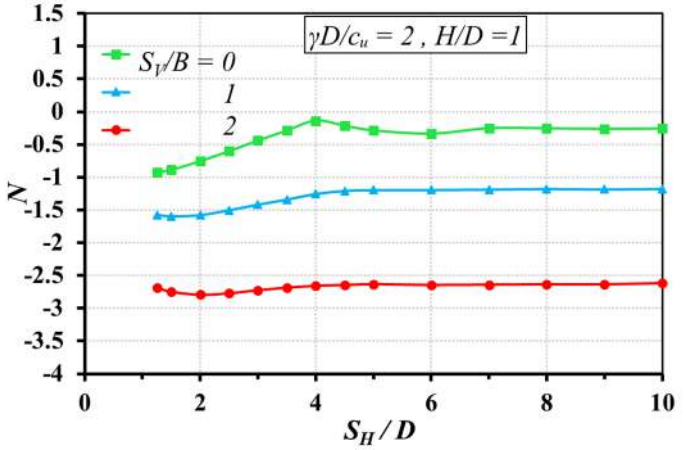

(a)

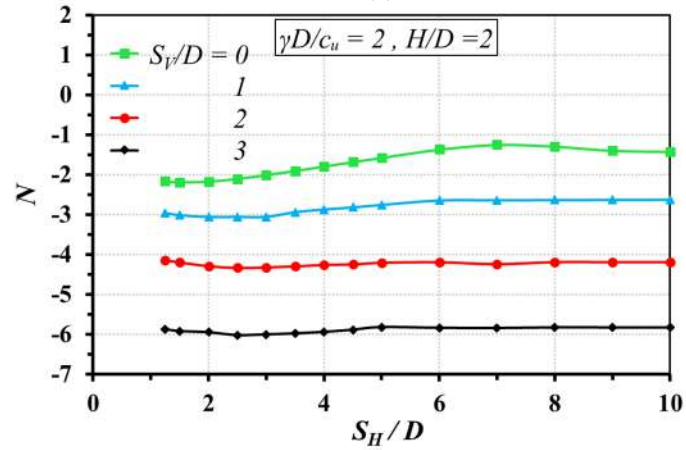

(b)

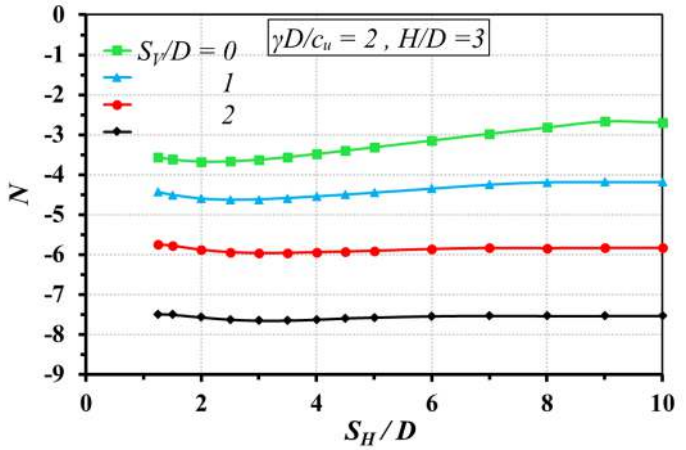

(c)

Fig. 5.13: Variation of Stability Numbers (*N*) in Load Multiplier with S_H/D for $\gamma B/c_u = 2$ and for different S_V/D and for (a) $H/D = 1$, (b) $H/D = 2$, and (c) $H/D = 3$

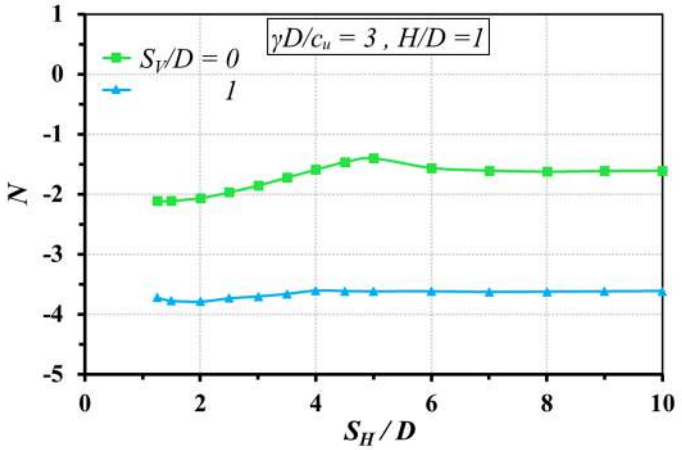

(a)

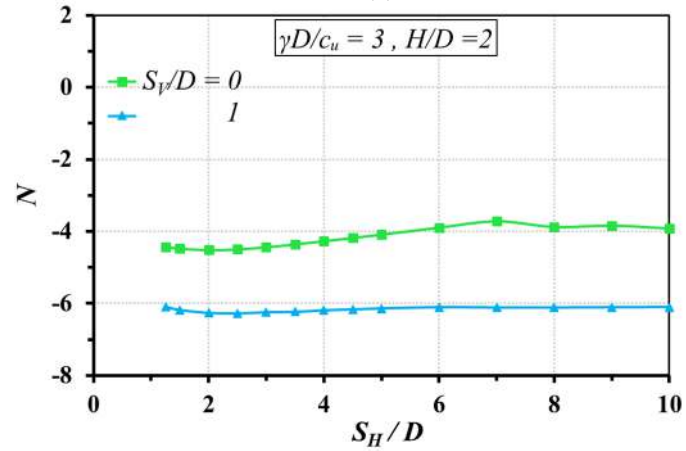

(b)

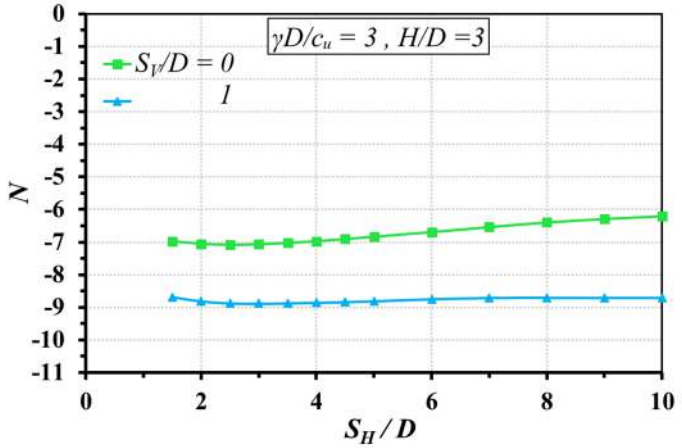

(c)

Fig. 5.14: Variation of Stability Numbers (N) in Load Multiplier with S_H/D for $\gamma B/c_u = 3$ and for different S_V/D and for (a) $H/D = 1$, (b) $H/D = 2$, and (c) $H/D = 3$

5.4.1.2. Variation of stability number with clear cover (*H/D*)

The variation of stability numbers with *H/D* are presented graphically from Figure 5.15 to Figure 5.17. It is seen that even with all parameters kept the same, with the cover of the tunnel (*H*) increasing, the stability factor decreases.

This decrease, however, seems uniform with depth of the tunnel. However, when relative depth S_V/D is increased to 2 and 3, if the unit weight of soil becomes such that $\gamma D/c_u$ is 2 to 3, the shallow depth of the tunnels results in instability of the tunnels. Even when the solutions of *N* are obtained, the negative values indicate the need of internal tunnel pressure σ_t in excess of the surcharge pressure.

The range of *N* for *H/D* of 1 to 3 varies with 100% to 200% for S_V/D of 0 to 1, whereas the variation covers a wider range for higher values of S_V/D.

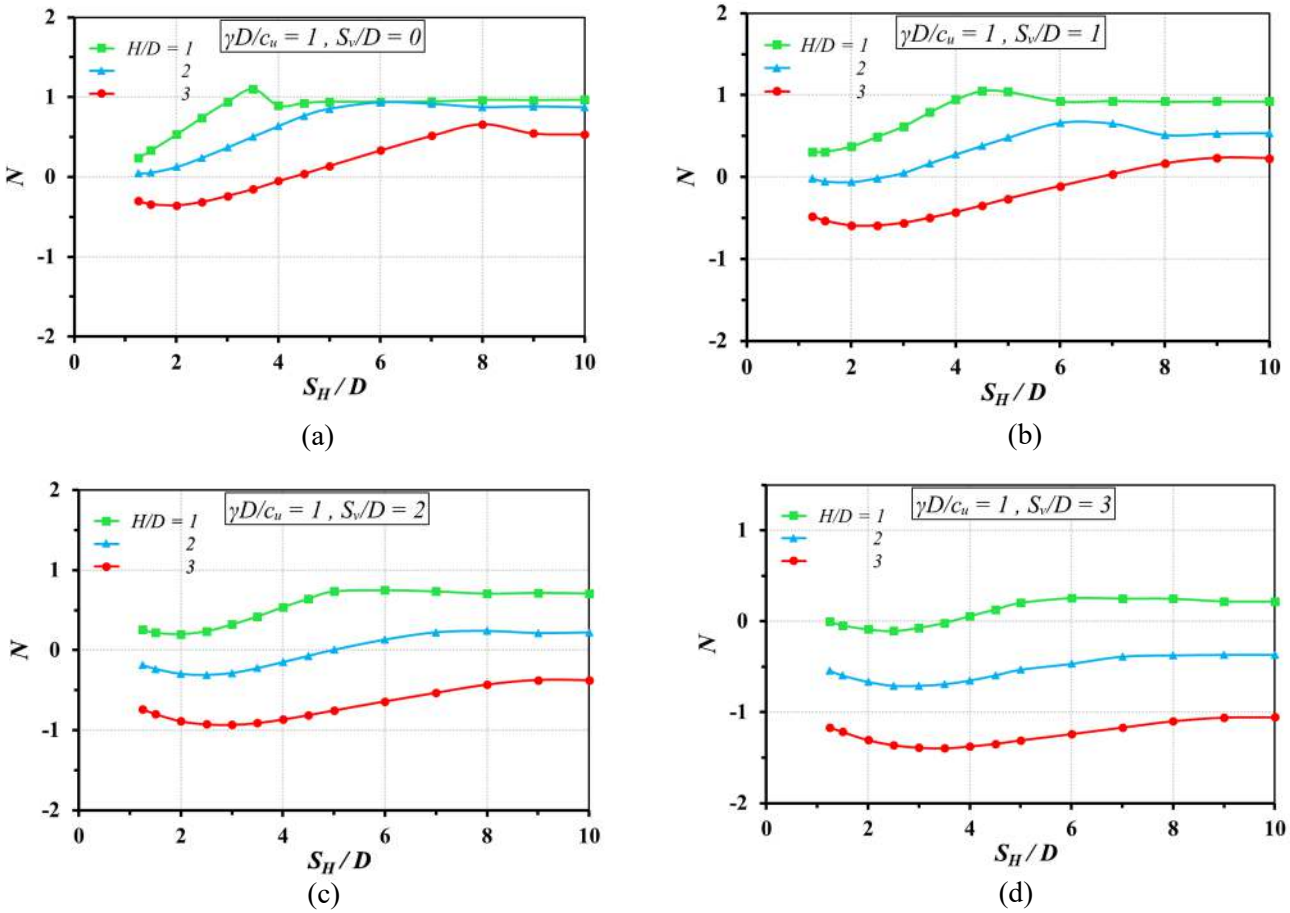

Fig. 5.15: Variation of Stability Numbers (*N*) in Load Multiplier with S_H/D for $\gamma D/c_u = 1$ and for different *H/D* and for (a) $S_V/D = 0$, (b) $S_V/D = 1$, (c) $S_V/D = 2$ and (d) $S_V/D = 3$

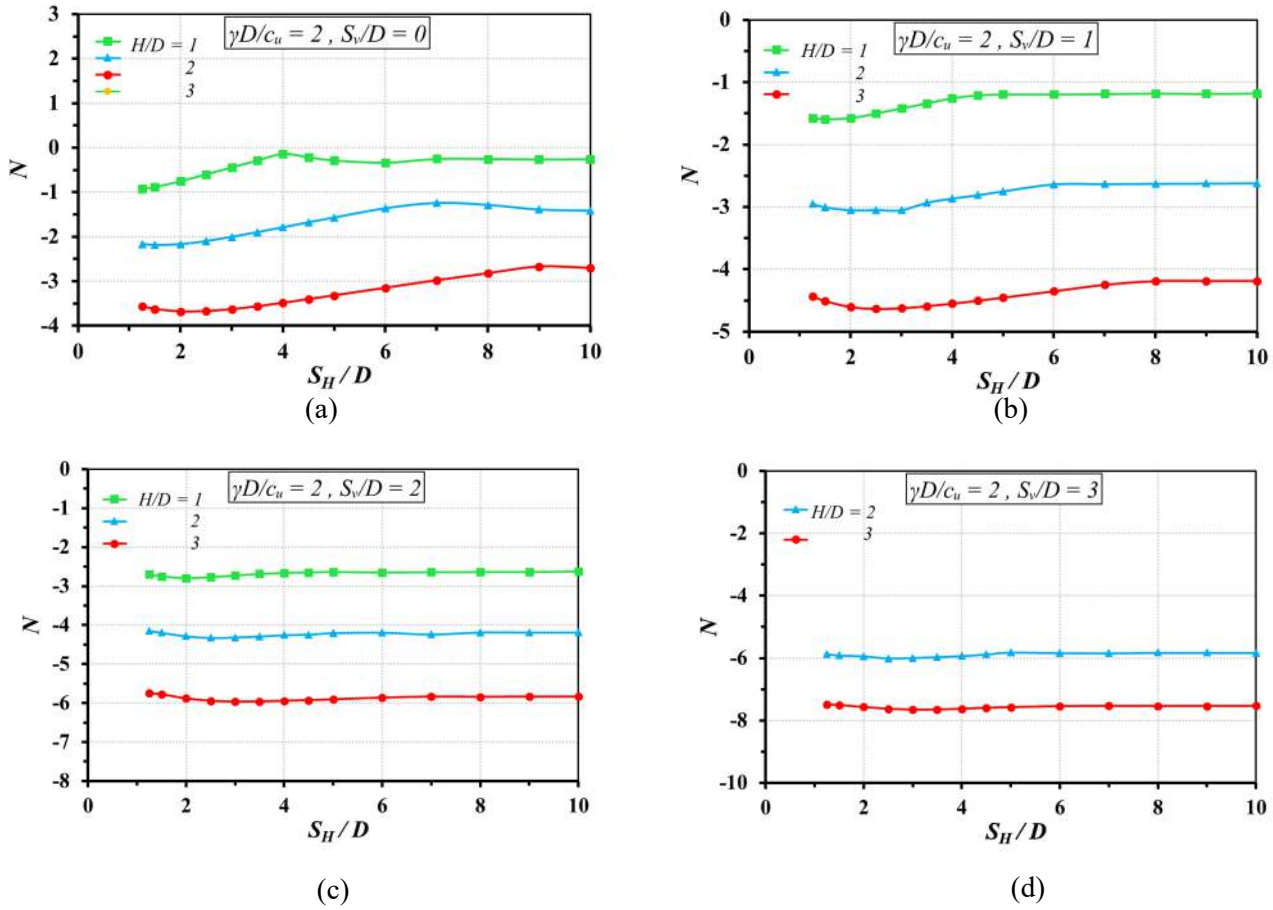

Fig. 5.16: Variation of Stability Numbers (*N*) in Load Multiplier with S_H/D for $\gamma D/c_u = 2$ and for different *H/D* and for (a) $S_v/D = 0$, (b) $S_v/D = 1$, (c) $S_v/D = 2$ and (d) $S_v/D = 3$

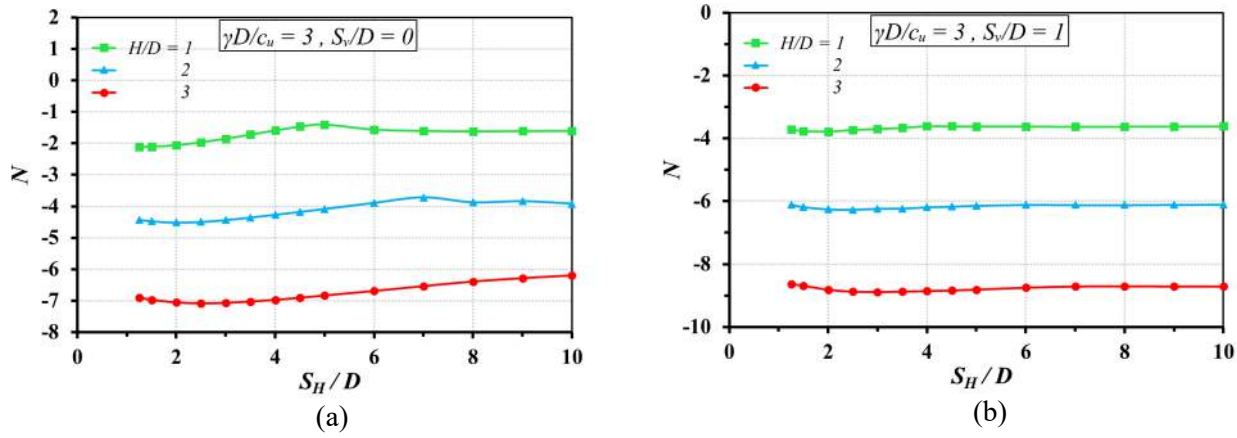

Fig. 5.17: Variation of Stability Numbers (*N*) in Load Multiplier with S_H/D for $\gamma D/c_u = 3$ and for different *H/D* and for (a) $S_v/D = 0$ and (b) $S_v/D = 1$

5.4.1.3. Variation of stability number with unit weight of soil and undrained cohesion ($\gamma D/c_u$)

In this study, the effects of unit weight of soil and cohesion are assessed in terms of $\gamma D/c_u$. The results are presented in graphs from Fig. 5.18 to 5.20. It is obvious that with increase in unit weight of soil or decrease in cohesion the stability will also decrease. But it is found that with increase in $\gamma D/c_u$, if the relative depth is also high, the tunnel is stable with greater overburden above the tunnel (H).

This can be further illustrated with Fig, 5.18(d), 5.19(d) and 5.20(d). Consider $\gamma D/c_u$ to be 3. Even though N is decreasing with higher H/D, the solutions and hence, the charts are available only when H/D = 3. As a result, it can be stated that with increasing of depth of the tunnels, the chance of stability increases.

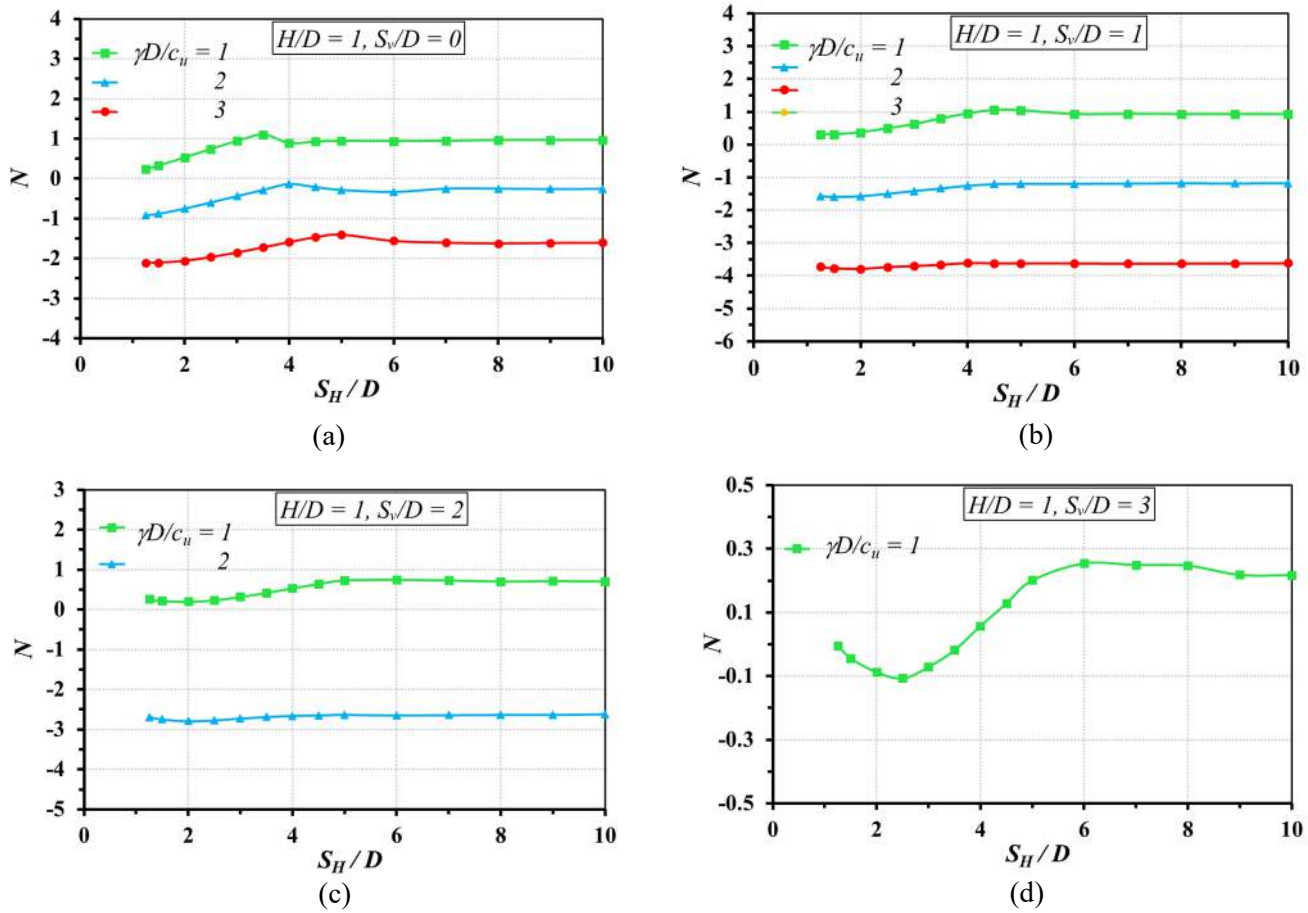

Fig. 5.18: Variation of Stability Numbers (N) in Load Multiplier with S_H/D for H/D = 1 and for different $\gamma D/c_u$ and for (a) S_V/D = 0, (b) S_V/D = 1, (c) S_V/D = 2 and (d) S_V/D = 3

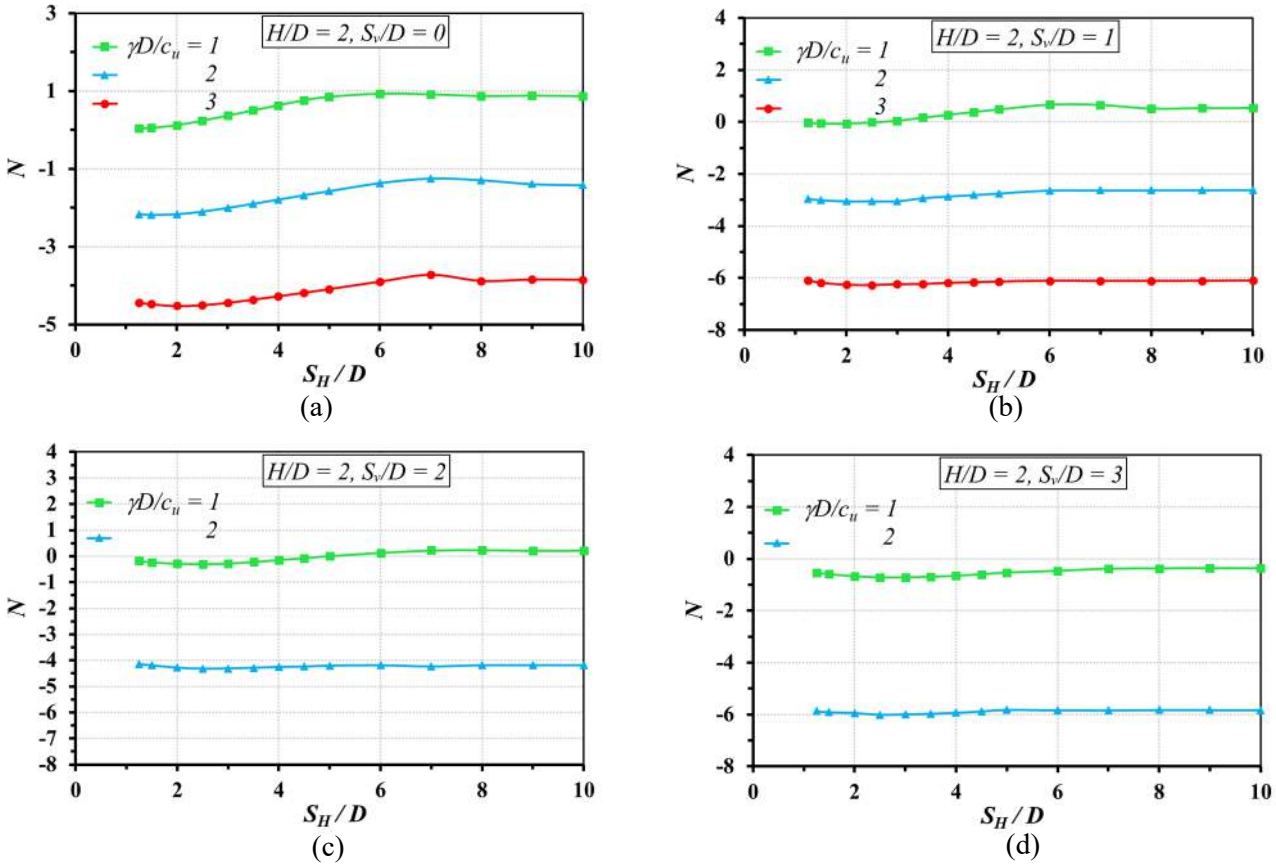

Fig. 5.19: Variation of Stability Numbers (N) in Load Multiplier with S_H/D for H/D = 2 and for different $\gamma D/c_u$ and for (a) S_V/D = 0, (b) S_V/D = 1, (c) S_V/D = 2 and (d) S_V/D = 3

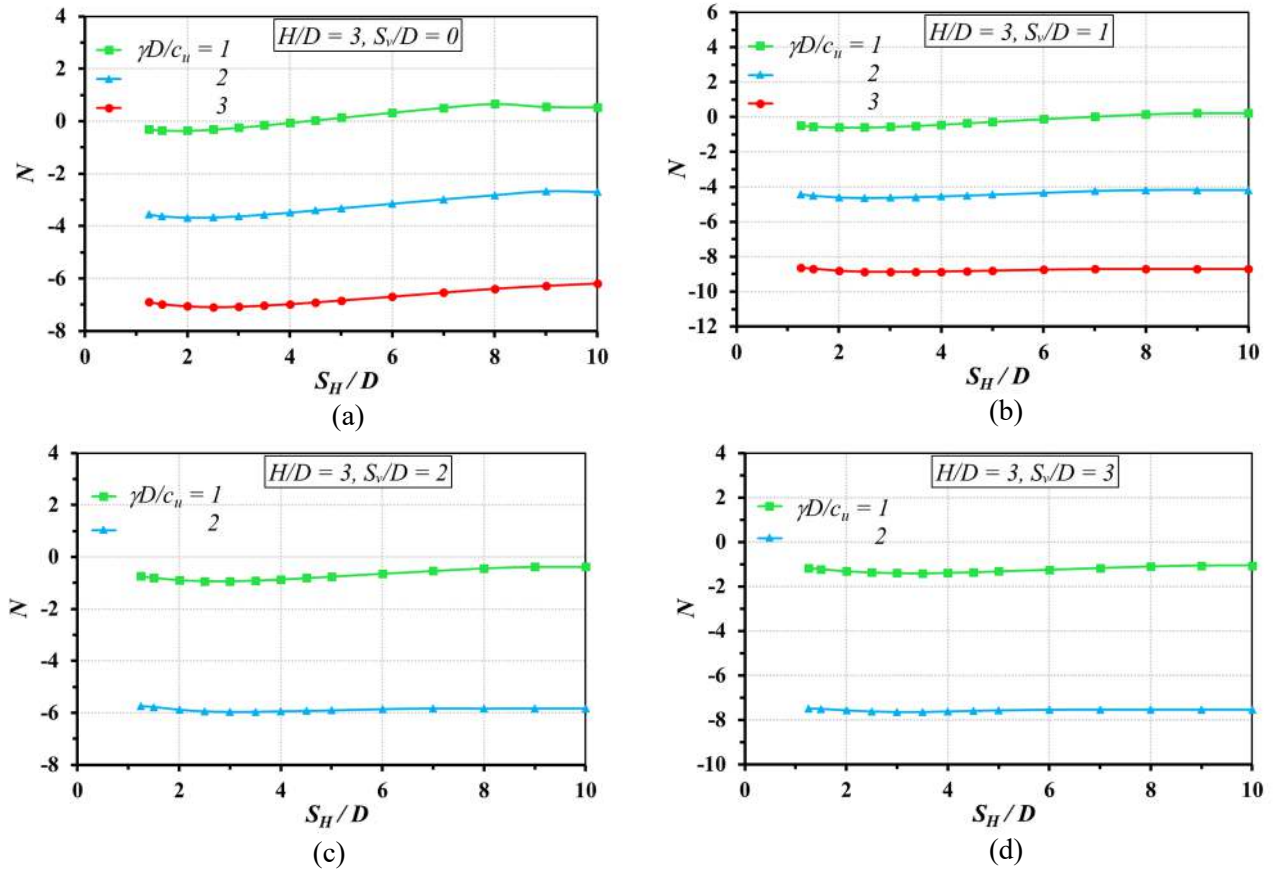

Fig. 5.20: Variation of Stability Numbers (N) in Load Multiplier with S_H/D for H/D = 3 and for different $\gamma D/c_u$ and for (a) S_V/D = 0, (b) S_V/D = 1, (c) S_V/D = 2 and (d) S_V/D = 3

5.4.2. GRAVITY MULTIPLIER METHOD:

After analyzing the dual circular tunnels using gravity multiplier method, the results are tabulated under Annexure 1. As already discussed, S_V/D of 0 indicates that both the tunnels are at the same level. Here, it is considered that there is no internal tunnel pressure, hence a collapse multiplier less than 1 means it is required to apply σ_t to maintain stability.

5.4.2.1. Variation of stability number with relative depth (S_V/D)

The variation of stability numbers (S_n) with S_V/D are presented graphically in Fig. 5.21. The increase in relative depth, has the most effect on stability of the tunnels. However, the reduction of *Sn* with increase of S_V/D is decreased with each increment. This is due to the effect of overburden and interaction effect of the first tunnel. from Figure 5.70 to Figure 5.72. As observed in load multiplier method, it is seen that the stability number decreases with increasing relative depth.

The critical distance, i,e, the distance at which S_n tend to become constant is in the range of 4-6. However, for comparatively deep tunnels the effect is far-reached and the critical S_H/D is found to be more than 7-8. For higher relative depths, e.g. S_V/D of 3 causes the stability factor to be up from 1.05 to 1.86 for higher *H/D.*

These stability charts sometimes show a stability factor of 1. In gravity multiplier method, this means that the tunnel is already loaded to its capacity.

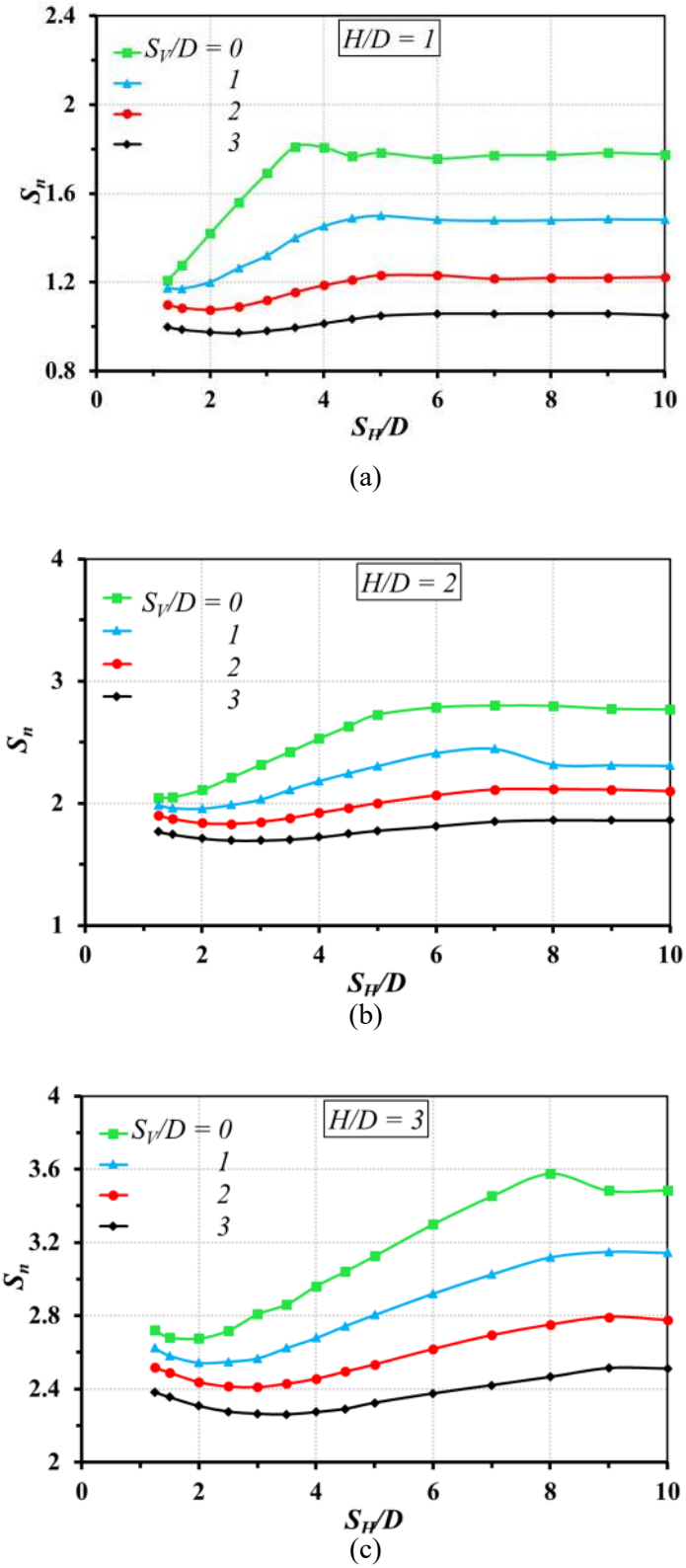

Fig. 5.21: Variation of Stability Numbers (*N*) in Gravity Multiplier with S_H/D for different S_V/D and for (a) $H/D = 1$, (b) $H/D = 2$ and (c) $H/D = 3$

5.4.2.2. Variation of stability number with clear cover (*H/D*)

The variation of stability numbers (S_n) with depth or cover thickness (in terms of dimensionless parameter *H/D*) are presented graphically in Fig.5.22. As discussed above, as with increase in *H*, S_n increases, the same is reflected in the following plots. This is due to the manner at which S_n is derived using equation 5.3..

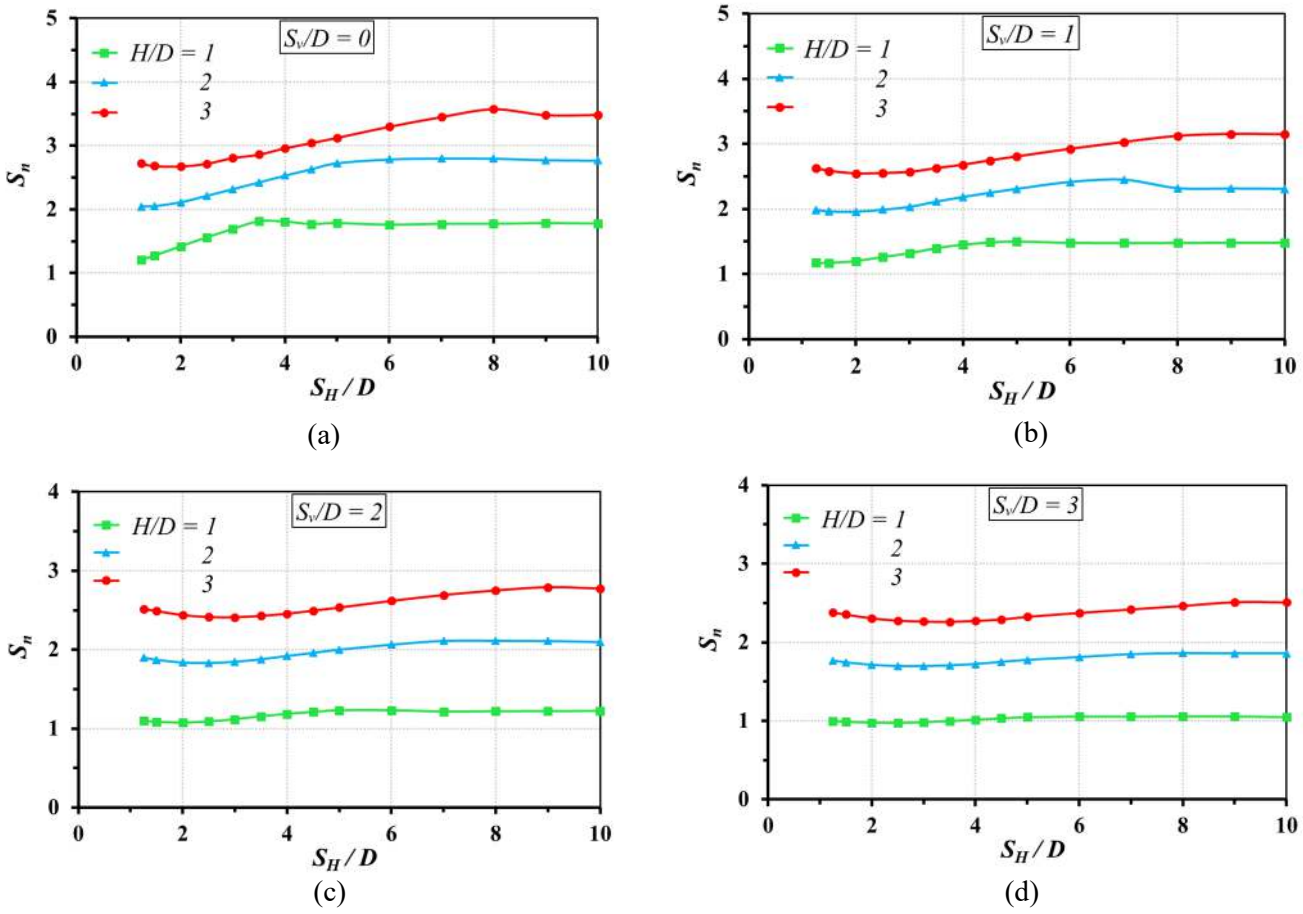

Fig. 5.22: Variation of Stability Numbers (S_n) in Load Multiplier with S_H/D for H/Dc_u and for (a) S_V/D = 0, (b) S_V/D = 1, (c) S_V/D = 2 and (d) S_V/D = 3

5.5. FAILURE PATTERNS:

5.5.1. USE OF ADAPTIVE MESHING:

In OptumG2, a technique called adaptive meshing technique is used which basically densifies the meshes where the stress is high. This way a more precise result is obtained AFTER ADAPTIVE ITERATIONS. Because of accuracy of meshes where it is needed, lesser computation time is required. A comparison is drawn in Fig. 5.23. The stability number is plotted against number of adaptive iterations. It can be seen that the results tend to converge with increase in number of iterations, indicating better accuracy. The iteration number of 1 indicates no use of adaptive iteration.

A few comparisons with and without adaptive meshing are shown in Fig. 5.24 and 5.25.

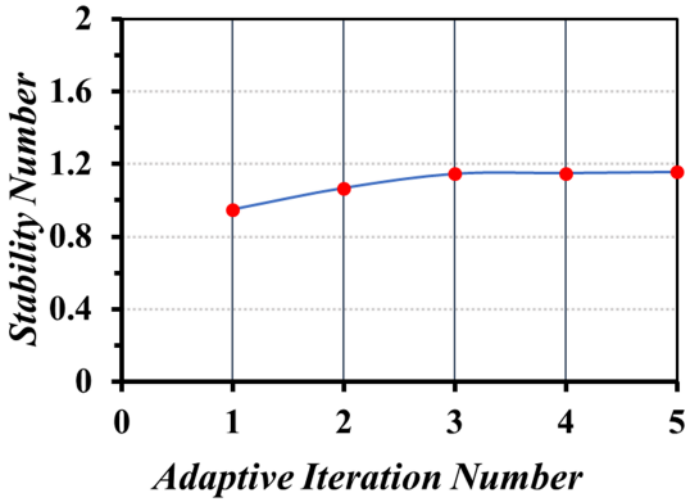

Fig. 5.23: Variation of Stability number with number of adaptive iterations for circular tunnels for H/D = 1, $\gamma B/c_u$ = 1, S_V/D = 2 & S_H/D = 3.5 in gravity multiplier method

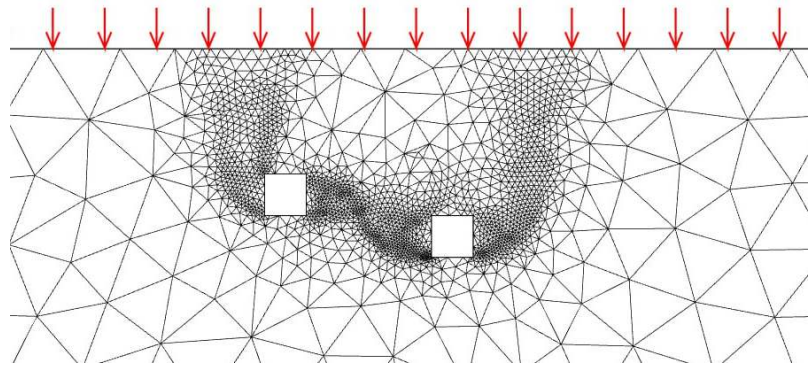

(a)

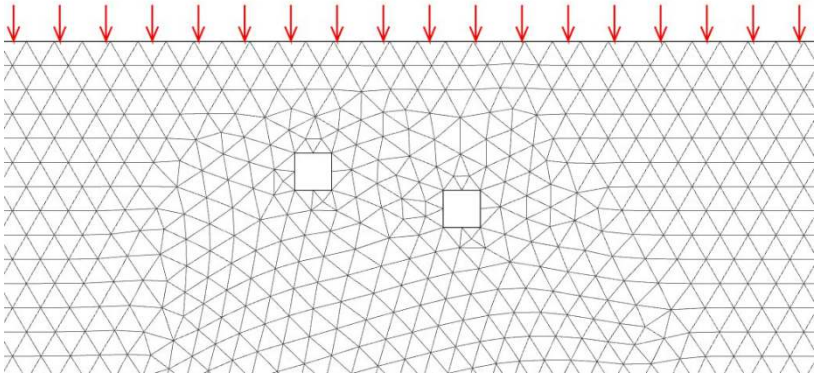

(b)

Fig. 5.24: Meshing pattern (a) with 5 adaptive iteration and (b) without adaptive iteration for square tunnels for $H/B = 3$, $\gamma B/c_u = 1$, $S_V/B = 1$ & $S_H/B = 4$ in load multiplier method

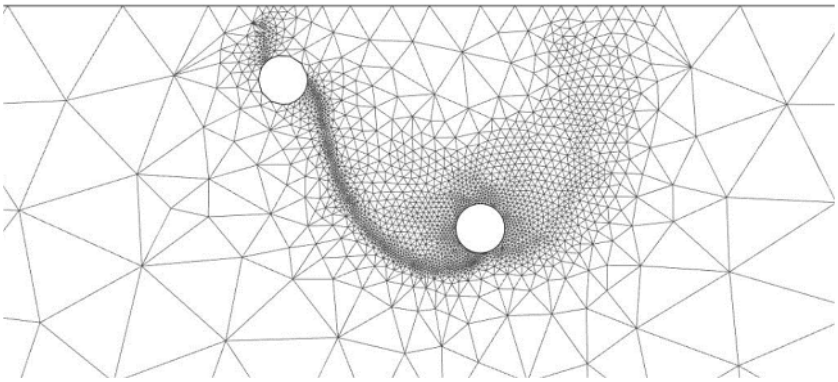

(a)

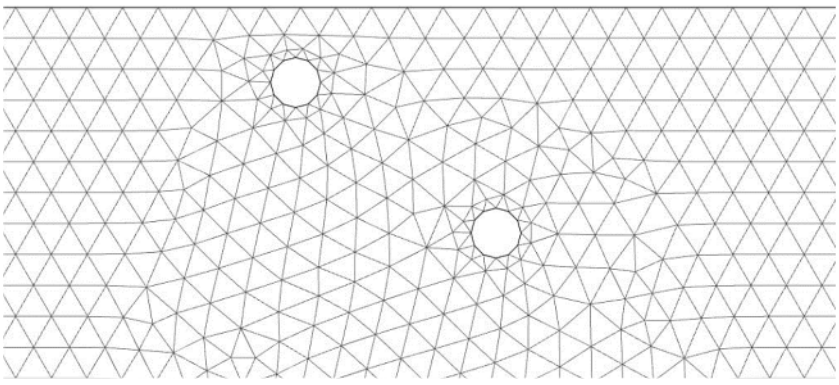

(b)

Fig. 5.25: Meshing pattern (a) with 5 adaptive iteration and (b) without adaptive iteration for square tunnels for $H/D = 1$, $\gamma B/c_u = 1$, $S_V/D = 3$ & $S_H/D = 4$ in gravity multiplier method

5.5.2. EFFECT OF HORIZONTAL DISTANCE BETWEEN THE TUNNELS:

If observed from Fig. 5.1. to 5.22, it is clear that in any case, with increase in horizontal distance between the tunnels, the stability number first decreases and then increases. After a while, the stability factor becomes constant. This indicates that, after some distance the two tunnels tend to behave as single tunnels. The failure surfaces also indicate that with increasing S_H/B or S_H/D, the failure surfaces of the two tunnels first overlap, then the interference decreases and eventually, becomes independent of each other. This is shown under Figure 5.26 and 5.27.

5.5.3. EFFECT OF VERTICAL DISTANCE BETWEEN THE TUNNELS:

It is observed that when the depth of the one tunnel increases with respect to the other, the failure is more and more governed by the bottom tunnel. When the tunnels are at the same level, i.e. $S_V/B = 0$ (for square tunnels) or $S_V/D = 0$ (for circular tunnels), the failure pattern is similar for both tunnels. However, with higher relative depth, the similarity reduces and the two failure surfaces pattern interferes with each other. This is shown Fig. 5.28 and 5.29

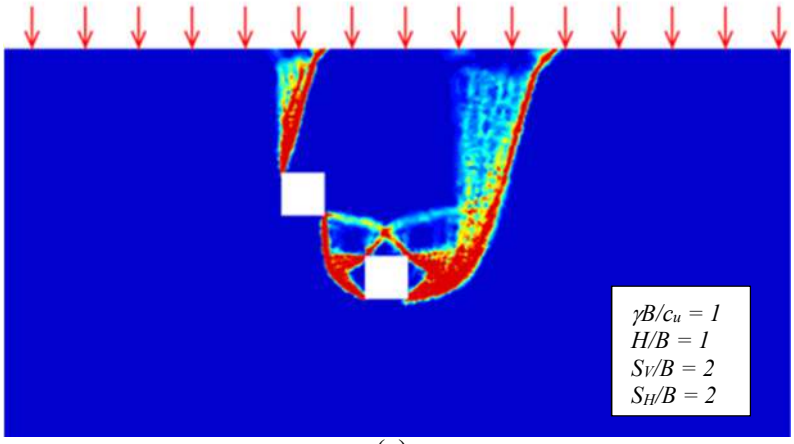

(a)

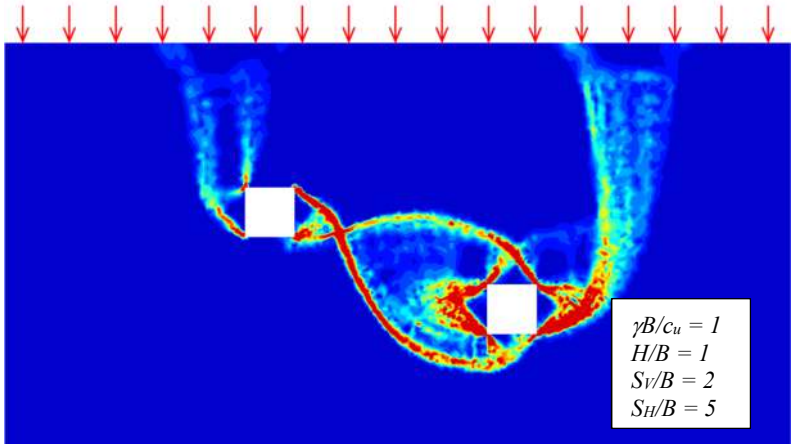

(b)

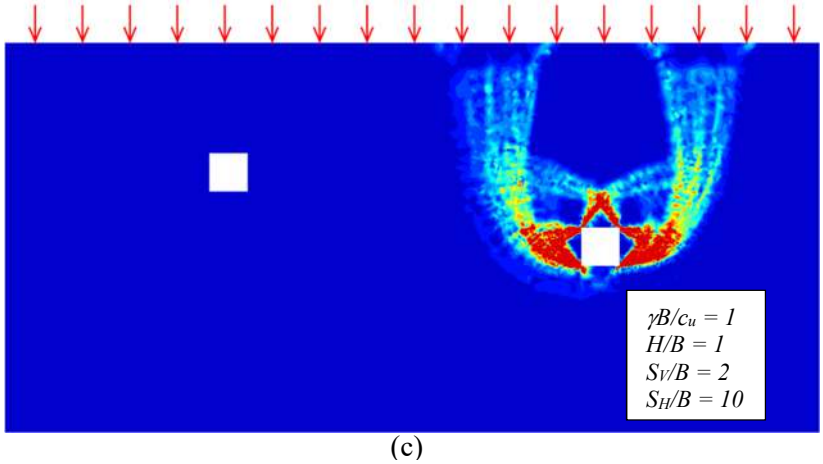

(c)

Fig. 5.26: Failure patterns for (a) S_H/B = 2, (b) S_H/B = 5 and (c) S_H/B = 10 for square tunnels in load multiplier method

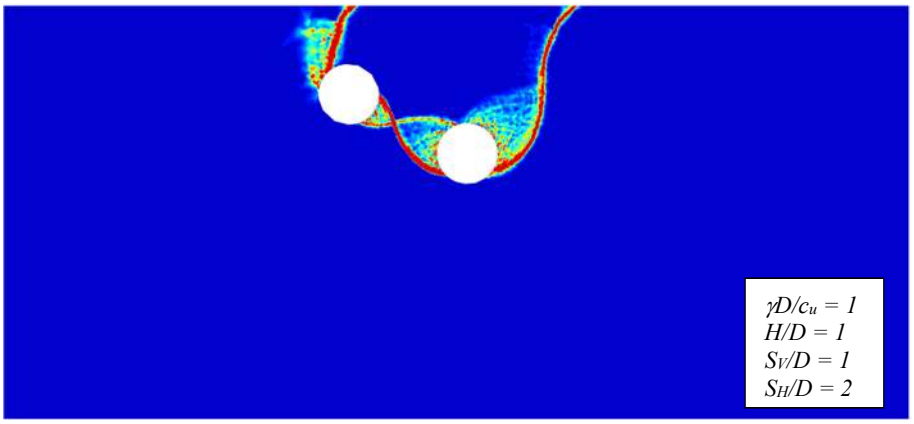

(a)

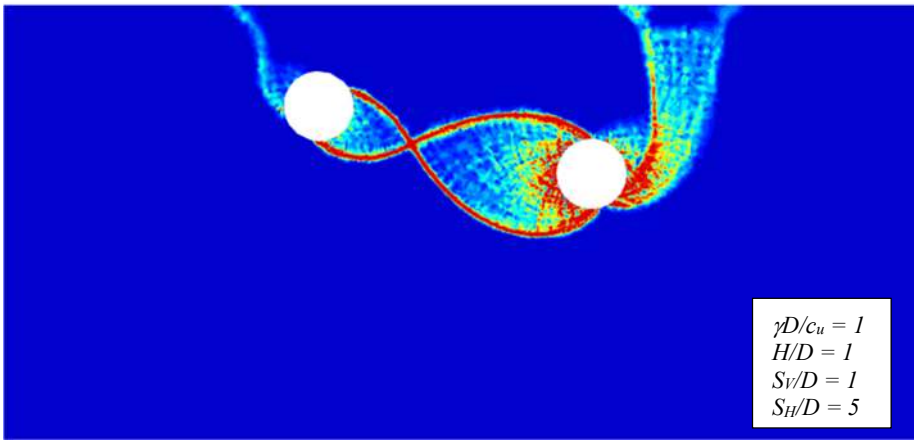

(b)

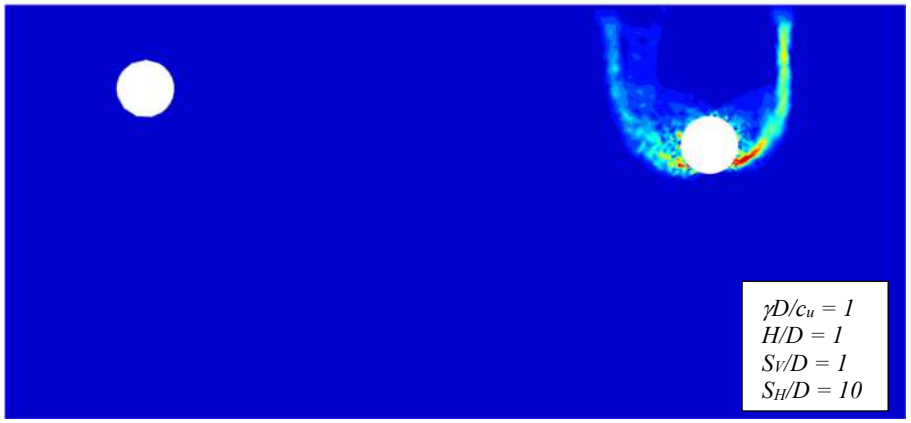

(c)

Fig. 5.27: Failure patterns for (a) S_H/D = 2, (b) S_H/D = 5 and (c) S_H/D = 10 for circular tunnels in gravity multiplier method

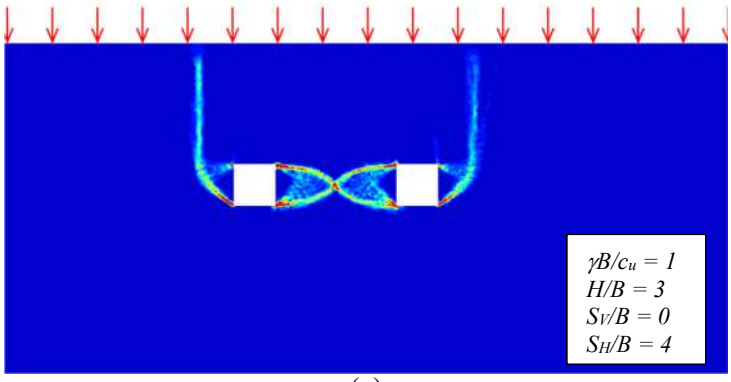

(a)

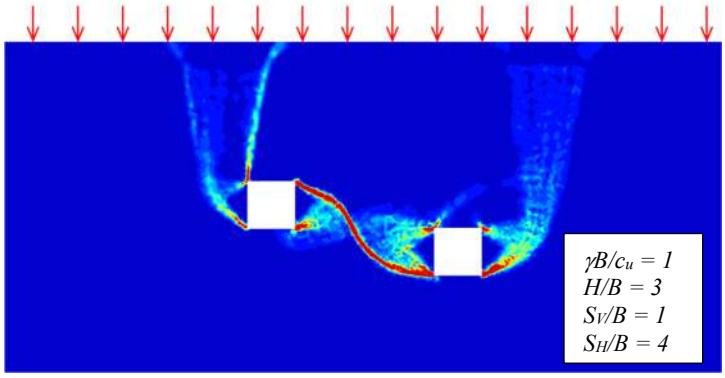

(b)

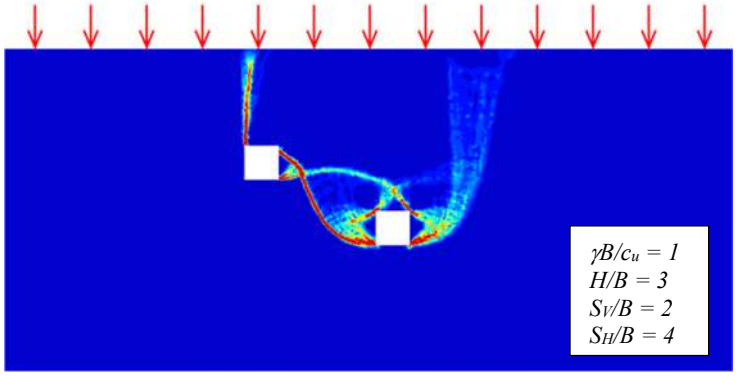

(c)

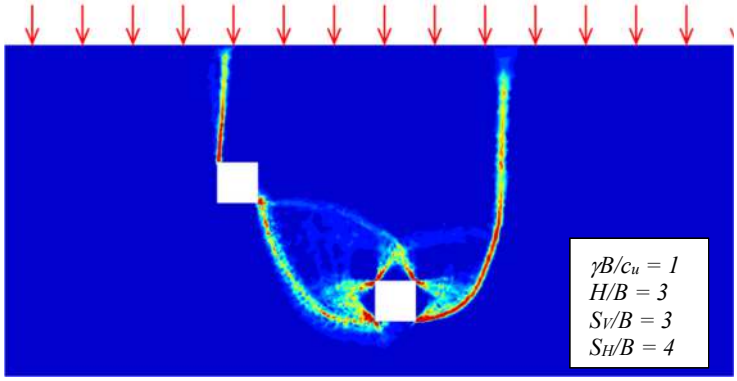

(d)

Fig. 5.28: Failure patterns for (a) $S_V/B = 0$, (b) $S_V/B = 1$, (c) $S_V/B = 2$ and (d) $S_V/B = 3$ for square tunnels in load multiplier method

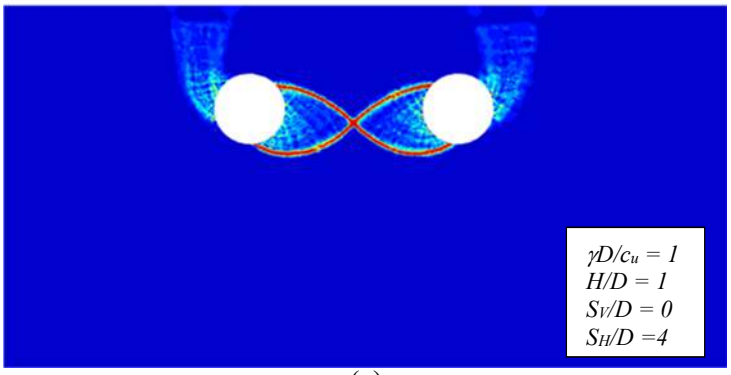

(a)

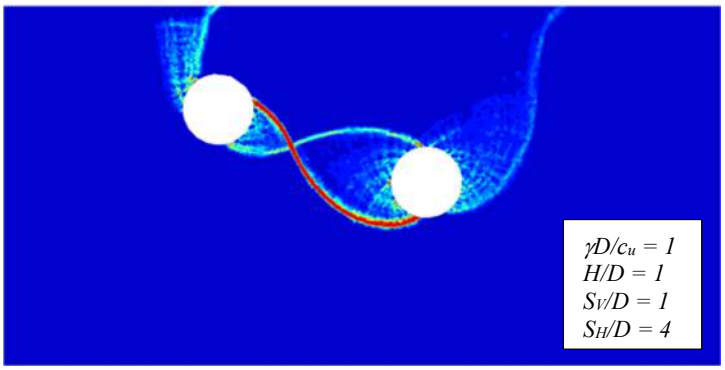

(b)

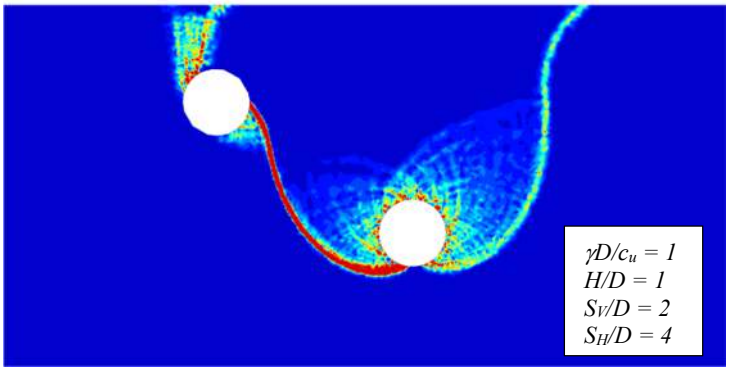

(c)

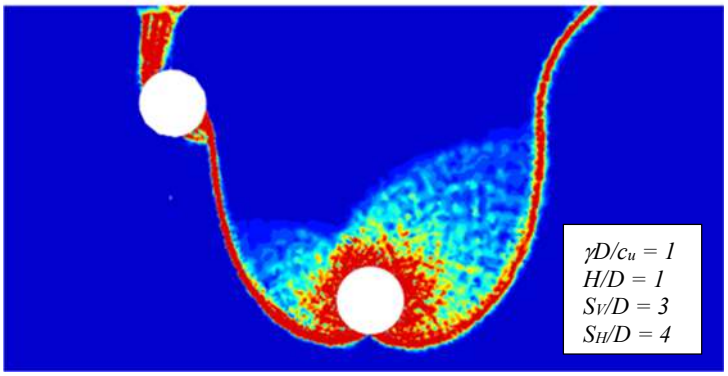

(d)

Fig. 5.29: Failure patterns for (a) S_V/D = 0, (b) S_V/D = 1, (c) S_V/D = 2 and (d) S_V/D = 3 for circular tunnels in gravity multiplier method

CHAPTER – 6: CONCLUSIONS AND FUTURE SCOPES

6.1. CONCLUSIONS:

The present study investigates the stability of two square as well circular tunnels placed at relative depths in clayey deposit. This study uses adaptive lower bound – finite element limit analysis. The OptumG2 software is used to perform the analysis using load multiplier as well as gravity multiplier method. The major conclusions from this study can be summarized as follows.

1. Finite element limit analysis is an efficient method to analyze complex soil-structure system. Moreover, with increasing crisis in resources and need for sustainable development, the lower bound finite element provides the lower bound of the true collapse load instead of assuming high factor of safety to obtain overly-conservative results. As there is no failure plane assumed before the analysis, for complex problems like studied in this thesis, FELA provides reasonably better solution that limit equilibrium methods. Moreover, it is not required to ensure the non-convergence by genuine load as in the case of strength reduction finite element analysis. Hence, in comparison, FELA provides a solution with lesser computation time.
2. Adaptive meshing techniques are used in this study. It gives better result in less computing time. This is due to the fact that in adaptive meshing, the mesh density increases where the stresses are high. As a result, the researcher finds solution in less time with greater accuracy.
3. As the stability numbers in the two methods are defined by different authors, the values are not the same for any given combination. However, these can be related with each other. It is seen that the results from these two methods are in well agreement with other.
4. The stability numbers show distinct characteristics with respect to different dimensionless parameters. With load multiplier and gravity multiplier methods, the charts can be used as reference and boundary to assess stability of twin tunnels as discussed in this thesis.
5. The stability number initially decreases with increase in spacing between the tunnels. This is particularly prominent for H/B or H/D of more than 1. This decrease varies from 20% to 50% in general. After that, the stability number starts rising with S_H/B or S_H/D

till it reaches a point and then becomes constant. The horizontal distance (S_H) may be called critical distance, i.e. distance at which the two tunnels tend to behave as single individual tunnels. The S_H/B or S_H/D at critical distance typically varies from 3 to 8 with a general median of 7.

6. With increase in depth of the tunnels the overburden pressure increases, therefore the stability of the tunnels decreases requiring additional internal pressure from the tunnels. However, if the soil parameters become such that $\gamma B/c_u$ or $\gamma D/c_u$ is more than 1, H/B or H/D of 1 hardly provides solution for stability for greater relative depths. In those cases, deeper the depth of the tunnel, higher chance of stable tunnels is found.
7. The stability of the tunnels decreases exponentially as the relative depths between the tunnels increases. It is also seen that with large overburden pressure because of unit weight, in high relative depths of 2 to 3, the tunnels required internal pressure to maintain stability.

6.2. FUTURE SCOPES:

1. In this study, for the problems addressed only lower bound solution is obtained. However, the true collapse load will lie between the upper and lower bound solutions. Additional studies should be done to assess the range of true collapse load. stability of the tunnels decreases requiring additional internal pressure from the tunnels.
2. In this study, the subsoil is considered to be homogeneous and isotropic. Hence, for more realistic soils, anisotropic and heterogeneous conditions may be assumed in future.
3. The loading condition is considered to be uniformly distributed. However, for practical situations, moving varying loads may be taken for analysis.
4. The tunnel internal pressure is taken to be σ_t for all the tunnels. Whatsoever, more complex analysis can be done where the internal pressure will vary in both the tunnels depending upon relative depth. This way, a correlation between the internal pressures required to maintain stability in the two tunnels may be established.
5. This study can also be extended for 3-D conditions.

References

1. Assadi, A., & Sloan, S. W. (1991). *Undrained stability of shallow square tunnel*. Journal of geotechnical engineering, 117(8), 1152-1173.
2. Atkinson, J.H., and Potts, D.M. 1977. *Stability of a shallow circular tunnel in cohesionless soil*. Geotechnique, 27(2), 203-215.
3. Bottero, A., Negre, R., Pastor, J., & Turgeman, S. (1980). *Finite element method and limit analysis theory for soil mechanics problems*. Computer Methods in Applied Mechanics and Engineering, 22(1), 131-149.
4. Caporaletti, P., Burghignoli, A., & Taylor, R. (2005, June). *Centrifuge study of tunnel movements and their interaction with structures*. In Geotechnical aspects of underground construction in soft ground: proceedings of the 5th international symposium TC28, Amsterdam, The Netherlands (pp. 99-106). CRC Press, London, UK.
5. Chapman, D. N., Ahn, S. K., Hunt, D. V., & Chan, A. H. (2006). *The use of model tests to investigate the ground displacements associated with multiple tunnel construction in soil*. Tunnelling and underground space technology, 21(3), 413.
6. Chen WF. Limit Analysis and Soil Plasticity. Elsevier: Amsterdam, 1975
7. Clayton, C. R. I., Van Der Berg, J. P., & Thomas, A. H. (2006). *Monitoring and displacements at Heathrow Express Terminal 4 station tunnels*. Géotechnique, 56(5), 323-334.
8. Clough G.W. and Schmidt B. (1977). *Design and performance of excavation and tunnels in soft clay*. State of the Art Report, International Symposium on Soft Clay, Bangkok, Thailand.
9. Davis, E.H., Gunn, M.J., Mair, R.J., and Seneviratne, H.N. 1980. *The stability of shallow tunnels and underground openings in cohesive material*. Geotechnique, 30, 397-416
10. Drucker, D. C., Greenberg, W. & Prager, W. (1951). *The safety factor of an elastic plastic body in plane strain*. Trans. ASME J. Appl. Mech. 73, 371–378.
11. Farrell, R. P. (2011). *Tunnelling in sands and the response of buildings* (Doctoral dissertation, University of Cambridge).
12. Fotieva, N. N., & Sheinin, V. I. (1966). *Distribution of stresses in the lining of a circular tunnel when driving a parallel tunnel*. Soil Mechanics and Foundation Engineering, 3(6), 417-422.
13. Fritz, P. (1984). *An analytical solution for axisymmetric tunnel problems in elasto-viscoplastic media*. International journal for numerical and analytical methods in geomechanics, 8(4), 325-342.
14. Hendron, A. J., & Aiyer, A. K. (1972). *Stresses and strains around a cylindrical tunnel in an elasto-plastic material with dilatancy* (No. 10). Army Engineer District, Omaha.
15. Keawsawasvong, S., & Ukritchon, B. (2022). *Design equation for stability of a circular tunnel in anisotropic and heterogeneous clay*. Underground Space, *7*(1), 76-93.
16. Kim, S. H., Burd, H. J., & Milligan, G. W. E. (1998). *Model testing of closely spaced tunnels in clay*. Geotechnique, *48*(3), 375-388.
17. Kim, S., & Kim, S.-H. (1996). *Model testing and analysis of interactions between tunnels in clay* [PhD thesis]. University of Oxford.
18. Kimura, T., & Mair, R. J. (1981). *Centrifugal testing of model tunnels in soft clay*. In Proceedings of the 10th international conference on soil mechanics and foundation engineering. Stockholm (Vol. 1, pp. 319–322).
19. Lee, C. J., Wu, B. R., Chen, H. T., & Chiang, K. H. (2006). *Tunnel stability and arching effects*

during tunneling in soft clayey soil. Tunnelling and Underground Space Technology, 21(2), 119-132.

20. Li, T., Gong, W., & Yang, X. (2021). *Stability analysis of a non-circular tunnel face in soils characterized by modified Mohr-Coulomb yield criterion*. Tunnelling and Underground Space Technology, 109, 103785.
21. Liu, J., Ding, W., & Wang, M. (2018). *Analysis of Face Stability of Circular Tunnel in Purely Cohesive Soils Driven by Shield*.
22. Lyamin, A. V., & Sloan, S. W. (2002). *Upper bound limit analysis using linear finite elements and non-linear programming*. International Journal for Numerical and Analytical Methods in Geomechanics, 26(2), 181-216.
23. Lysmer, J. (1970). *Limit analysis of plane problems in soil mechanics*. Journal of the Soil Mechanics and Foundations Division, 96(4), 1311-1334.
24. Ma, Y., Lu, A., Cai, H., & Zeng, X. (2022). *Analytical solution for determining the plastic zones around two unequal circular tunnels*. Tunnelling and Underground Space Technology, 120, 104267.
25. Mair R.J. (1979). *Centrifugal modelling of tunnel construction in soft clay*. Ph.D thesis, University of Cambridge.
26. Marshall, A. M., Farrell, R. P., Klar, A., & Mair, R. (2012). *Tunnels in sands: the effect of size, depth and volume loss on greenfield displacements*. Géotechnique, 62(5), 385-399.
27. Meguid, M. A., & Rowe, R. K. (2006). *Stability of D-shaped tunnels in a Mohr Coulomb material under anisotropic stress conditions*. Canadian Geotechnical Journal, 43(3), 273-281.
28. Nguyen, H. C., & Nguyen-Son, L. (2022). *A stable CS-FEM for the static and seismic stability of a single square tunnel in the soil where the shear strength increases linearly with depth*. Journal of Rock Mechanics and Geotechnical Engineering, 14(4), 1253-1265.
29. Osman, A. S. (2010). *Stability of unlined twin tunnels in undrained clay*. Tunnelling and Underground Space Technology, 25(3), 290-296
30. Osman, A. S., Mair, R. J., & Bolton, M. D. (2006). *On the kinematics of 2D tunnel collapse in undrained clay*. Geotechnique, 56(9), 585-595.
31. Peck, B. B. (1969). *Deep excavation and tunnelling in soft ground*, State of the art volume. In 7th ICSMFE (Vol. 4, pp. 225-290).
32. Rankin, W. J. (1988). *Ground movements resulting from urban tunnelling: predictions and effects*. Geological Society, London, Engineering Geology Special Publications, 5(1), 79-92.
33. Sahoo, J. P., & Kumar, J. (2013). *Stability of long unsupported twin circular tunnels in soils*. Tunnelling and Underground Space Technology, 38, 326-335.
34. Shiau, J., & Al-Asadi, F. (2020). *Three-dimensional heading stability of twin circular tunnels*. Geotechnical and Geological Engineering, 38, 2973-2988
35. Sloan, S. W. (1988). *Lower bound limit analysis using finite elements and linear programming*. International Journal for Numerical and Analytical Methods in Geomechanics, 12(1), 61-77.
36. Sloan, S. W., & Assadi, A. (1991). *Undrained stability of a square tunnel in a soil whose strength increases linearly with dept*h. Computers and Geotechnics, 12(4), 321-346.
37. Sloan, S. W. (2013). *Geotechnical stability analysis*. Géotechnique, *63*(7), 531-571.
38. Sulem, J., Panet, M., & Guenot, A. (1987, June). *An analytical solution for time-dependent displacements in a circular tunnel*. In International journal of rock mechanics and mining sciences & geomechanics abstracts (Vol. 24, No. 3, pp. 155-164). Pergamon.

39. Terzaghi, K., 1946. "*An introduction to tunnel geology*", In: Proctor, R.V. and White, T.L. (Eds.), Rock Tunnelling with Steel Supports. The Commercial Shearing and Stamping Co. Youngstown, Ohio, USA.

40. Wang, H. N., Zeng, G. S., & Jiang, M. J. (2018). *Analytical stress and displacement around non-circular tunnels in semi-infinite ground*. Applied Mathematical Modelling, 63, 303-328

41. Wilson, D. W., Abbo, A. J., Sloan, S. W., & Lyamin, A. V. (2011). *Undrained stability of a circular tunnel where the shear strength increases linearly with depth*. Canadian geotechnical journal, 48(9), 1328-1342.

42. Wilson, D. W., Abbo, A. J., Sloan, S. W., & Lyamin, A. V. (2014*). Undrained stability of dual circular tunnels*. International Journal of Geomechanics, 14(1), 69-79.

43. Wilson, D. W., Abbo, A. J., Sloan, S. W., & Lyamin, A. V. (2015). *Undrained stability of dual square tunnels*. Acta Geotechnica, 10, 665-682.

44. Yamamoto, K., Lyamin, A. V., Wilson, D. W., Sloan, S. W., & Abbo, A. J. (2011). *Stability of a circular tunnel in cohesive-frictional soil subjected to surcharge loading*. Computers and Geotechnics, 38(4), 504-514.

45. Yamamoto, K., Lyamin, A. V., Wilson, D. W., Sloan, S. W., & Abbo, A. J. (2011). *Stability of a single tunnel in cohesive–frictional soil subjected to surcharge loading*. Canadian Geotechnical Journal, 48(12), 1841-1854.

46. Yamamoto, K., Lyamin, A. V., Wilson, D. W., Sloan, S. W., & Abbo, A. J. (2013). *Stability of dual circular tunnels in cohesive-frictional soil subjected to surcharge loading*. Computers and Geotechnics, 50, 41-54.

47. Yamamoto, K., Lyamin, A. V., Wilson, D. W., Sloan, S. W., & Abbo, A. J. (2014). *Stability of dual square tunnels in cohesive-frictional soil subjected to surcharge loading*. Canadian Geotechnical Journal, 51(8), 829-843

48. Zhang, J., Feng, T., Yang, J., Yang, F., & Gao, Y. (2018). *Upper-bound stability analysis of dual unlined horseshoe-shaped tunnels subjected to gravity.* Computers and Geotechnics, 97, 103-110.

49. Zhang, J., Yang, F., Yang, J., Zheng, X., & Zeng, F. (2016). *Upper-bound stability analysis of dual unlined elliptical tunnels in cohesive-frictional soils*. Computers and Geotechnics, 80, 283-289.

Annexure A

Table A1: Stability Factors for Dual Square Tunnels in Load Multiplier Method

H/B	$\gamma B/c_u$	S_H/B	Stability Number N for			
			$S_V/B = 0$	$S_V/B = 1$	$S_V/B = 2$	$S_V/B = 3$
H/B = 1	$\gamma B/c_u = 1$	1.25	-0.007	-0.094	-0.187	-0.431
H/B = 1	$\gamma B/c_u = 1$	1.5	0.008	-0.101	-0.240	-0.513
H/B = 1	$\gamma B/c_u = 1$	2	0.121	-0.068	-0.298	-0.607
H/B = 1	$\gamma B/c_u = 1$	2.5	0.250	0.047	-0.250	-0.629
H/B = 1	$\gamma B/c_u = 1$	3	0.428	0.178	-0.143	-0.587
H/B = 1	$\gamma B/c_u = 1$	3.5	0.633	0.317	-0.022	-0.499
H/B = 1	$\gamma B/c_u = 1$	4	0.717	0.487	0.088	-0.409
H/B = 1	$\gamma B/c_u = 1$	4.5	0.618	0.643	0.183	-0.343
H/B = 1	$\gamma B/c_u = 1$	5	0.635	0.643	0.250	-0.297
H/B = 1	$\gamma B/c_u = 1$	6	0.627	0.504	0.258	-0.254
H/B = 1	$\gamma B/c_u = 1$	7	0.616	0.523	0.243	-0.262
H/B = 1	$\gamma B/c_u = 1$	8	0.614	0.528	0.255	-0.252
H/B = 1	$\gamma B/c_u = 1$	9	0.632	0.513	0.241	-0.250
H/B = 1	$\gamma B/c_u = 1$	10	0.629	0.499	0.243	-0.253
H/B = 1	$\gamma B/c_u = 2$	1.25	-1.144	-1.934	-3.269	--
H/B = 1	$\gamma B/c_u = 2$	1.5	-1.149	-2.040	-3.346	--
H/B = 1	$\gamma B/c_u = 2$	2	-1.098	-2.087	-3.375	--
H/B = 1	$\gamma B/c_u = 2$	2.5	-1.007	-1.962	-3.263	--
H/B = 1	$\gamma B/c_u = 2$	3	-0.868	-1.859	-3.200	--
H/B = 1	$\gamma B/c_u = 2$	3.5	-0.711	-1.774	-3.163	--
H/B = 1	$\gamma B/c_u = 2$	4	-0.539	-1.697	-3.124	--
H/B = 1	$\gamma B/c_u = 2$	4.5	-0.453	-1.666	-3.135	--
H/B = 1	$\gamma B/c_u = 2$	5	-0.441	-1.664	-3.138	--
H/B = 1	$\gamma B/c_u = 2$	6	-0.578	-1.662	-3.108	--
H/B = 1	$\gamma B/c_u = 2$	7	-0.561	-1.665	-3.082	--
H/B = 1	$\gamma B/c_u = 2$	8	-0.572	-1.669	-3.091	--
H/B = 1	$\gamma B/c_u = 2$	9	-0.562	-1.668	-3.080	--
H/B = 1	$\gamma B/c_u = 2$	10	-0.560	-1.662	-3.087	--
H/B = 1	$\gamma B/c_u = 3$	1.25	-2.318	-4.238	--	--
H/B = 1	$\gamma B/c_u = 3$	1.5	-2.355	-4.354	--	--
H/B = 1	$\gamma B/c_u = 3$	2	-2.377	-4.438	--	--
H/B = 1	$\gamma B/c_u = 3$	2.5	-2.331	-4.294	--	--
H/B = 1	$\gamma B/c_u = 3$	3	-2.244	-4.174	--	--
H/B = 1	$\gamma B/c_u = 3$	3.5	-2.102	-4.120	--	--
H/B = 1	$\gamma B/c_u = 3$	4	-1.977	-4.087	--	--
H/B = 1	$\gamma B/c_u = 3$	4.5	-1.884	-4.080	--	--
H/B = 1	$\gamma B/c_u = 3$	5	-1.875	-4.061	--	--
H/B = 1	$\gamma B/c_u = 3$	6	-1.962	-4.060	--	--
H/B = 1	$\gamma B/c_u = 3$	7	-1.957	-4.068	--	--
H/B = 1	$\gamma B/c_u = 3$	8	-1.924	-4.064	--	--
H/B = 1	$\gamma B/c_u = 3$	9	-1.986	-4.071	--	--
H/B = 1	$\gamma B/c_u = 3$	10	-1.995	-4.057	--	--
H/B = 2	$\gamma B/c_u = 1$	1.25	-0.211	-0.453	-0.665	-1.006
H/B = 2	$\gamma B/c_u = 1$	1.5	-0.231	-0.495	-0.719	-1.067
H/B = 2	$\gamma B/c_u = 1$	2	-0.250	-0.527	-0.808	-1.172
H/B = 2	$\gamma B/c_u = 1$	2.5	-0.219	-0.474	-0.807	-1.218
H/B = 2	$\gamma B/c_u = 1$	3	-0.122	-0.394	-0.752	-1.212
H/B = 2	$\gamma B/c_u = 1$	3.5	0.015	-0.304	-0.678	-1.178
H/B = 2	$\gamma B/c_u = 1$	4	0.158	-0.191	-0.599	-1.129
H/B = 2	$\gamma B/c_u = 1$	4.5	0.300	-0.076	-0.525	-1.066
H/B = 2	$\gamma B/c_u = 1$	5	0.421	0.022	-0.461	-1.021
H/B = 2	$\gamma B/c_u = 1$	6	0.623	0.184	-0.354	-0.942
H/B = 2	$\gamma B/c_u = 1$	7	0.524	0.274	-0.266	-0.872
H/B = 2	$\gamma B/c_u = 1$	8	0.521	0.255	-0.251	-0.862
H/B = 2	$\gamma B/c_u = 1$	9	0.535	0.250	-0.250	-0.859
H/B = 2	$\gamma B/c_u = 1$	10	0.527	0.245	-0.245	-0.859
H/B = 2	$\gamma B/c_u = 2$	1.25	-2.406	-3.368	-4.567	--
H/B = 2	$\gamma B/c_u = 2$	1.5	-2.476	-3.449	-4.674	--
H/B = 2	$\gamma B/c_u = 2$	2	-2.529	-3.530	-4.804	--
H/B = 2	$\gamma B/c_u = 2$	2.5	-2.509	-3.502	-4.867	--
H/B = 2	$\gamma B/c_u = 2$	3	-2.439	-3.433	-4.812	--
H/B = 2	$\gamma B/c_u = 2$	3.5	-2.338	-3.369	-4.768	--
H/B = 2	$\gamma B/c_u = 2$	4	-2.225	-3.307	-4.733	--
H/B = 2	$\gamma B/c_u = 2$	4.5	-2.127	-3.240	-4.701	--

H/B	$\gamma B/c_u$	S_H/B	Stability Number N for			
			$S_V/B = 0$	$S_V/B = 1$	$S_V/B = 2$	$S_V/B = 3$
H/B = 2	$\gamma B/c_u = 2$	5	-2.047	-3.179	-4.664	--
H/B = 2	$\gamma B/c_u = 2$	6	-1.875	-3.097	-4.625	--
H/B = 2	$\gamma B/c_u = 2$	7	-1.881	-3.083	-4.635	--
H/B = 2	$\gamma B/c_u = 2$	8	-1.890	-3.102	-4.628	--
H/B = 2	$\gamma B/c_u = 2$	9	-1.879	-3.094	-4.631	--
H/B = 2	$\gamma B/c_u = 2$	10	-1.903	-3.098	-4.635	--
H/B = 2	$\gamma B/c_u = 3$	1.25	-4.656	-6.465	--	--
H/B = 2	$\gamma B/c_u = 3$	1.5	-4.774	-6.609	--	--
H/B = 2	$\gamma B/c_u = 3$	2	-4.861	-6.785	--	--
H/B = 2	$\gamma B/c_u = 3$	2.5	-4.854	-6.762	--	--
H/B = 2	$\gamma B/c_u = 3$	3	-4.802	-6.714	--	--
H/B = 2	$\gamma B/c_u = 3$	3.5	-4.747	-6.687	--	--
H/B = 2	$\gamma B/c_u = 3$	4	-4.687	-6.649	--	--
H/B = 2	$\gamma B/c_u = 3$	4.5	-4.622	-6.629	--	--
H/B = 2	$\gamma B/c_u = 3$	5	-4.548	-6.596	--	--
H/B = 2	$\gamma B/c_u = 3$	6	-4.401	-6.537	--	--
H/B = 2	$\gamma B/c_u = 3$	7	-4.260	-6.538	--	--
H/B = 2	$\gamma B/c_u = 3$	8	-4.181	-6.548	--	--
H/B = 2	$\gamma B/c_u = 3$	9	-4.206	-6.553	--	--
H/B = 2	$\gamma B/c_u = 3$	10	-4.181	-6.542	--	--
H/B = 3	$\gamma B/c_u = 1$	1.25	-0.612	-0.921	-1.178	-1.626
H/B = 3	$\gamma B/c_u = 1$	1.5	-0.660	-0.980	-1.251	-1.686
H/B = 3	$\gamma B/c_u = 1$	2	-0.740	-1.049	-1.374	-1.797
H/B = 3	$\gamma B/c_u = 1$	2.5	-0.770	-1.050	-1.407	-1.863
H/B = 3	$\gamma B/c_u = 1$	3	-0.722	-1.024	-1.403	-1.881
H/B = 3	$\gamma B/c_u = 1$	3.5	-0.640	-0.961	-1.354	-1.871
H/B = 3	$\gamma B/c_u = 1$	4	-0.532	-0.881	-1.299	-1.841
H/B = 3	$\gamma B/c_u = 1$	4.5	-0.427	-0.794	-1.247	-1.805
H/B = 3	$\gamma B/c_u = 1$	5	-0.325	-0.727	-1.187	-1.768
H/B = 3	$\gamma B/c_u = 1$	6	-0.139	-0.571	-1.092	-1.690
H/B = 3	$\gamma B/c_u = 1$	7	0.045	-0.450	-1.010	-1.640
H/B = 3	$\gamma B/c_u = 1$	8	0.152	-0.340	-0.935	-1.588
H/B = 3	$\gamma B/c_u = 1$	9	0.189	-0.262	-0.869	-1.542
H/B = 3	$\gamma B/c_u = 1$	10	0.183	-0.265	-0.862	-1.534
H/B = 3	$\gamma B/c_u = 2$	1.25	-3.901	-4.866	-6.132	-8.244
H/B = 3	$\gamma B/c_u = 2$	1.5	-3.969	-4.953	-6.221	-8.336
H/B = 3	$\gamma B/c_u = 2$	2	-4.068	-5.083	-6.365	-8.455
H/B = 3	$\gamma B/c_u = 2$	2.5	-4.095	-5.096	-6.448	-8.492
H/B = 3	$\gamma B/c_u = 2$	3	-4.074	-5.056	-6.442	-8.467
H/B = 3	$\gamma B/c_u = 2$	3.5	-4.010	-5.018	-6.434	-8.338
H/B = 3	$\gamma B/c_u = 2$	4	-3.930	-4.972	-6.411	-8.277
H/B = 3	$\gamma B/c_u = 2$	4.5	-3.858	-4.940	-6.395	-8.217
H/B = 3	$\gamma B/c_u = 2$	5	-3.800	-4.898	-6.372	-8.148
H/B = 3	$\gamma B/c_u = 2$	6	-3.651	-4.801	-6.328	-8.075
H/B = 3	$\gamma B/c_u = 2$	7	-3.502	-4.714	-6.288	-8.034
H/B = 3	$\gamma B/c_u = 2$	8	-3.353	-4.664	-6.285	-8.007
H/B = 3	$\gamma B/c_u = 2$	9	-3.212	-4.638	-6.288	-8.008
H/B = 3	$\gamma B/c_u = 2$	10	-3.138	-4.642	-6.289	-8.009
H/B = 3	$\gamma B/c_u = 3$	1.25	-7.177	-8.977	--	--
H/B = 3	$\gamma B/c_u = 3$	1.5	-7.315	-9.120	--	--
H/B = 3	$\gamma B/c_u = 3$	2	-7.442	-9.298	--	--
H/B = 3	$\gamma B/c_u = 3$	2.5	-7.479	-9.335	--	--
H/B = 3	$\gamma B/c_u = 3$	3	-7.461	-9.330	--	--
H/B = 3	$\gamma B/c_u = 3$	3.5	-7.427	-9.323	--	--
H/B = 3	$\gamma B/c_u = 3$	4	-7.385	-9.304	--	--
H/B = 3	$\gamma B/c_u = 3$	4.5	-7.349	-9.279	--	--
H/B = 3	$\gamma B/c_u = 3$	5	-7.304	-9.268	--	--
H/B = 3	$\gamma B/c_u = 3$	6	-7.192	-9.215	--	--
H/B = 3	$\gamma B/c_u = 3$	7	-7.060	-9.167	--	--
H/B = 3	$\gamma B/c_u = 3$	8	-6.927	-9.163	--	--
H/B = 3	$\gamma B/c_u = 3$	9	-6.898	-9.159	--	--
H/B = 3	$\gamma B/c_u = 3$	10	-6.886	-9.163	--	--

Table A2: Stability Factors for Dual Square Tunnels in Gravity Multiplier Method

H/B	S_H/B	Stability Number S_n for			
		S_V/B = 0	S_V/B = 1	S_V/B = 2	S_V/B = 3
H/B = 1	1.25	0.978	0.957	0.935	0.873
H/B = 1	1.5	1.015	0.944	0.906	0.850
H/B = 1	2	1.100	0.963	0.886	0.828
H/B = 1	2.5	1.198	1.026	0.906	0.823
H/B = 1	3	1.330	1.099	0.947	0.836
H/B = 1	3.5	1.477	1.175	0.990	0.863
H/B = 1	4	1.614	1.241	1.031	0.893
H/B = 1	4.5	1.612	1.296	1.061	0.915
H/B = 1	5	1.519	1.276	1.080	0.928
H/B = 1	6	1.550	1.299	1.083	0.940
H/B = 1	7	1.564	1.278	1.084	0.944
H/B = 1	8	1.555	1.274	1.082	0.942
H/B = 1	9	1.557	1.281	1.083	0.943
H/B = 1	10	1.553	1.284	1.084	0.941
H/B = 2	1.25	1.826	1.690	1.650	1.562
H/B = 2	1.5	1.794	1.654	1.604	1.526
H/B = 2	2	1.776	1.642	1.566	1.484
H/B = 2	2.5	1.808	1.672	1.570	1.466
H/B = 2	3	1.896	1.726	1.592	1.474
H/B = 2	3.5	2.012	1.790	1.630	1.492
H/B = 2	4	2.136	1.870	1.670	1.524
H/B = 2	4.5	2.252	1.950	1.720	1.548
H/B = 2	5	2.344	2.014	1.766	1.580
H/B = 2	6	2.500	2.116	1.826	1.622
H/B = 2	7	2.478	2.152	1.872	1.658
H/B = 2	8	2.434	2.152	1.878	1.680
H/B = 2	9	2.434	2.146	1.882	1.678
H/B = 2	10	2.426	2.150	1.886	1.682
H/B = 3	1.25	2.451	2.304	2.244	2.136
H/B = 3	1.5	2.394	2.241	2.190	2.094
H/B = 3	2	2.322	2.196	2.127	2.037
H/B = 3	2.5	2.298	2.199	2.106	2.001
H/B = 3	3	2.343	2.214	2.115	2.001
H/B = 3	3.5	2.418	2.256	2.133	2.007
H/B = 3	4	2.523	2.319	2.151	2.025
H/B = 3	4.5	2.622	2.388	2.196	2.043
H/B = 3	5	2.712	2.457	2.244	2.067
H/B = 3	6	2.862	2.571	2.319	2.121
H/B = 3	7	3.021	2.667	2.388	2.166
H/B = 3	8	3.117	2.742	2.445	2.208
H/B = 3	9	3.063	2.787	2.499	2.247
H/B = 3	10	3.048	2.796	2.505	2.259

Table A3: Stability Factors for Dual Circular Tunnels in Load Multiplier Method

H/D	$\gamma D/c_u$	S_H/D	Stability Number N for			
			$S_V/D = 0$	$S_V/D = 1$	$S_V/D = 2$	$S_V/D = 3$
H/D =1	$\gamma D/c_u = 1$	1.25	0.239	0.308	0.259	-0.004
H/D =1	$\gamma D/c_u = 1$	1.5	0.331	0.308	0.218	-0.044
H/D =1	$\gamma D/c_u = 1$	2	0.531	0.371	0.201	-0.088
H/D =1	$\gamma D/c_u = 1$	2.5	0.742	0.492	0.237	-0.107
H/D =1	$\gamma D/c_u = 1$	3	0.940	0.619	0.321	-0.071
H/D =1	$\gamma D/c_u = 1$	3.5	1.098	0.791	0.421	-0.018
H/D =1	$\gamma D/c_u = 1$	4	0.891	0.946	0.538	0.058
H/D =1	$\gamma D/c_u = 1$	4.5	0.925	1.053	0.644	0.129
H/D =1	$\gamma D/c_u = 1$	5	0.942	1.042	0.734	0.202
H/D =1	$\gamma D/c_u = 1$	6	0.939	0.925	0.749	0.255
H/D =1	$\gamma D/c_u = 1$	7	0.944	0.929	0.734	0.250
H/D =1	$\gamma D/c_u = 1$	8	0.963	0.922	0.707	0.248
H/D =1	$\gamma D/c_u = 1$	9	0.962	0.924	0.716	0.219
H/D =1	$\gamma D/c_u = 1$	10	0.965	0.923	0.709	0.218
H/D =1	$\gamma D/c_u = 2$	1.25	-0.921	-1.573	-2.690	--
H/D =1	$\gamma D/c_u = 2$	1.5	-0.881	-1.597	-2.748	--
H/D =1	$\gamma D/c_u = 2$	2	-0.750	-1.578	-2.792	--
H/D =1	$\gamma D/c_u = 2$	2.5	-0.598	-1.503	-2.770	--
H/D =1	$\gamma D/c_u = 2$	3	-0.439	-1.418	-2.723	--
H/D =1	$\gamma D/c_u = 2$	3.5	-0.286	-1.339	-2.687	--
H/D =1	$\gamma D/c_u = 2$	4	-0.137	-1.254	-2.659	--
H/D =1	$\gamma D/c_u = 2$	4.5	-0.215	-1.207	-2.648	--
H/D =1	$\gamma D/c_u = 2$	5	-0.285	-1.195	-2.636	--
H/D =1	$\gamma D/c_u = 2$	6	-0.335	-1.194	-2.647	--
H/D =1	$\gamma D/c_u = 2$	7	-0.252	-1.187	-2.642	--
H/D =1	$\gamma D/c_u = 2$	8	-0.253	-1.179	-2.637	--
H/D =1	$\gamma D/c_u = 2$	9	-0.263	-1.185	-2.638	--
H/D =1	$\gamma D/c_u = 2$	10	-0.257	-1.178	-2.620	--
H/D =1	$\gamma D/c_u = 3$	1.25	-2.107	-3.723	--	--
H/D =1	$\gamma D/c_u = 3$	1.5	-2.106	-3.770	--	--
H/D =1	$\gamma D/c_u = 3$	2	-2.059	-3.784	--	--
H/D =1	$\gamma D/c_u = 3$	2.5	-1.965	-3.731	--	--
H/D =1	$\gamma D/c_u = 3$	3	-1.852	-3.701	--	--
H/D =1	$\gamma D/c_u = 3$	3.5	-1.720	-3.661	--	--
H/D =1	$\gamma D/c_u = 3$	4	-1.588	-3.608	--	--
H/D =1	$\gamma D/c_u = 3$	4.5	-1.464	-3.616	--	--
H/D =1	$\gamma D/c_u = 3$	5	-1.400	-3.619	--	--
H/D =1	$\gamma D/c_u = 3$	6	-1.559	-3.619	--	--
H/D =1	$\gamma D/c_u = 3$	7	-1.603	-3.629	--	--
H/D =1	$\gamma D/c_u = 3$	8	-1.621	-3.624	--	--
H/D =1	$\gamma D/c_u = 3$	9	-1.609	-3.619	--	--
H/D =1	$\gamma D/c_u = 3$	10	-1.604	-3.614	--	--
H/D =2	$\gamma D/c_u = 1$	1.25	0.047	-0.018	-0.183	-0.543
H/D =2	$\gamma D/c_u = 1$	1.5	0.055	-0.056	-0.233	-0.595
H/D =2	$\gamma D/c_u = 1$	2	0.125	-0.063	-0.295	-0.667
H/D =2	$\gamma D/c_u = 1$	2.5	0.240	-0.016	-0.308	-0.710
H/D =2	$\gamma D/c_u = 1$	3	0.369	0.049	-0.285	-0.710
H/D =2	$\gamma D/c_u = 1$	3.5	0.503	0.165	-0.224	-0.693
H/D =2	$\gamma D/c_u = 1$	4	0.636	0.275	-0.148	-0.652
H/D =2	$\gamma D/c_u = 1$	4.5	0.764	0.380	-0.071	-0.596
H/D =2	$\gamma D/c_u = 1$	5	0.852	0.480	0.005	-0.532
H/D =2	$\gamma D/c_u = 1$	6	0.933	0.663	0.132	-0.466
H/D =2	$\gamma D/c_u = 1$	7	0.915	0.653	0.223	-0.386
H/D =2	$\gamma D/c_u = 1$	8	0.872	0.513	0.240	-0.372
H/D =2	$\gamma D/c_u = 1$	9	0.882	0.531	0.213	-0.367
H/D =2	$\gamma D/c_u = 1$	10	0.870	0.537	0.222	-0.367
H/D =2	$\gamma D/c_u = 2$	1.25	-2.163	-2.952	-4.144	-5.871
H/D =2	$\gamma D/c_u = 2$	1.5	-2.187	-3.007	-4.195	-5.913
H/D =2	$\gamma D/c_u = 2$	2	-2.170	-3.053	-4.284	-5.944
H/D =2	$\gamma D/c_u = 2$	2.5	-2.101	-3.052	-4.326	-6.013
H/D =2	$\gamma D/c_u = 2$	3	-2.005	-3.051	-4.314	-5.997
H/D =2	$\gamma D/c_u = 2$	3.5	-1.900	-2.932	-4.289	-5.972
H/D =2	$\gamma D/c_u = 2$	4	-1.790	-2.864	-4.255	-5.936
H/D =2	$\gamma D/c_u = 2$	4.5	-1.678	-2.811	-4.242	-5.880
H/D =2	$\gamma D/c_u = 2$	5	-1.572	-2.749	-4.205	-5.817
H/D =2	$\gamma D/c_u = 2$	6	-1.364	-2.636	-4.191	-5.835
H/D =2	$\gamma D/c_u = 2$	7	-1.245	-2.632	-4.238	-5.840

H/D	$\gamma D/c_u$	S_H/D	Stability Number N for			
			$S_V/D = 0$	$S_V/D = 1$	$S_V/D = 2$	$S_V/D = 3$
H/D =2	$\gamma D/c_u = 2$	8	-1.288	-2.627	-4.188	-5.825
H/D =2	$\gamma D/c_u = 2$	9	-1.392	-2.623	-4.189	-5.826
H/D =2	$\gamma D/c_u = 2$	10	-1.419	-2.619	-4.189	-5.828
H/D =2	$\gamma D/c_u = 3$	1.25	-4.429	-6.104	--	--
H/D =2	$\gamma D/c_u = 3$	1.5	-4.471	-6.184	--	--
H/D =2	$\gamma D/c_u = 3$	2	-4.516	-6.260	--	--
H/D =2	$\gamma D/c_u = 3$	2.5	-4.493	-6.272	--	--
H/D =2	$\gamma D/c_u = 3$	3	-4.434	-6.240	--	--
H/D =2	$\gamma D/c_u = 3$	3.5	-4.354	-6.233	--	--
H/D =2	$\gamma D/c_u = 3$	4	-4.267	-6.190	--	--
H/D =2	$\gamma D/c_u = 3$	4.5	-4.179	-6.169	--	--
H/D =2	$\gamma D/c_u = 3$	5	-4.086	-6.142	--	--
H/D =2	$\gamma D/c_u = 3$	6	-3.896	-6.111	--	--
H/D =2	$\gamma D/c_u = 3$	7	-3.721	-6.118	--	--
H/D =2	$\gamma D/c_u = 3$	8	-3.878	-6.119	--	--
H/D =2	$\gamma D/c_u = 3$	9	-3.841	-6.111	--	--
H/D =2	$\gamma D/c_u = 3$	10	-3.918	-6.106	--	--
H/D =3	$\gamma D/c_u = 1$	1.25	-0.299	-0.479	-0.736	-1.166
H/D =3	$\gamma D/c_u = 1$	1.5	-0.342	-0.535	-0.796	-1.215
H/D =3	$\gamma D/c_u = 1$	2	-0.355	-0.593	-0.885	-1.306
H/D =3	$\gamma D/c_u = 1$	2.5	-0.314	-0.593	-0.924	-1.362
H/D =3	$\gamma D/c_u = 1$	3	-0.238	-0.560	-0.930	-1.390
H/D =3	$\gamma D/c_u = 1$	3.5	-0.154	-0.499	-0.907	-1.397
H/D =3	$\gamma D/c_u = 1$	4	-0.052	-0.429	-0.863	-1.376
H/D =3	$\gamma D/c_u = 1$	4.5	0.040	-0.349	-0.809	-1.347
H/D =3	$\gamma D/c_u = 1$	5	0.138	-0.265	-0.751	-1.309
H/D =3	$\gamma D/c_u = 1$	6	0.332	-0.110	-0.638	-1.239
H/D =3	$\gamma D/c_u = 1$	7	0.515	0.033	-0.532	-1.168
H/D =3	$\gamma D/c_u = 1$	8	0.662	0.165	-0.430	-1.097
H/D =3	$\gamma D/c_u = 1$	9	0.545	0.234	-0.373	-1.057
H/D =3	$\gamma D/c_u = 1$	10	0.533	0.229	-0.376	-1.055
H/D =3	$\gamma D/c_u = 2$	1.25	-3.561	-4.434	-5.744	-7.490
H/D =3	$\gamma D/c_u = 2$	1.5	-3.623	-4.509	-5.775	-7.504
H/D =3	$\gamma D/c_u = 2$	2	-3.677	-4.604	-5.880	-7.569
H/D =3	$\gamma D/c_u = 2$	2.5	-3.669	-4.635	-5.942	-7.625
H/D =3	$\gamma D/c_u = 2$	3	-3.627	-4.623	-5.964	-7.652
H/D =3	$\gamma D/c_u = 2$	3.5	-3.562	-4.590	-5.959	-7.649
H/D =3	$\gamma D/c_u = 2$	4	-3.486	-4.550	-5.942	-7.626
H/D =3	$\gamma D/c_u = 2$	4.5	-3.401	-4.502	-5.926	-7.594
H/D =3	$\gamma D/c_u = 2$	5	-3.318	-4.453	-5.906	-7.574
H/D =3	$\gamma D/c_u = 2$	6	-3.148	-4.352	-5.861	-7.541
H/D =3	$\gamma D/c_u = 2$	7	-2.979	-4.249	-5.833	-7.531
H/D =3	$\gamma D/c_u = 2$	8	-2.822	-4.190	-5.839	-7.536
H/D =3	$\gamma D/c_u = 2$	9	-2.673	-4.187	-5.834	-7.535
H/D =3	$\gamma D/c_u = 2$	10	-2.704	-4.188	-5.833	-7.531
H/D =3	$\gamma D/c_u = 3$	1.25	-6.896	-8.630	--	--
H/D =3	$\gamma D/c_u = 3$	1.5	-6.971	-8.685	--	--
H/D =3	$\gamma D/c_u = 3$	2	-7.056	-8.811	--	--
H/D =3	$\gamma D/c_u = 3$	2.5	-7.085	-8.871	--	--
H/D =3	$\gamma D/c_u = 3$	3	-7.070	-8.882	--	--
H/D =3	$\gamma D/c_u = 3$	3.5	-7.027	-8.870	--	--
H/D =3	$\gamma D/c_u = 3$	4	-6.974	-8.854	--	--
H/D =3	$\gamma D/c_u = 3$	4.5	-6.907	-8.834	--	--
H/D =3	$\gamma D/c_u = 3$	5	-6.834	-8.807	--	--
H/D =3	$\gamma D/c_u = 3$	6	-6.690	-8.747	--	--
H/D =3	$\gamma D/c_u = 3$	7	-6.536	-8.708	--	--
H/D =3	$\gamma D/c_u = 3$	8	-6.390	-8.704	--	--
H/D =3	$\gamma D/c_u = 3$	9	-6.282	-8.707	--	--
H/D =3	$\gamma D/c_u = 3$	10	-6.196	-8.708	--	--

Table A4: Stability Factors for Dual Circular Tunnels in Gravity Multiplier Method

H/D	S_H/D	Stability Number S_n for			
		$S_V/D = 0$	$S_V/D = 1$	$S_V/D = 2$	$S_V/D = 3$
H/D = 1	1.25	1.209	1.173	1.098	0.998
H/D = 1	1.5	1.276	1.170	1.085	0.987
H/D = 1	2	1.419	1.200	1.076	0.976
H/D = 1	2.5	1.560	1.263	1.090	0.971
H/D = 1	3	1.691	1.320	1.119	0.981
H/D = 1	3.5	1.810	1.400	1.156	0.995
H/D = 1	4	1.806	1.453	1.187	1.015
H/D = 1	4.5	1.768	1.487	1.211	1.033
H/D = 1	5	1.782	1.500	1.232	1.048
H/D = 1	6	1.757	1.482	1.232	1.057
H/D = 1	7	1.771	1.478	1.216	1.057
H/D = 1	8	1.772	1.480	1.220	1.058
H/D = 1	9	1.782	1.484	1.221	1.058
H/D = 1	10	1.775	1.483	1.224	1.050
H/D = 2	1.25	2.046	1.986	1.900	1.766
H/D = 2	1.5	2.050	1.962	1.872	1.744
H/D = 2	2	2.110	1.958	1.838	1.712
H/D = 2	2.5	2.210	1.988	1.832	1.696
H/D = 2	3	2.316	2.032	1.848	1.696
H/D = 2	3.5	2.422	2.112	1.880	1.704
H/D = 2	4	2.530	2.184	1.922	1.722
H/D = 2	4.5	2.630	2.246	1.962	1.750
H/D = 2	5	2.726	2.306	2.002	1.776
H/D = 2	6	2.786	2.412	2.066	1.812
H/D = 2	7	2.800	2.446	2.114	1.850
H/D = 2	8	2.798	2.318	2.116	1.862
H/D = 2	9	2.774	2.312	2.112	1.860
H/D = 2	10	2.768	2.308	2.100	1.860
H/D = 3	1.25	2.721	2.625	2.517	2.382
H/D = 3	1.5	2.682	2.583	2.490	2.355
H/D = 3	2	2.676	2.544	2.439	2.307
H/D = 3	2.5	2.718	2.550	2.415	2.277
H/D = 3	3	2.808	2.568	2.412	2.265
H/D = 3	3.5	2.862	2.625	2.430	2.262
H/D = 3	4	2.961	2.679	2.457	2.274
H/D = 3	4.5	3.042	2.745	2.496	2.292
H/D = 3	5	3.126	2.805	2.535	2.325
H/D = 3	6	3.300	2.922	2.619	2.376
H/D = 3	7	3.453	3.027	2.694	2.421
H/D = 3	8	3.576	3.120	2.751	2.466
H/D = 3	9	3.483	3.150	2.793	2.514
H/D = 3	10	3.486	3.144	2.775	2.511